1-1-2011

The Role of Apolipoprotein E Concentration and Isoform in Amyloid-beta Metabolism In Vivo

Joseph Castellano
Washington University in St. Louis

WASHINGTON UNIVERSITY IN ST. LOUIS

Division of Biology and Biomedical Sciences
Neurosciences

Dissertation Examination Committee:
David M. Holtzman, Chair
Alison M. Goate
Jin-Moo Lee
Timothy M. Miller
Daniel S. Ory
Conrad C. Weihl

The Role of Apolipoprotein E Concentration and Isoform in Amyloid-β Metabolism In Vivo

by

Joseph Michael Castellano

A dissertation presented to the
Graduate School of Arts and Sciences
of Washington University in
partial fulfillment of the
requirements for the degree
of Doctor of Philosophy

December 2011

Saint Louis, Missouri

ABSTRACT OF THE DISSERTATION

The Role of Apolipoprotein E Concentration and Isoform

in Amyloid-β Metabolism In Vivo

by

Joseph Michael Castellano

Doctor of Philosophy in Neurosciences

Washington University in St. Louis, 2011

David M. Holtzman, M.D., Chair

Alzheimer's disease is a progressive, neurodegenerative disease characterized by several pathological lesions, one of which is the accumulation of the amyloid-β (Aβ) peptide into extracellular amyloid plaques. Several autosomal dominant mutations have been shown to cause familial forms of early-onset Alzheimer's disease, but factors that modulate the risk and onset for the more common sporadic, late-onset Alzheimer's disease are less understood. The strongest identified genetic risk factor for sporadic, late-onset Alzheimer's disease is the *APOE* ε4 allele, the presence of which dramatically increases risk and hastens the onset of the disease relative to non-carriers of the allele. Evidence that *APOE* ε4-carriers exhibit accelerated onset of amyloid accumulation has led to the hypothesis that *APOE* genotype differentially modulates AD risk and onset via regulation of Aβ metabolism. Thus, we sought to characterize the extent to which modulating the concentration and isoform of apoE regulates brain Aβ metabolism. To this end, we created transgenic mice overexpressing the low-density lipoprotein receptor (LDLR), a major receptor for apoE in the central nervous system, which led to a significant reduction of brain apoE concentration. After crossing these mice to a mouse

model of β-amyloidosis, the resulting mice exhibited a marked reduction in Aβ deposition. To examine the mechanism by which Aβ deposition is reduced with increased LDLR expression, we performed in vivo microdialysis in young mice, finding that early decreases in the steady state concentration of Aβ in the brain interstitial fluid (ISF) could be explained by enhanced Aβ clearance. To further investigate the mechanism by which LDLR regulates Aβ metabolism prior to amyloid plaque deposition, we utilized a brain Aβ efflux method to show that LDLR overexpression increased Aβ clearance from the brain. To complement this approach, we developed a novel method to directly assess the plasma appearance rate of brain-derived Aβ, which revealed that LDLR overexpression increased brain to blood efflux of Aβ. We next examined the role of specific apoE isoforms in modulating amyloid accumulation in humans and in a mouse model of β-amyloidosis in which human apoE isoforms were expressed. We found that cerebral Aβ deposition varied in both humans and in mice in a manner that corresponded to *APOE* genotype. Using in vivo microdialysis, we found in both young and old mice that the concentration and clearance of Aβ from the ISF differed according to the isoform of apoE expressed. In vivo stable isotopic labeling kinetics experiments in young mice revealed that fractional synthesis rates of Aβ did not vary according to human apoE isoform. Moreover, we infused recombinant apoE particles during in vivo microdialysis to demonstrate that intrinsic differences in apoE isoforms contribute to differences in the steady state concentration of ISF Aβ. Together, these results suggest a mechanism by which *APOE* alleles modulate AD risk through differential regulation of brain Aβ clearance. Furthermore, our results suggest that apoE receptors and other molecules involved in Aβ clearance may represent useful therapeutic targets for AD prevention.

Acknowledgements

First and foremost, I would like to thank my mentor, Dave Holtzman. In addition to facilitating my training and development on a number of levels in the past 5-6 years, he has given me opportunity beyond what I expected from graduate school. Dave has the unique ability to provide valuable guidance while allowing those in his lab to grow as independent scientists. It has truly been an honor and a privilege to be a student in your laboratory.

I would like to extend my gratitude to all members of my thesis committee for their valuable insights and useful advice. Thank you for pointing me in the right direction when experiments failed and for encouraging me when experiments went well. Each one of you has served as a role model for me as I begin my scientific career.

I am indebted to members of the Holtzman laboratory, all of whom have helped me in different ways to get to this point and made my graduate school experience enjoyable. To the "Goodfellows" of Bay 2, Adam and Philip, I have appreciated all our scientific discussions and debates, and most of all, the laughs. Thank you for tolerating my inane humor and for imparting some of your own.

My family has been an enduring source of support and encouragement. Above all else, my parents taught me the value of strong work ethic and success with humility. To my four brothers, thank you for reminding me of life outside the laboratory when I needed reminding.

To Katherine, my best friend and loving wife, your relationship has been especially meaningful to me. I cannot imagine getting to this point without your love and support

along the way. In addition to providing the occasional (much-needed) statistical advice, you have been my top supporter, for which I have always been grateful. I cannot wait to continue on with you as we take the next step of our journey.

Table of Contents **Page**

Chapter 4. Human apoE isoforms differentially regulate brain amyloid-β peptide clearance

Chapter 5. Conclusions and Future Directions

Appendices

Figure and Table List

Page

Chapter 2

Page

Chapter 3

Chapter 4

Page

Chapter 4 (continued)

Appendices

Page

Appendices (continued)

Chapter 1.

Introduction and Perspective

Alzheimer's disease

Alzheimer's disease (AD), the most common cause of dementia, is a progressive, neurodegenerative disease that currently affects over 26 million individuals worldwide. The disease affects a striking proportion of the elderly population—over 12% of individuals over the age of 65 and nearly half of individuals over the age of 85. Moreover, total healthcare costs for AD treatment and caregiving in the U.S. are expected to exceed $183 billion in 2011 (Thies and Bleiler, 2011). Although great strides have been made in the last several decades, there are currently no treatments capable of halting AD progression or restoring loss of cognitive function. Faced with an aging population and the associated increase in prevalence and healthcare costs, a molecular understanding of the roles of various risk factors in AD pathogenesis will be important to guide therapeutic strategies for this devastating disease.

In terms of clinical presentation, AD dementia is initially characterized by an early impairment in short-term memory as well as decline in attention, executive function, and problem-solving abilities. Difficulty understanding spatial relationships, confusion with time and location, language dysfunction, and personality change are characteristic clinical features as the disease progresses. Toward the end of the typically 7 to 10-year course of dementia that terminates in death, memory and cognitive dysfunction becomes severe and the ability to independently perform daily activities and personal care is lost.

Over a century ago, at a conference in Tübingen, Germany, Alois Alzheimer presented a clinicopathological description of a 51 year-old female dementia patient

named Auguste Deter. Using the Bielschowsky silver impregnation method to examine neuropathological changes in her cerebral cortex at autopsy, Alzheimer reported the presence of extracellular "foci" and changes of the "neurofibrils," later known as two of the disease's hallmark pathological features, amyloid plaques and neurofibrillary tangles, respectively (Alzheimer et al., 1995). Nearly 80 years later, cerebrovascular and parenchymal amyloid plaques were isolated from AD/Down's Syndrome brain and discovered to contain aggregated species of a "β protein," now known as the amyloid-β (Aβ) peptide (Glenner and Wong, 1984; Masters et al., 1985).

Cerebral β-amyloidosis and the amyloid-β peptide

The principal component of extracellular amyloid plaques is the amyloid-β (Aβ) peptide, a proteolytic derivative of the amyloid precursor protein (APP) that varies in length from 38-43 amino acids. Expressed in many cells throughout different organ systems, APP is highly expressed in the central nervous system by neurons as a type I transmembrane protein. Aβ, a peptide of unknown physiological function, is naturally secreted (Haass et al., 1992; Seubert et al., 1992; Shoji et al., 1992) following the sequential proteolysis of APP by both β- (Vassar et al., 1999) and γ-secretases (De Strooper et al., 1998). During this amyloidogenic processing of APP, γ-secretase performs a unique intramembranous cleavage at varying C-terminal residues in the Aβ sequence, generating Aβ peptides of varying length and potential for aggregation. Although Aβ40 is the most abundant of the Aβ species, Aβ42 is considered to be central to AD pathogenesis as it is more hydrophobic and, thus, more capable of initiating Aβ aggregation in the brain. Based on various lines of evidence from genetic, biochemical,

and animal model studies, it has been hypothesized that the accumulation of Aβ initiates a pathogenic cascade that ultimately culminates in synaptic dysfunction, neuronal loss, and loss of cognitive function (Hardy and Selkoe, 2002). Indeed, deposition of Aβ in amyloid plaques has been shown to be associated with various toxic effects in the brain, including neuritic dystrophy, synaptic and network dysfunction, and neuroinflammation (Bolmont et al., 2008; Busche et al., 2008; D'Amore et al., 2003; Knowles et al., 1999; Kuchibhotla et al., 2008; Lombardo et al., 2003; Meyer-Luehmann et al., 2008). The aggregation of soluble Aβ into higher-order soluble species has also been an area of active research in the past decade. However, there remains a great deal of controversy in separating the toxic role of soluble oligomers from that of other forms of aggregated Aβ that are present in and around plaques that may act as a reservoir of oligomers while independently exerting toxic effects (Selkoe, 2011). Plaques are either diffuse or fibrillar in nature, consisting of non-fibrillar or fibrillar (β-sheet-rich) conformations of aggregated Aβ, respectively. Fibrillar amyloid plaques can be visualized histologically using congophilic dyes such as Congo Red or Thioflavin-S or with compounds such as Pittsburgh Compound B *in vivo*. Microscopically, fibrillar plaques are associated with dystrophic neurites, gliosis, and an active neuroinflammatory process (neuritic plaques) (Lucin and Wyss-Coray, 2009). Interestingly, the brain exhibits region-specific vulnerability to amyloid plaque deposition, with the most prominent deposition occurring in a network of brain regions in humans known as the "default-mode network," a network characterized by elevated metabolic activity during self-referential mental activity (Buckner et al., 2005; Raichle et al., 2001; Vlassenko et al., 2010). This network includes the hippocampal formation as well as lateral and medial prefrontal, retrosplenial,

posterior cingulate, and medial prefrontal areas, all of which are more susceptible to amyloid plaque deposition than other brain regions, perhaps as a result of elevated neuronal activity and the associated increase in Aβ secretion (Bero et al., 2011).

Several groups have characterized molecular and neuroimaging biomarkers of key neuropathological hallmarks of AD (Fagan et al., 2006; Fagan et al., 2007; Jack et al., 2008; Rowe et al., 2007; Shaw et al., 2009). For example, reduced concentrations of Aβ42 in isolated cerebrospinal fluid (CSF) from living subjects reflect the presence of cerebral Aβ deposition. It is widely hypothesized that this finding reflects a process by which Aβ42 is sequestered into amyloid plaques, changing the equilibrium between brain and CSF pools of Aβ (Clark et al., 2003; Fagan et al., 2009; Hong et al., 2011; Sunderland et al., 2003). Using positron emission tomography (PET) in combination with amyloid-binding compounds such as the [^{11}C]-benzothiazole radiotracer, Pittsburgh Compound B (PIB), brain amyloid in living subjects can be visualized and compared with other biomarkers of the disease and related to the clinical disease course (Ikonomovic et al., 2008; Klunk et al., 2004; Leinonen et al., 2008). A large body of evidence has supported the concept that biomarkers such as PIB uptake and CSF Aβ42 concentration are reliable surrogate markers of amyloid plaque pathology in living subjects (Fagan et al., 2006; Fagan et al., 2007; Jack et al., 2008; Rowe et al., 2007; Shaw et al., 2009), the combination of which will likely be critical for preclinical intervention strategies as well as accurate diagnosis (Perrin et al., 2009).

The role of genetics in familial and sporadic AD

A relatively small percentage of AD cases is inherited in an autosomal dominant manner; these cases are referred to as familial AD (FAD) and typically have early onset (30-60 years of age). Although mutations in *APP*, *PSEN1* (*presenilin 1*), and *PSEN2* (*presenilin 2)* account for a small percentage of all AD cases, these mutations have, nonetheless, provided enormous mechanistic insight into AD pathogenesis in addition to serving as the basis for animal models of β-amyloidosis. Missense mutations in the coding sequence of *APP* were the first identified as being causative for FAD and/or cerebral amyloid angiopathy (CAA) (Goate et al., 1991; Haass et al., 1994; Levy et al., 1990; Mullan et al., 1992; Suzuki et al., 1994; Van Broeckhoven et al., 1990). These mutations preferentially increase the ratio of Aβ42 to Aβ40 or the overall production of Aβ species, depending on the position of the mutation. Mutations in *PSEN1* cause FAD, likely as a result of shifting the ratio of Aβ42/Aβ40 in favor of greater Aβ42 production (De Strooper, 2007; Holtzman et al., 2011). The vast majority of AD cases (>99%), however, are sporadic with late-onset (age >60) and cannot be attributed uniformly to one genetic determinant.

In addition to risk factors such as aging, family history (Fratiglioni et al., 1993; Mayeux et al., 1991), and traumatic brain injury (Mayeux et al., 1993; Plassman et al., 2000), several genes have been found to be associated with risk for AD. Large-scale genome-wide association studies (GWAS) have revealed associations between AD risk and various genes encoding proteins responsible for lipid metabolism and/or immune system function, and membrane trafficking. For example, by comparing a large set of samples from cognitively normal elderly controls and AD cases, GWAS have revealed AD risk associations with *CLU* (clusterin), *APOE* (apolipoprotein E), *PICALM*

(phosphatidylinositol-binding clathrin assembly protein), *CR1* (complement receptor 1), *BIN1* (bridging integrator protein 1), *CD33* (sialic acid-binding immunoglobulin-like lectin), *MS4A4A* (membrane spanning 4A gene cluster), *CD2AP* (CD2-associated protein), *EPHA1* (Ephrin receptor A1), and *ABCA7* (ATP-binding cassette transporter) (Bertram et al., 2008; Harold et al., 2009; Hollingworth et al., 2011; Lambert et al., 2009; Naj et al., 2011; Seshadri et al., 2010). While the identification of these novel associations should motivate new mechanistic investigations in AD research, *APOE* remains, to a large extent, the strongest identified genetic risk factor, an association for which the underlying mechanism remains unclear.

APOE and the link to AD

Of the several susceptibility genes implicated in influencing AD risk, *APOE* ε4 is the strongest identified gene confirmed to confer increased risk for sporadic, late-onset AD (age > 60) (Corder et al., 1993). The *APOE* ε3 allele is the most frequent in all populations, with a frequency ranging from 50 to 90%, whereas *APOE* ε4 and *APOE* ε2 allele frequency ranges from 5-35% and 1-5%, respectively (Mahley and Rall, 2000). Risk for AD is associated with *APOE* isoform (*ε4 > ε3> ε2*), with the *APOE* ε4 allele present in ~50% of patients who develop late-onset AD (Corder et al., 1993; Saunders, 2000; Saunders et al., 1993). Having one or two copies of the *APOE* ε4 allele increases sporadic AD risk approximately 3- to 12-fold, respectively. Moreover, one or two copies of *APOE* ε4 results in earlier age of onset by approximately one to two decades relative to non-carriers in late-onset AD (Corder et al., 1993). *APOE* ε2 individuals have reduced risk for developing late-onset AD as well as in early-onset AD caused by *APP* mutations

and a *PS1* mutation (Corder et al., 1993; Pastor et al., 2003; Saunders, 2000; Saunders et al., 1993; West et al., 1994). Epidemiological studies from various populations have confirmed the increased frequency of the *APOE* ε4 allele in sporadic AD patients compared to non-carriers, though the frequency varies in different ethnicities (Roses, 1996). However, it is important to note that *APOE* ε4 is neither necessary nor sufficient for the development of AD so that apoE polymorphism cannot be utilized alone for the diagnosis of AD (Meyer et al., 1998; Tiraboschi et al., 2004). This suggests that apoE-independent and dependent mechanisms likely interact with other genetic and non-genetic components to modulate AD pathogenesis. It will be critical to identify additional unknown risk or protective components and how they interact with apoE to accelerate or delay the onset of the disease.

There is controversy as to whether *APOE* polymorphism associates with the rate of progression of cognitive decline in AD after its onset (Corder et al., 1995; Saunders, 2000). In particular, there is discrepancy regarding the role of *APOE* ε4 in the rate of cognitive and functional decline after the onset of cognitive decline in AD. Several reports suggest patients homozygous for *APOE* ε4 experience a more rapid rate of cognitive and functional decline (Saunders, 2000), suggesting that the factors that determine the onset of disease may also have a major role in the rate of progression and clinical outcome. However, others have reported that disease onset and rate of progression as factors are different in the context of *APOE* ε4 (Craft et al., 1998; Hoyt et al., 2005; Saunders, 2000). An MRI study from a large, cognitively normal population suggested that *APOE* ε4 carriers have decreased entorhinal cortex volume in children and adolescents, suggesting a potential developmental effect (Shaw et al., 2007). In

longitudinal MRI studies of subjects already diagnosed with AD, the rate of volume decrease of entorhinal cortex and hippocampus is greater in those who are *APOE* ε4 positive (Bookheimer and Burggren, 2009). A recent large study of cognitively normal individuals younger than 60 found that age-related memory decline was greater in *APOE* ε4 carriers vs. non-carriers (Caselli et al., 2009), suggesting that the consequences of AD pathology may manifest in the brain as early as the sixth decade of life. The role of apoE isoforms in the predisposition to AD is well established; however, additional studies are needed to understand how apoE4 accelerates onset and possibly, the rate of progression of the disease.

ApoE biology and function in the CNS

Human apolipoprotein E (apoE) is an exchangeable lipoprotein of 299 amino acids expressed in multiple organs with the highest expression in liver followed by the brain (Mahley and Rall, 2000). ApoE exists mainly as a component of lipoprotein particles along with other apolipoproteins and proteins in plasma and CSF (Mahley and Rall, 2000). In humans, there are three polymorphic forms of apoE that vary at two amino acid positions: apoE2 (Cys-112, Cys-158), apoE3 (Cys-112, Arg-158), and apoE4 (Arg-112, Arg-158) (Zannis et al., 1982). These critical amino acid substitutions alter the charge and structural properties of the protein, ultimately influencing the functional properties of apoE isoforms (Mahley and Rall, 2000).

ApoE is one of the key lipoproteins of lipoprotein particles that regulate the metabolism of lipids by directing their transport, delivery, and distribution from one tissue or cell type to another through apoE receptors and proteins associated with lipid

transfer and lipolysis (Mahley, 1988; Mahley and Rall, 2000). ApoE isoform-specific associations with lipoprotein particles in the plasma and uptake of apoE lipoprotein complexes through LDL receptors have significant effects on lipid metabolism, having important implications in diseases like Type III Hyperlipoproteinemia (HLP) (Ruiz et al., 2005), atherosclerosis, and diseases of the CNS. ApoE2 is defective in low density lipoprotein receptor (LDLR) binding, delaying the clearance of remnant lipoproteins (β-very low density lipoproteins (VLDL) and increasing cholesterol and triglycerides in plasma. *APOE* ε2 homozygous individuals have defective lipid clearance and, along with other genetic and environmental factors, possession of *APOE* ε2 contributes to the development of Type III HLP (Mahley et al., 1999). ApoE4 preferentially associates with VLDL in plasma and may have a differential effect on VLDL and remnant lipid clearance and LDL receptor expression (Gregg et al., 1986). Most *APOE* ε4 homozygous individuals have increased plasma LDL cholesterol levels, which serves as a risk factor for atherosclerosis (Gregg et al., 1986; Mahley and Rall, 2000).

Structural studies, including X-ray crystallography and site-directed mutagenesis studies, have suggested a model in which arginine-61 extends out from the four-helix bundle of apoE4, forming a putative salt bridge with glutamic acid-255 (Hatters et al., 2006). In apoE2 and apoE3, however, arginine-61 has been predicted to not interact with glutamic acid-255 (Hatters et al., 2006). The spatial proximity of the two domains of apoE were probed using fluorescence resonance energy transfer (FRET) and electron paramagnetic resonance spectroscopy (EPR), revealing that the two domains are closer in both lipid-free and lipid-bound apoE4 than in apoE3, supporting the concept of "domain interaction" (Hatters et al., 2005). Based on this concept, it has been suggested that the

putative salt bridge between the two domains in apoE4 results in an altered conformation that changes the lipid binding preference from plasma HDL to VLDL. Although FRET and EPR experiments have suggested a domain interaction solely for apoE4 (Hatters et al., 2005), NMR studies with monomeric apoE3 have suggested that domain-domain interaction may also exist in lipid-free or partially lipidated apoE3 (Chen et al., 2011; Garai et al.; Zhang et al., 2008; Zhang et al., 2007). Structural studies with reconstituted phospholipids containing apoE3 and apoE4 have yielded conflicting results in terms of the isoform-specific differences in how apoE is arranged in the lipid milieu (Hatters et al., 2006; Schneeweis et al., 2005). However, the dynamic nature of apoE-lipid interactions may generate multiple protein conformational states, making it challenging to interpret how these states may influence physiological function. New approaches are needed to assess apoE structure, the role of domain interaction, and its functional consequences in diseases both of the periphery and the CNS.

In the brain, apoE is mostly produced by astrocytes, followed by microglia and, under certain conditions, by neurons (Kim et al., 2009a). In the CSF, apoE is associated predominantly with cholesterol and phospholipid-rich, high-density lipoprotein (HDL)-like complexes. Unlike plasma, CSF exclusively contains HDL-like lipoproteins and no LDL or VLDL. ApoE's association with HDL-like particles in the CSF occurs without any known isoform specificity (Bandaru et al., 2009; LaDu et al., 1998; Pitas et al., 1987). ApoE4 is likely less stable than apoE2 or apoE3 in vitro as it loses its structure in lower concentrations of chaotropic agents and at lower temperatures, suggesting an altered conformational organization. This observation is consistent with reports of lower

apoE4 protein levels in the brains of *APOE*4 knockin mice despite no differences in transcription across isoforms (Bales et al., 2009; Fryer et al., 2005a; Riddell et al., 2008).

Aβ-dependent roles of apoE in AD: human studies

In vitro and in vivo animal experiments suggest that the accumulation of Aβ in the brain is the initial driving force for AD pathogenesis (Hardy and Selkoe, 2002). While the mechanism by which apoE isoforms affect AD risk is not entirely understood, there is strong evidence that apoE differentially modulates Aβ metabolism (Verghese et al., 2011). Extracellular amyloid plaques represent a major pathological hallmark of the disease. ApoE is present in Aβ plaques in postmortem tissue from AD patients (Strittmatter and Roses, 1996). Several studies have observed an increase in senile and neuritic plaques in *APOE ε*4 homozygous AD patients compared to *APOE ε*4/*ε3* or *APOE ε3* homozygous AD patients (Hyman et al., 1995), although others found no significant effect on plaque density or number (Hyman et al., 1995; Kim et al., 2009a). In a large cohort study in Caucasian, autopsy-confirmed AD patients, it was observed that the presence of both *APOE ε*4 alleles is a crucial factor for increasing neuritic plaque accumulation in all neocortical areas of brain. *APOE ε2* individuals with AD had reduced plaque accumulation, though the sample size was very small (Tiraboschi et al., 2004). Perhaps most relevant in understanding how *APOE* status influences AD risk is how it influences AD pathology in relation to the time course of disease onset. Converging evidence suggests that the initial pathological feature of AD is Aβ deposition in the brain, which is estimated to begin 10-15 years prior to the onset of any clinical signs and symptoms of cognitive decline (Perrin et al., 2009). A variety of events appear

downstream of Aβ deposition in the AD pathological process, including neurofibrillary tangle formation, neuroinflammation, and neuronal/synaptic loss. If *APOE* genotype is linked to AD risk by influencing the probability of onset of Aβ accumulation, one would predict that cognitively normal individuals at any given age would exhibit brain amyloid plaque burden in the following order: *ε4 > ε3> ε2*. In fact, in both CSF biomarker and amyloid neuroimaging studies, apoE isoform-specific brain Aβ pathology (*ε4 > ε3> ε2)* has been reported in cognitively normal individuals aged 45-90 (Morris et al., 2010; Reiman et al., 2009; Sunderland et al., 2004). These data suggest that *APOE* modulates AD risk by affecting the likelihood that Aβ begins to deposit such that the timing of Aβ accumulation is shifted earlier or later in the preclinical phase depending on *APOE* status (Verghese et al., 2011). Given the clear effect of *APOE ε*4 in modulating AD risk and Aβ pathology, a major hypothesis for which there is emerging evidence is that apoE4 increases Aβ aggregation and/or impairs Aβ clearance relative to other apoE isoforms.

Aβ-dependent roles of apoE in AD: in vitro & animal studies

Once the link between apoE isoform and AD risk had been described, several groups focused on characterizing the putative interaction between apoE and Aβ and the extent to which this interaction influenced the aggregation of Aβ in vitro. These studies revealed apoE isoform-specific differences in Aβ binding, with most studies reporting that lipidated apoE2 and apoE3 bind Aβ more strongly than lipidated apoE4 (Aleshkov et al., 1997; LaDu et al., 1994; Yang et al., 1997). Consistent with the increased amyloid plaque load reported in *APOE ε*4 individuals, several groups have reported that apoE4 is more efficient in increasing Aβ fibrillization in vitro relative to apoE3 or apoE2 (Castano

et al., 1995; Ma et al., 1994; Wisniewski et al., 1994); however, others have reported that human apoE isoforms may inhibit the process of Aβ aggregation (Beffert and Poirier, 1998; Evans et al., 1995; Wood et al., 1996). However, due to differences in the preparations of apoE and Aβ used in these studies, a consensus as to the precise biochemical nature of the physical interaction between apoE and Aβ, and the extent to which it influences aggregation, has yet to be reached. To investigate human apoE's role in Aβ aggregation and clearance and how these interactions modulate the disease process, work has focused on generating and analyzing mouse models of β-amyloidosis that express human apoE isoforms using a variety of genetic approaches.

Following the demonstration that murine apoE greatly facilitates amyloid formation in neuritic plaques and CAA (Bales et al., 1997; Holtzman et al., 2000b), several groups created lines of mice expressing human apoE transgenes in order to understand the role of human apoE in Aβ accumulation in vivo. One series of studies demonstrated that GFAP-driven expression of human apoE isoforms in PDAPP mice on an apoE null background results in an apoE isoform-dependent pattern of Aβ deposition and amyloid burden in the hippocampus (E4 > E3) (Fagan et al., 2002; Holtzman et al., 2000a). Consistent with these findings, lentiviral-mediated delivery of apoE4 in the brains of PDAPP mice on an apoE null background increased insoluble levels of parenchymal Aβ42 (Dodart et al., 2005). To further examine the effect of human apoE on Aβ accumulation, mice were engineered to express human apoE isoforms under the control of mouse regulatory elements (*APOE* knockin mice) and then crossbred with Tg2576 or PDAPP mice. In Tg2576 mice, apoE4 increased Aβ deposition and CAA relative to apoE3 (Fryer et al., 2005b); in PDAPP mice, human apoE resulted in a clear

isoform-dependent pattern of Aβ accumulation, i.e., E4> E3> E2 (Bales et al., 2009). One hypothesis to explain the higher amyloid plaque load in individuals expressing *APOE* ε4 is that apoE4 impairs the clearance of Aβ from a pool where it is likely to aggregate in the brain, leading to aberrant accumulation. It was recently demonstrated in mice that complexes of lipidated apoE4 and Aβ were transported across the blood-brain barrier more slowly than apoE3-Aβ or apoE2-Aβ complexes (Deane et al., 2008). However, in the context of endogenous production of apoE and Aβ within the mouse brain, the possibility that human apoE clears Aβ in an apoE isoform-dependent manner remains critically untested. Although several in vitro studies have attempted to clarify the role of human apoE isoforms in modulating Aβ uptake (Jiang et al., 2008), additional in vivo studies are needed to probe the question in the context of all possible clearance routes. Additionally, the possible role of human apoE in directly modulating Aβ aggregation remains a challenging, yet critical untested question in vivo.

A number of human studies have sought to test whether apoE protein concentration may be associated with AD (Kim et al., 2009a). Given apoE's role in facilitating amyloid formation, the concentration of human apoE may represent an important aspect of AD pathogenesis. Due perhaps to inherent limitations in postmortem analysis and sample heterogeneity, studies assessing differences in apoE concentration in the brain parenchyma from patients have been conflicting (Beffert et al., 1999; Bray et al., 2004; Growdon et al., 1999; Harr et al., 1996). A recent study demonstrated that the concentration of apoE in the brain parenchyma of *APOE* ε4 carriers was not statistically different from non-carriers of the *APOE* ε4 allele (Sullivan et al., 2009). There is relative consensus, however, among studies analyzing apoE levels in mice expressing human

apoE isoforms. Most groups report that while the transcription of apoE does not vary across isoforms (Bales et al., 2009), apoE protein concentration among isoforms differs significantly, i.e., E2 >> E3 > E4 (Bales et al., 2009; Fryer et al., 2005b; Riddell et al., 2008); a recent study, however, did not observe isoform-dependent differences in apoE concentration (Korwek et al., 2009). Intrinsic differences in the structure of apoE isoforms may alter the stability of apoE isoforms, thus influencing apoE concentration, as suggested for apoE4 in a recent in vitro study (Riddell et al., 2008). Additional studies are needed to understand whether isoform-dependent differences in apoE concentration account for the effect of *APOE* on Aβ accumulation; alternatively, concentration-independent differences among the isoforms may also account for the effect of *APOE* on Aβ accumulation.

ApoE receptors and the interaction with Aβ metabolism

Based on the interaction between apoE and Aβ, the role of apoE receptors in modulating Aβ metabolism has been an area of active research in the past decade. Brown and Goldstein, in work that earned them the Nobel Prize in Medicine, showed that the low-density lipoprotein receptor (LDLR) endocytoses lipoprotein particles containing apoB or apoE, in a process known as receptor-mediated endocytosis (Brown and Goldstein, 1986). The LDL receptor family consists of a class of receptors of varied function that includes LDLR, LDLR-related protein 1 (LRP1), LRP1B, megalin, very low-density lipoprotein receptor (VLDLR), apoE receptor 2 (apoER2), sorting protein-related receptor (sorLA), among others (Bu, 2009). An early study assessed whether members of the LDLR family regulate apoE and Aβ metabolism in the CNS, finding that

mice lacking an LDLR-stabilizing protein known as receptor-associated protein (RAP) had lower levels of LDLR and LRP1 in the brain in addition to increased Aβ accumulation (Van Uden et al., 2002). LRP1 has been shown to interact with APP to modulate its trafficking and subsequent processing to Aβ (Cam et al., 2005; Kinoshita et al., 2001; Trommsdorff et al., 1998; Ulery et al., 2000). Although soluble Aβ levels were increased when an LRP1 minireceptor was overexpressed in the PDAPP mouse model of β-amyloidosis, no differences in amyloid plaque load were observed between PDAPP mice and PDAPP mice overexpressing LRP1 (Zerbinatti et al., 2004). Furthermore, several subsequent studies suggested a role for LRP1 in cellular-mediated Aβ42 clearance (Fuentealba et al., 2010; Zerbinatti et al., 2006) as well as blood-brain barrier-mediated clearance of radiolabeled Aβ (Bell et al., 2007; Deane et al., 2004). Both ApoER2 and VLDLR have been demonstrated to regulate neuronal migration during brain development via reelin signaling (Herz and Chen, 2006); recently, apoE4 was demonstrated in vitro to interfere with the ability of apoER2 to modulate synaptic activity via reelin signaling (Chen et al., 2010). A role for VLDLR has recently been suggested in mediating blood-brain barrier-mediated apoE/Aβ complex clearance in an apoE isoform-dependent manner (Deane et al., 2008).

Although many roles for LRP1 in APP/Aβ metabolism have been characterized, the potential roles of LDLR in Aβ metabolism have not been thoroughly investigated. Utilizing mice expressing human apoE isoforms but in the context of LDLR deletion, Fryer and colleagues revealed that LDLR is a major receptor for apoE in the CNS (Fryer et al., 2005a). In contrast to apoE3 and apoE4, which were elevated by 2- to 3-fold with LDLR deletion, apoE2 was unchanged in the absence of LDLR. This result is consistent

with the poor reported affinity of apoE2 for LDLR (1-2%) compared to the other isoforms of apoE (Knouff et al., 2004; Weisgraber, 1994; Yamamoto et al., 2008). Furthermore, when LDLR is deleted in PDAPP mice, murine apoE levels were significantly increased, while there was a trend towards an increase in Aβ deposition at 10 months of age compared to PDAPP mice expressing LDLR (Fryer et al., 2005a). Using the Tg2576 mouse model of β-amyloidosis, a subsequent study revealed that LDLR deletion increased Aβ deposition (Cao et al., 2006). Based on these studies, further investigation is needed to assess the role of LDLR in Aβ clearance and accumulation in vivo. Another important area to be explored is the extent to which different components of Aβ clearance pathways may be involved in the regulation of Aβ metabolism, for example, the blood-brain barrier, which could have important implications for targeting apoE receptors therapeutically.

Chapter 2.

Overexpression of low-density lipoprotein receptor in the brain markedly inhibits amyloid deposition and increases extracellular Aβ clearance

PREFACE

The following work was published in *Neuron* in December, 2009. Jungsu Kim (primary author) performed the study with experimental assistance from Hong Jiang, Jacob Basak, Maia Parsadanian, Stephanie Mason, Vi Pham. Joseph Castellano performed and designed in vivo microdialysis experiments and wrote the corresponding sections for the manuscript. Steven Paul contributed valuable reagents for the study.

ABSTRACT

Apolipoprotein E (APOE) is the strongest genetic risk factor for Alzheimer's disease (AD). Previous studies suggest that the effect of apoE on amyloid-β (Aβ) accumulation plays a major role in AD pathogenesis. Therefore, understanding proteins that control apoE metabolism may provide new targets for regulating Aβ levels. LDLR, a member of the LDL receptor family, binds to apoE, yet its potential role in AD pathogenesis remains unclear. We hypothesized that LDLR overexpression in the brain would decrease apoE levels, enhance Aβ clearance and decrease Aβ deposition. To test our hypothesis, we created several transgenic mice that overexpress LDLR in the brain and found that apoE levels in these mice decreased by 50–90%. Furthermore, LDLR overexpression dramatically reduced Aβ aggregation and enhanced Aβ clearance from the brain extracellular space. Plaque-associated neuroinflammatory responses were attenuated in LDLR transgenic mice. These findings suggest that increasing LDLR levels may represent a novel AD treatment strategy.

INITRODUCTION

Accumulation of the amyloid β peptide (Aβ) in the brain is hypothesized to trigger pathogenic cascades that eventually lead to Alzheimer's disease (AD) (Hardy, 2006). Therefore, strategies modulating production, clearance, and aggregation of Aβ are actively being pursued as disease modifying therapies in AD (Golde, 2006). Aβ peptides are generated by the sequential proteolytic processing of amyloid β precursor protein (APP) by the β- and γ-secretase (Cole and Vassar, 2007; Sisodia and St George-Hyslop, 2002; Steiner and Haass, 2000). Extensive genetic research on familial AD (FAD) led to the identification of mutations in the APP, presenilin 1 (PSEN1) and presenilin 2 (PSEN2) genes and provided strong support for the critical role of Aβ accumulation in AD pathogenesis (Hardy, 2006). Many research groups have utilized this genetic information to develop transgenic mouse models that recapitulate key pathological phenotypes of AD. These transgenic mice models have been useful in understanding the etiology of AD and for testing potential therapeutic approaches for preventing Aβ-dependent pathologies. Although mutations in FAD-liked genes are known to cause rare forms of FAD, the ε4 allele of apolipoprotein E (*APOE*) is the only firmly established genetic risk factor for more common forms of AD (Bertram et al., 2007b). ApoE functions as a ligand in the receptor-mediated endocytosis of lipoprotein particles (Kim et al., 2009a). After apoE binds to low density lipoprotein (LDL) receptor family members, the ligand-receptor complex is taken up by clathrin-mediated endocytosis and dissociated in endosomes. Upon dissociation, the apoE receptor recycles back to the cell surface, whereas the apoE-containing lipoprotein particle is targeted to the lysosome wherein cholesterol becomes available for cellular needs. Although it is not completely clear how

apoE influences the various pathogenic processes implicated in AD, several lines of evidence suggest that the effects of apoE on Aβ aggregation and clearance play a major role in AD pathogenesis (Kim et al., 2009a). Previous studies demonstrated that the absence of apoE leads to a dramatic decrease in the levels of fibrillar Aβ deposits in APP transgenic mouse models (Bales et al., 1999; Bales et al., 1997; Holtzman et al., 2000a; Holtzman et al., 2000b). Furthermore, recent studies strongly suggest that apoE regulates both extracellular and intracellular Aβ clearance in the brain (Bell et al., 2007; Deane et al., 2008; DeMattos et al., 2004; Jiang et al., 2008). Therefore, modulating the function of proteins that control apoE metabolism in the brain will likely alter the extent of amyloid deposition and ultimately affect the disease process. In support of this possibility, it was recently demonstrated that ATP-binding cassette transporter A1 (ABCA1)-mediated lipidation of apoE modulates amyloid plaque formation (Hirsch-Reinshagen et al., 2005; Koldamova et al., 2005; Wahrle et al., 2005; Wahrle et al., 2008). Consequently, further insight into how apoE levels can be regulated in the brain may lead to novel therapeutic avenues for the prevention and treatment of AD.

ApoE binds to a group of structurally related proteins known as the low density lipoprotein receptor (LDLR) family. This family includes LDLR, lipoprotein receptor-related protein 1 (LRP1), lipoprotein receptor with 11 binding repeats (LR11), apolipoprotein receptor 2 (ApoER2), very low density lipoprotein receptor (VLDLR) and others (Herz and Bock, 2002). They share several common structural characteristics, such as complement-type ligand binding repeats, β-propeller domain, and epidermal growth factor type repeats. The prototype of this family member is LDLR, which has been extensively studied in the peripheral tissues for its role in mediating the removal of

cholesterol and cholesteryl ester from the circulation (Brown and Goldstein, 1986). Genetic defects in LDLR lead to an impaired lipoprotein clearance from the bloodstream and massive accumulation of cholesterol in the circulation, resulting in familial hypercholesterolemia. Due to its critical role in the metabolism of apoB-containing LDL particles, LDLR has been the focus of much attention in better understating the pathogenesis of atherosclerosis and coronary heart disease (Soutar and Naoumova, 2007). However, the physiological and pathological function of LDLR in the nervous system remains unclear. In contrast, the roles of other LDL receptor family members in brain development and synaptic plasticity are better understood (Herz, 2009). Furthermore, the modulatory effects of other LDL receptors on Aβ clearance and APP trafficking have been thoroughly examined in cellular and animal model systems (Cam and Bu, 2006). However, the potential role of LDLR in AD pathogenesis has not been studied extensively. To address this issue, we created several transgenic mouse lines that overexpress LDLR in the brain and bred two transgenic lines with the APPswe/PSEN1ΔE9 (APP/PS1) transgenic mouse model (Jankowsky et al., 2004). The effects of LDLR overexpression on Aβ accumulation and its clearance from the brain interstitial fluid (ISF) were investigated.

RESULTS

Generation and Characterization of LDLR Transgenic Mice

In order to achieve widespread expression of the LDLR transgene in the brain, we created a construct using the mouse prion promoter (Borchelt et al., 1996). Six transgenic founders with LDLR transgene were generated and maintained on a B6/CBA background. One transgenic line transmitted the LDLR transgene only in males and did not have any detectable transgene expression in the brain. The five remaining transgenic lines were screened for LDLR overexpression by western blotting (Figure 1A). As expected, multiple bands of LDLR proteins were detected due to extensive posttranslational modifications (Filipovic, 1989). Two to eleven fold increases in LDLR protein levels, relative to non-transgenic (NTG) mice, were detected in the various founder lines (Figure 1A). The high-expressing B line and low-expressing E line were selected for further experiments. To characterize the regional expression pattern of the LDLR transgene, brain sections were immunostained using an anti-hemagglutinin (HA) antibody for the detection of the HA tag placed in the amino-terminal region of the LDLR sequence. As expected, the immunostaining pattern with anti-HA antibody overlapped very well with that of anti-LDLR antibody staining (Figure S1). Transgene expression, analyzed by anti-HA antibody, was detected in cortex, hippocampus, and cerebellum (Figure 1B–1D). Double immunofluorescence staining with anti-NeuN, a neuron-specific marker, and anti-HA antibody demonstrated that most neurons expressed LDLR from the transgene (Figure 1E). To further examine which cell types express the transgene, primary neurons or astrocytes were cultured from LDLR transgenic line B mice. LDLR expression was analyzed with anti-LDLR antibody or anti-HA antibody

(Figure 1F–1G). Higher levels of LDLR protein were detected in both neurons and astrocytes. This expression pattern is consistent with a previous study characterizing the prion promoter expression vector (Borchelt et al., 1996).

To analyze the functional effect of LDLR overexpression in the brain, the levels of apoE protein in the brain was analyzed by apoE enzyme-linked immunosorbent assay (ELISA). Since LDLR is one of the major apoE endocytic receptors in the brain (Fryer et al., 2005a), we expected that LDLR overexpression would lead to a reduction in apoE protein levels through enhanced receptor-mediated endocytosis. There was a significant decrease in apoE protein levels in all five lines, ranging from 50 to 90%, compared to NTG littermates (Figure 2A). Interestingly, only two-fold overexpression in LDLR transgenic line E mice was sufficient to decrease apoE levels by ~50% in the brain. Overexpression of LDLR by more than five-fold, relative to NTG mice, led to 80–90% reduction in apoE levels. We also analyzed apoE mRNA levels by quantitative RT-PCR. There were no significant differences in apoE mRNA levels between LDLR transgenic lines B (> 10-fold overexpression) and E (2-fold overexpression) and their NTG littermates (Figure S2). This suggests that the higher levels of LDLR in the transgenic mice facilitate apoE endocytosis from the extracellular space, leading to a decrease in the amount of extracellular apoE. The higher levels of LDLR in the transgenic mice may facilitate apoE endocytosis from the extracellular space, leading to a decrease in the amount of extracellular apoE.

LDLR Overexpression Decreases ApoE Levels Even in the Presence of APPswe and PSEN1ΔE9 Overexpression

A recent study demonstrated that the APP intracellular domain may increase apoE protein levels by suppressing the transcription of LRP1, another major apoE receptor in the brain (Liu et al., 2007). Furthermore, altered γ-secretase activity by a PSEN1ΔE9 mutation has been shown to increase apoE protein levels by interfering with the endocytosis of LDLR (Tamboli et al., 2008). Therefore, we evaluated the possibility that overexpression of APP and PSEN1ΔE9 in APP/PS1 transgenic mice used in our study might attenuate the effect of LDLR overexpression on apoE levels. To determine whether LDLR overexpression still has a functional effect on apoE protein in the presence of the APP and PSEN1E9 transgenes, soluble apoE levels were analyzed from APP/PS1/LDLR and APP/PS1 transgenic mice at 2.5 months of age. ApoE levels in cortical and hippocampal tissues from LDLR line B transgenic mice were significantly decreased by ~90%, compared with NTG mice (Figure 2B). In the low-expressing line E transgenic mice, there was a 55–60% reduction of apoE protein levels in both cortex and hippocampus (Figure 2C). The effect size of LDLR overexpression on apoE protein levels was not different in the absence (Figure 2A) or presence (Figure 2B and 2C) of APP and PSEN1ΔE9 overexpression. Taken together, these results strongly suggest that overexpression of APP and PSEN1ΔE9 does not interfere with the function of LDLR in our transgenic mice. In addition to the strong effect of the LDLR transgene on apoE levels, there was also a sex difference in apoE protein levels. In the absence of LDLR transgene overexpression, male APP/PS1 mice had 10–20% less apoE protein in the cortex and hippocampus compared with female littermates ($p=0.05$ and $p=0.06$ for B line

Ctx and Hip, respectively, p=0.02 and p=0.0008 for E line Ctx and Hip, respectively) (Figure 2B and 2C). The difference in apoE protein levels between female and male mice was unlikely due to differences in endogenous LDLR protein levels, since LDLR levels were not significantly different between female and male APP/PS1 mice (Figure S3C). Previous studies suggest that there may be functional redundancy among LDL receptor family members (Mahley and Ji, 1999; Wouters et al., 2005). Apolipoprotein J (ApoJ) and ApoE are the two most abundant apolipoproteins in the brain. ApoJ, also known as clusterin, has been shown to facilitate fibrillar amyloid plaque formation (DeMattos et al., 2002b). To determine whether LDLR overexpression had a selective effect on apoE, we assessed apoJ protein levels by western blot analysis. No significant difference in the levels of apoJ was found between LDLR transgenic and NTG mice (Figure S3B). This finding suggests that even more than 10-fold overexpression of LDLR does not affect the metabolism of a similar apolipoprotein.

Strong LDLR Overexpression Leads to Marked Decreases in Amyloid Deposition

Previous studies demonstrated that the lack of apoE led to a dramatic decrease of amyloid deposition in APP transgenic mouse models (Bales et al., 1997; Holtzman et al., 2000b). Given the critical role of apoE in Aβ deposition, we hypothesized that the reduction of extracellular apoE levels by LDLR overexpression may lead to a decrease in Aβ accumulation. To determine whether LDLR overexpression affects Aβ accumulation and deposition, the high-expressing LDLR transgenic line B mice were bred with APP/PS1 transgenic mice. The extent of Aβ deposition was analyzed by histochemical and biochemical methods. Brain sections from 7 month old APP/PS1 mice (Figure 3A and 3C) and APP/PS1/LDLR mice (Figure 3B and 3D) were immunostained with

biotinylated-3D6 antibody (anti-Aβ 1–5). In our preliminary studies with APP/PS1 transgenic mice, there was a significant difference in amyloid plaque load between female and male mice. Therefore, we planned to analyze the extent of Aβ accumulation by sex in this study. In the absence of LDLR overexpression, male APP/PS1 mice had a 50–60% decrease in amyloid plaque load, compared with female APP/PS1 littermates ($p=0.0087$ and $p=0.0022$ for Ctx and Hip, respectively) (Figure 3E). Quantitative analyses of anti-Aβ immunostaining demonstrated that amyloid plaque loads in the cortex and hippocampus were markedly decreased in APP/PS1/LDLR transgenic mice compared with APP/PS1 mice (Figure 3E). The inhibitory effects of LDLR overexpression on Aβ accumulation were observed in both female and male mice. To further characterize the nature of the deposited plaques, brain sections were subsequently stained with X-34 dye that detects fibrillar amyloid deposits. In line with the results from Aβ immunostaining (Figure 3E), there were strong sex differences in fibrillar amyloid deposition. Female APP/PS1 mice deposited significantly more fibrillar plaques than did male APP/PS1 littermates ($p=0.0234$ and $p=0.0087$ for Ctx and Hip, respectively) (Figure 3F). Importantly, APP/PS1/LDLR transgenic mice exhibited a dramatic 40–70% decrease in the X-34 positive fibrillar plaque load in the cortex and hippocampus, compared with sex-matched APP/PS1 mice (Figure 3F). Consistent with the histochemical analyses, biochemical analyses of Aβ levels demonstrated a 50–75% reduction in insoluble Aβ40 levels (Figure 4A) and a 45–70% reduction in insoluble Aβ42 levels in the cortex and hippocampus of APP/PS1/LDLR transgenic mice (Figure 4B). Taken together, our results from high-expressing LDLR transgenic line B mice demonstrate that 10-fold LDLR overexpression markedly decreases Aβ accumulation and amyloid deposition.

Two-fold Overexpression of LDLR is Sufficient to Inhibit Amyloid Formation

To determine whether lower levels of LDLR overexpression would also have a protective effect against Aβ accumulation and deposition, LDLR transgenic line E mice that overexpress LDLR by approximately 2-fold were bred to APP/PS1 transgenic mice. Levels of Aβ accumulation were analyzed by anti-Aβ immunohistochemistry and X-34 staining (Figures 5A and 5B). Amyloid plaque loads in the cortex and hippocampus were markedly lower in female APP/PS1/LDLR transgenic mice, compared with female APP/PS1 mice (Figure 5C). In addition, female APP/PS1/LDLR mice had a 50–55% decrease in fibrillar plaque load in the cortex and hippocampus (Figure 5D). In line with the histochemical findings, biochemical measurement of Aβ levels demonstrated a 30–55% reduction in total (soluble plus insoluble) Aβ40 levels and an approximately 35% reduction in total Aβ42 levels in the cortex and hippocampus of APP/PS1/LDLR transgenic mice (Table S1). In contrast to the effects in females, there was no significant difference between plaque load or Aβ levels in male APP/PS1 versus APP/PS1/LDLR transgenic mice from line E. Collectively, these findings strongly suggest that even a small increase of LDLR protein levels can be effective in preventing Aβ accumulation in female mice (Figure 5C and 5D).

Attenuation of Neuroinflammatory Responses in APP/PS1/LDLR Transgenic Mice

Abnormal activation of microglia and astrocytes is observed in the brains of AD patients and transgenic mouse models of amyloidosis (Wyss-Coray, 2006). Previous studies suggest that fibrillar amyloid plaques may trigger neuroinflammatory cascades (Meyer-Luehmann et al., 2008). To quantitatively examine the extent of gliosis, we established a

semi-automated imaging processing method and assessed the activation of microglia by using CD11b (Figure 6A and 6B) and CD45 (Figure 6D and 6E) as markers. There was an ~70% decrease in the CD11b-positive activated microglial load in APP/PS1/LDLR line B transgenic mice, compared with APP/PS1 littermates (Figure 6C). Similarly, analysis of CD45-positive microglia indicated an ~80% reduction in area covered by activated microglia in LDLR transgenic mice (Figure 6F). In addition, brain sections were stained with anti-glial fibrillary acidic protein (GFAP) antibody to quantify the extent of astrogliosis (Figure 6G and 6H). Clusters of activated astrocytes were often associated with amyloid plaques (Figure S4A). APP/PS1/LDLR transgenic mice had ~45% less GFAP load in cortex, compared with APP/PS1 littermates (Figure 6I). The extent of microgliosis and astrogliosis were correlated very well with the amount of compact fibrillar plaques detected with the X-34 dye (Figure S4B–S4D). These findings demonstrate that the reduction of fibrillar plaque formation by LDLR overexpression is closely associated with the decreased activation of microglia and astrocytes.

LDLR Overexpression Decreases Steady-state ISF eAβ Levels in Young Mice and Increases the Elimination of eAβ from the ISF

We reasoned that the marked reduction in Aβ deposition in mice overexpressing LDLR may be the result of altered soluble Aβ metabolism early in life in the extracellular space of the brain where it is prone to aggregate (Meyer-Luehmann et al., 2003). To assess this possibility, we performed in vivo microdialysis in APP/PS1/LDLR line B transgenic mice and APP/PS1 littermates prior to the onset of amyloid deposition to compare levels of soluble Aβ in the hippocampal ISF. Soluble ISF Aβ exchangeable across a 38kDa dialysis membrane (eAβ) has previously been shown to be tightly correlated with the

levels of total soluble Aβ present in extracellular pools of the brain (Cirrito et al., 2003). Theoretically, the actual in vivo steady state concentration of an analyte being dialyzed exists at the point at which there is no flow of the perfusion buffer (Menacherry et al., 1992). To obtain this value, we varied the flow rate of the perfusion buffer from 0.3μL/min to 1.6μL/min during microdialysis in the hippocampus of young APP/PS1/LDLR and APP/PS1 mice (Figure 7A1). After extrapolating back to the point of zero flow for each mouse, we found that the mean steady state concentration of ISF eAβ1-x was significantly lower in APP/PS1/LDLR mice compared to mice expressing normal levels of LDLR (Figure 7A2). This difference was not due to differential recovery of eAβ by the probe between groups at any of the flow rates tested (Figure S5). Since the extent of Aβ deposition observed in Figure 3 was found to depend on the sex of the mice analyzed, we stratified microdialysis experiments in the same way. We found that both male and female APP/PS1 mice overexpressing LDLR had lower steady state ISF eAβ1-x levels compared to their sex-matched APP/PS1 counterparts (Figure 7A3). Though we did not observe a similar change in Aβ levels as assessed by conventional biochemical means (Table S2), it is likely that the Aβ sampled during in vivo microdialysis more closely reflects the extracellular pool than total Aβ measured from tissue homogenates.

Given that LDLR overexpression did not appear to alter APP processing (Figure S3B), and based on our previous finding that apoE decreased the elimination rate of soluble Aβ from the ISF (DeMattos et al., 2004), we hypothesized that the lower steady state concentration of eAβ in APP/PS1/LDLR mice is likely the result of increased elimination from the brain ISF (Deane et al., 2008; DeMattos et al., 2004). To test this hypothesis, we injected young APP/PS1 and APP/PS1/LDLR mice intraperitoneally with

a potent γ-secretase inhibitor in order to halt Aβ production, thus allowing sensitive measurement of the elimination rate of eAβ from the ISF, as previously described (Figures 7B1 and 7B2) (Cirrito et al., 2003; DeMattos et al., 2004). The half-life of elimination from the ISF for eAβ1-x was decreased by about two-fold in APP/PS1/LDLR mice compared to that measured in APP/PS1 mice (Figure 7B3). The increase of eAβ elimination in LDLR transgenic mice was observed in both males and females (Figure 7B4). Taken together, these results demonstrate that increasing expression of LDLR promotes the elimination of soluble Aβ from the ISF, leading to lower levels of the peptide in the hippocampal extracellular space. It is likely that the enhanced Aβ elimination from the ISF early in the life of the mice underlies the resulting strong decrease in Aβ accumulation and its consequences such as inflammation that progress with age.

DISCUSSION

In the current study, we hypothesized that overexpression of LDLR in the brain would decrease brain apoE protein levels, subsequently decreasing amyloid deposition. To test this hypothesis, we created several transgenic mouse lines that overexpress LDLR in the brain and then bred them with APP/PS1 transgenic mice. Brain apoE levels in LDLR transgenic mice were decreased by 50–90% in a dose-dependent manner. Most importantly, LDLR overexpression led to dramatic reductions in Aβ aggregation and neuroinflammatory responses. In addition, increasing expression of LDLR facilitated the elimination of soluble Aβ from the ISF, leading to lower levels of Aβ in the hippocampal extracellular space. This result strongly suggests that LDLR enhances brain Aβ clearance, serving as an important pathway that modulates Aβ metabolism. Overall, the results suggest that LDLR may be an attractive therapeutic target for AD.

Although numerous putative susceptibility genes for AD have been reported so far, the strongest genetic risk factor is *APOE* genotype; the ε4 allele is an AD risk factor and the ε2 allele appears to be protective (Bertram et al., 2007b). Given the considerable genetic evidence and the immunoreactivity of apoE in amyloid plaques, the effect of apoE isoforms on Aβ aggregation has been investigated extensively in vitro (Kim et al., 2009a). Later, in vivo studies demonstrated that the lack of apoE led to a dramatic reduction of fibrillar Aβ deposition in APP transgenic mouse models (Bales et al., 1999; Bales et al., 1997; Holtzman et al., 2000a; Holtzman et al., 2000b). Furthermore, apoE has been shown to regulate Aβ clearance in the brain (Bell et al., 2007; Deane et al., 2008; DeMattos et al., 2004; Jiang et al., 2008). These and other findings strongly suggest that the effects of apoE on Aβ aggregation and clearance play a major role in AD

pathogenesis (Kim et al., 2009a). Consequently, modulating the function or levels of proteins that affect apoE metabolism in the brain seems to be a logical therapeutic strategy to alter Aβ-dependent pathogenic processes in AD. Results presented in the current study corroborate the feasibility and efficacy of apoE targeting therapeutics.

ApoE in the periphery is known to bind to several LDL receptor family members. Since the lipid composition and lipidation state of apoE-containing lipoprotein particles are different between brain and peripheral tissues, it would be important to know which LDL receptor members can regulate apoE protein levels in the brain (Kim et al., 2009a). Knockout mouse studies have provided direct evidence for LDLR and LRP1 as major apoE receptors in the brain (Elder et al., 2007; Fryer et al., 2005a; Liu et al., 2007). Fryer et al. also demonstrated that LDLR differentially regulates the levels of human apoE isoforms in the brain through its binding specificity. Zerbinatti et al. generated a LRP1 mini-receptor transgenic mouse model with 3.7-fold increased LRP1 levels in the brain (Zerbinatti et al., 2004). Although an ~25% reduction in brain apoE levels was observed in LRP1 transgenic mice, there was an increase in soluble and insoluble Aβ in old mice (Zerbinatti et al., 2006; Zerbinatti et al., 2004). The reason for the LRP1 mini-receptor overexpression causing an increase in Aβ levels is not entirely clear but is likely due to the effects of LRP1 on APP and not due to its effects on apoE. For example, unlike LDLR, LRP1 is an APP binding protein that influences APP endocytic trafficking and cellular distribution such that processing to Aβ and its extracellular release is enhanced (Pietrzik et al., 2002; Ulery et al., 2000). This effect of LRP1 on APP and Aβ may supersede the effects of the LRP1 minireceptor on decreasing apoE levels by 25% and its effects on Aβ in the brain. In the current study, only 2-fold overexpression of LDLR

protein was sufficient to decrease brain apoE levels and Aβ accumulation by more than 50%. Taken together, these data clearly demonstrate both LDLR and LRP1 regulate apoE protein levels in the brain. However, it is unclear whether other LDL receptor family members, such as LR11, ApoER2, and VLDLR, also efficiently mediate the endocytosis of apoE in the brain. Given the known apoE isoform-specific interactions with LDLR (Kim et al., 2009a), it would be interesting to determine whether the effect of LDLR overexpression differs in APP transgenic mouse models with humanized apoE isoforms. In addition, it will be important to determine the effects of LDLR overexpression on cognitive abnormalities observed in APP/PS1 mice.

Although the effects of LRP1 on Aβ clearance and APP processing have been extensively studied (Cam and Bu, 2006), the potential role of LDLR on AD pathogenesis has been unclear. Several studies reported that a few single-nucleotide polymorphisms (SNPs) in LDLR gene are associated with the risk of developing AD in case-control studies (Cheng et al., 2005; Gopalraj et al., 2005; Retz et al., 2001). However, others could not replicate the earlier studies and a meta-analysis of the previously reported case-control data failed to detect any significant summary odds ratios (Bertram et al., 2007a; Rodriguez et al., 2006). More recent findings suggest that other SNPs may be associated with a risk of AD in a sex-specific manner. SNP rs688 and haplotype GTT were significantly associated with an increased risk of AD in males and females, respectively (Lamsa et al., 2008; Zou et al., 2008). Unlike other studies, both studies also demonstrated functional effects of SNPs on LDLR splicing and Aβ42 levels.

In order to investigate the effect of LDLR deficiency on cholesterol and Aβ in the brain, several groups have analyzed LDLR knockout mice. Although LDLR deficiency

significantly increased murine brain apoE levels by ~50%, it did not alter brain cholesterol levels (Elder et al., 2007; Fryer et al., 2005a; Quan et al., 2003; Taha et al., 2009). Previously, we demonstrated that there was no significant change in brain Aβ levels both before and after the onset of amyloid deposition in PDAPP transgenic mice on a LDLR-deficient background (Fryer et al., 2005a). However, there was a trend for an increase in Aβ accumulation in PDAPP/LDLR knockout mice. Recently, Buxbaum and colleagues also reported that LDLR deficiency did not affect endogenous murine Aβ levels in the brain (Elder et al., 2007). In contrast, lack of LDLR was associated with increased amyloid deposition in Tg2576 mice (Cao et al., 2006).

Prior to our current study, it was unknown whether increased levels of LDLR in the brain would affect Aβ accumulation in vivo, and if so, via what mechanism. Given the role of apoE in Aβ clearance and aggregation, we hypothesized that the reduction of apoE levels by LDLR overexpression would promote the elimination of soluble Aβ from the brain ISF, i.e., via transcytosis across the blood-brain barrier into the plasma or by local cellular uptake and degradation within the brain. We predicted that increased elimination of soluble Aβ through either of these elimination routes would result in decreased Aβ accumulation. Our in vivo microdialysis results suggest that the mechanism by which LDLR overexpression alters Aβ metabolism is to enhance the extracellular clearance of Aβ peptide. It is possible that receptor-mediated clearance of Aβ-ApoE complex or Aβ alone from the brain ISF might be enhanced by LDLR overexpression. Interestingly, other LDL receptor family members, such as LRP1, LR11, and ApoER2, are known to directly or indirectly bind to APP and affect its amyloidogenic processing (Kim et al., 2009a). Since levels of carboxyl-terminal fragments of APP, generated by

APP processing, were not different between genotypes, it is unlikely that LDLR overexpression alters APP processing. Though it is likely that the reduction of apoE protein levels by LDLR overexpression enhanced Aβ clearance (DeMattos et al., 2004), we cannot exclude the possibility that LDLR may directly affect Aβ clearance independent of apoE.

Transgenic mouse models of amyloidosis have been invaluable for investigating AD pathogenic mechanisms and evaluating the efficacy of novel therapeutic targets. Interestingly, female APP/PS1 transgenic mice used in the current study had a more than 2-fold increase in plaque load and insoluble Aβ accumulation, compared with male littermates (Figure 3 and and 4). Our finding is consistent with a recent study that used APP/PS1 mice on a different genetic background (Halford and Russell, 2009). A similar sex-specific amyloid deposition phenotype has been previously reported with other APP transgenic mouse models (Callahan et al., 2001; Wang et al., 2003). The APP/PS1 transgenic mouse used in our study is one of the most commonly used Aβ amyloidosis models. Effects of genetic and pharmacological manipulations on Aβ accumulation and Aβ-related pathological changes have been tested using this model. However, most previous studies did not analyze the extent of Aβ accumulation by sex. It is possible that sex differences were not obviously recognized in other studies due to the limited sample size for each sex. Given the dramatic effect of sex on Aβ aggregation, the sex of APP/PS1 transgenic mice should be carefully considered for the proper interpretation of results. Since the prevalence of AD is higher in women even after adjusting for age and education levels (Andersen et al., 1999), it is intriguing that several mouse models of amyloidosis have similar sex-dependent phenotypes. Several studies suggest that female

hormones may, in part, contribute to sex differences in AD (Carroll et al., 2007; Yue et al., 2005). Given the inconsistent findings among studies, the exact mechanism underlying sex differences in AD pathogenesis requires further investigation. It is possible that the elevated apoE levels in the females APP/PS1 mice is related to why females develop more amyloid deposition (Figure 2). Interestingly, while the clearance of soluble Aβ in APP/PS1 males trended towards being faster than that for APP/PS1 females (Figure 7B4), we cannot rule out that an Aβ clearance-independent mechanism may account for the sex differences in plaque load and insoluble Aβ accumulation in older mice. Understanding the factors that regulate sex-dependent phenotypes may provide additional insight into new therapeutic targets.

Notably, an increase of LDLR protein levels by only ~2-fold was sufficient to decrease Aβ accumulation by ~50% in APP/PS1 female transgenic mice. Our findings suggest that even a small increase in LDLR levels or function in the brain may be exploited as a novel approach for developing AD therapeutics. Due to the critical role of LDLR in the metabolism of apoB-containing LDL particles in the circulation, strategies increasing the function and amount of LDLR protein in the liver have been extensively pursued as promising therapies for atherosclerosis and premature coronary heart disease (Soutar and Naoumova, 2007). Overexpression of LDLR in the liver facilitated LDL elimination by receptor-mediated endocytosis and prevented diet-induced hypercholesterolemia (Hofmann et al., 1988; Yokode et al., 1990). However, the modulation of LDLR function in the brain as a treatment modality for AD has not been previously investigated. Our study clearly demonstrates the beneficial effects of LDLR overexpression in the brain on pathogenic Aβ aggregation and subsequent

neuroinflammatory responses. Although other LDL receptor family members bind to multiple ligands (i.e. LRP1 having more than 20 ligands), there are only two known ligands, apoB and apoE, for LDLR. Since apoB is not expressed in the brain, modulating LDLR function in the brain is likely to target apoE specifically. A couple of recently identified genes are known to regulate LDLR protein levels by affecting the trafficking and degradation of LDLR in peripheral tissues (Soutar and Naoumova, 2007). Since these proteins are also expressed in the brain, their potential roles in the clearance and accumulation of Aβ warrant further investigations. In addition, several compounds have been identified to increase hepatic LDLR protein levels by modulating synthesis or degradation of LDLR and LDLR-regulating proteins. Given our results from transgenic mice overexpressing LDLR in the brain, the therapeutic potential of these lead compounds merit additional testing in animal models of Aβ amyloidosis.

EXPERIMENTAL PROCEDURES

Generation of LDLR Transgenic Mice

Murine LDLR was cloned from RNA isolated from mouse brain using the RNeasy kit (QIAGEN). Random primer RT-PCR was performed using the First Strand cDNA Synthesis Kit (Roche Applied Sciences). The sequence and orientation of the insert was verified by complete sequencing. LDLR cDNA was excised from pcDNA3.1 using XhoI and inserted into the cloning site of the mouse prion promoter vector (Borchelt et al., 1996), a gift from David Borchelt (University of Florida). The Mouse Genetics Core Laboratory at Washington University produced the transgenic mice on a B6/CBA background. Among 6 transgenic founders, 2 lines of LDLR transgenic mice were crossed with APPswe/PSEN1ΔE9 (APP/PS1) transgenic mice (line 85, Stock number 004462, The Jackson Laboratory). APP/PS1 transgenic mice overexpress a chimeric mouse/human APP695 swedish gene and human PSEN1 with an exon 9 deletion (Jankowsky et al., 2004). All comparisons between APP/PS1 transgenic mice with or without an LDLR transgene were littermates on the same genetic background.

Primary Astrocyte Cultures

Cortical primary murine astrocytes were obtained from P2 mouse pups. Cortices were dissected from the brain and placed in Hanks balanced salt solution then treated with trypsin/EDTA. Following trypsin digestion, the tissue was resuspended and triturated in growth media containing DMEM/F12, 20% fetal bovine serum (FBS), 10 ng/ml epidermal growth factor, 100 units/ml penicillin/streptomycin, and 1 mM sodium pyruvate. The cell suspension was then passed through a 100 μm nylon filter and plated

into T75 flasks coated with poly-D-lysine. Once the cells reached confluency, they were shaken at 100 rpm for three hours and the media was aspirated to remove the less adherent microglial cells. The cells were then passaged into 6 well plates for experiments.

Primary Neuron Cultures

Cortical primary murine neurons were obtained from E16 embryos. Cortices were dissected from the brain, cut into small pieces, and placed into HBSS. The tissue was then treated with trypsin/EDTA for 15 min at 37°C. FBS was then added to the tissue, and it was washed with HBSS (without calcium and magnesium). Following the wash steps, the tissue was resuspended in HBSS (-calcium/magnesium) and 500 U/mL of DNase I. The tissue was then triturated and the cells were resuspended in neurobasal medium with 10% FBS. Cells were then counted and plated into 6 well plates. 3 hrs following the plating, the seeding medium was replaced with neurobasal medium containing B27 supplement. To remove contaminating glial cells, a mixture of antimitotics (5-fluoro-2′-deoxyuridine, uridine, and cytosine β-D-arabinofuranoside) was added to the cultures on DIV5. The media was then changed to neurobasal media with B27 on DIV7.

Quantitative Analyses of Amyloid Deposition

Brain hemispheres were placed in 30% sucrose before freezing and cutting on a freezing sliding microtome. Serial coronal sections of the brain at 50 mm intervals were collected from the rostral anterior commisure to caudal hippocampus as landmarks. Sections were stained with biotinylated 3D6 (anti-Aβ1–5) antibody or X-34 dye. Stained brain sections were scanned with a NanoZoomer slide scanner (Hamamatsu Photonics). For quantitative

analyses of 3D6-biotin staining, scanned images were exported with NDP viewer software (Hamamatsu Photonics) and converted to 8-bit grayscale using ACDSee Pro 2 software (ACD Systems). Converted images were thresholded to highlight plaques and then analyzed by "Analyze Particles" function in the ImageJ software (National Institutes of Health) (Kim et al., 2007). Identified objects after thresholding were individually inspected to confirm the object as a plaque or not. X-34 stained sections were quantified following unbiased stereological principles (Cavalieri-point counting method) (Holtzman et al., 2000b). Three brain sections per mouse, each separated by 300 μm, were used for quantification. These sections correspond roughly to sections at Bregma −1.7, −2.0, and −2.3 mm in the mouse brain atlas. The average of 3 sections was used to represent a plaque load for each mouse. For analysis of Aβ plaque in the cortex, the cortex immediately dorsal to the hippocampus was assessed. All analyses were performed in a blinded manner.

Sandwich ELISA for Aβ and ApoE

Cortical and hippocampal tissues were sequentially homogenized with PBS and 5M guanidine buffer in the presence of 1x protease inhibitor mixture (Roche). The levels of Aβ and ApoE were measured by sandwich ELISA. For Aβ ELISA, HJ2 (anti-Aβ35–40) and HJ7.4 (anti-Aβ37–42) were used as capture antibodies and HJ5.1-biotin (anti-Aβ13–28) as the detection antibody. WUE4 (Krul et al., 1988) and anti-ApoE antibody (Calbiochem) were used for apoE ELISA. Pooled C57BL/6J plasma was used as a standard for murine apoE quantification(Fryer et al., 2005a). For in vivo microdialysis experiments, human Aβ1-x from collected fractions was measured using m266 antibody (anti-Aβ13–28) to capture and 3D6-biotinylated antibody (anti-Aβ1–5) to detect.

Quantitative Analyses of Neuroinflammatory Response

Brain sections cut with a freezing sliding microtome were immunostained with anti-CD11b antibody (BD Pharmingen), anti-CD45 antibody (Serotec), and anti-GFAP antibody (Chemicon). The percent area covered by CD11b and CD45 staining was analyzed in the hippocampus by using NDP viewer, ACDSee Pro 2, and NIH Image J softwares, as described above. For GFAP quantification, cortical regions were assessed. The overall area covered by GFAP staining signals was measured with NDP viewer. Three brain sections per mouse, each separated by 300 μm, were used for quantification. The average of 3 sections was used to estimate the area covered by immunoreactivity with each antibody. All analyses were performed in a blinded manner.

Western Blot

Cortical tissues, primary neurons, and astrocytes cultures were sonicated in radioimmunoprecipitation assay (RIPA) buffer (1% NP-40, 1% sodium deoxycholate, 0.1% SDS, 25mM Tris-HCl, 150mM NaCl) or 1% Triton X-100 in the presence of 1x protease inhibitor mixture (Roche). Cortical tissue homogenates were centrifuged at 18,000 rcf for 30 min. Primary cells were spun down at 14,000 rcf for 15 min. Protein concentration in supernatants was determined using the BCA protein assay kit (Pierce). Equal amounts of protein for each sample were run on 3–8% Tris-Acetate or 4–12% Bis-Tris XT gels (Bio-Rad) and transferred to PVDF membranes. Blots were probed for LDLR (Novus, Abcam, and a gift from Dr. Guojun Bu at Washington University), CT22 (Zymed), HA (Covance) and ApoJ (Covance). Normalized band intensity was quantified using NIH ImageJ software (Kim et al., 2007).

In Vivo Microdialysis

In vivo microdialysis in 2.5 month old APP/PS1 and APP/PS1/LDLR (B-line) littermates was performed essentially as described (Cirrito et al., 2003; DeMattos et al., 2004). Briefly, microdialysis using the zero flow extrapolated method was performed with an automated syringe pump (Univentor 864) connected to a laptop using Univentor 300 software. Zero flow data for each mouse were fit with an exponential decay regression as described (Menacherry et al., 1992). For clearance experiments, a stable baseline of ISF eAβ levels was obtained using a constant flow rate of 1.0µl/min before intraperitoneally injecting each mouse with 10 mg/kg of the gamma secretase inhibitor LY411,575 (prepared by dissolving in PBS and propylene glycol). The elimination of eAβ from the ISF followed first -order kinetics; therefore, for each mouse, the elimination half-life for eAβ was calculated using the slope of the linear regression that included all fractions until levels stopped decreasing.

Statistical Analyses

To determine the statistical significance (*$p<0.05$, **$p<0.01$, ***$p<0.001$), two-tailed Student's t-test was used, only if the data sets passed the equal variance test (Levene Median test) and normality test (Kolmogorov-Smirnov test) (SigmaStat 3.0.). When the data set did not meet the assumptions of a parametric test, Mann-Whitney Rank Sum Test was performed. The correlation between gliosis and X-34 plaque load was analyzed with Pearson product moment correlation test (SigmaStat 3.0.). Variability of the measurements was reported as SEM.

SUPPLEMENTARY EXPERIMENTAL PROCEDURES

Quantitative Real-time PCR (qPCR)

Frozen cortical tissues were placed in RNA*later*-ICE frozen tissue transition solution (Ambion) and stored at -20^{o}C. mRNA was extracted using the Dynabeads mRNA DIRECT kit (Invitrogen) and reverse transcribed with High Capacity cDNA Reverse Transcription kit (Applied Biosystems). qPCR was performed with TaqMan Universal PCR Master Mix and 7500 Fast Real-Time PCR system. The forward primer targeting exon 2 was 5'-CAATTGCGAAGATGAAGGCTC-3', and the reverse primer targeting exon 3 was 5'-TAATCCCAGAAGCGGTTCAG-3'. For 5' nucleases hydrolysis probe method, probe ATCAGCTCGAGTGGCAAAGCAAC was labeled with a 5' FAM fluorophore and 3' lowa Black non-fluorescent quencher (Integrated DNA Technologies). TaqMan mouse GAPDH endogenous control (Applied Biosystems) was used as a normalization reference. Relative mRNA levels were calculated by comparative Ct method using the Applied Biosystems 7500 software.

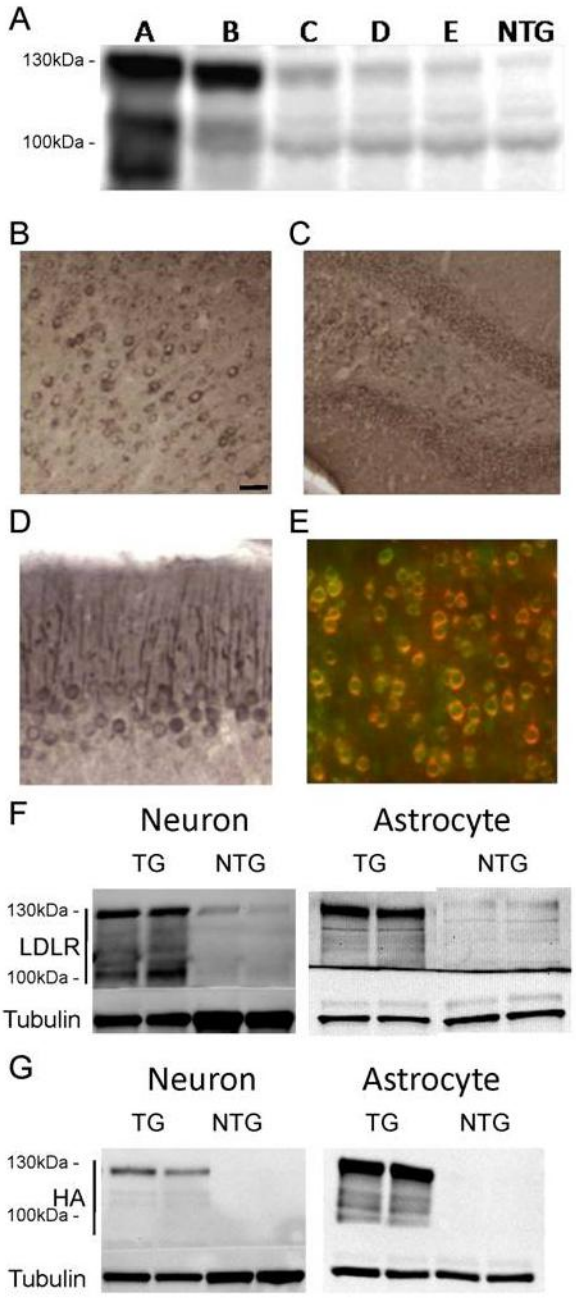

Figure 1

Figure 1. Expression of LDLR Transgene in Neurons and Astrocytes. (A) Levels of LDLR protein in the cortex of 5 different LDLR transgenic lines were assessed by western blotting. RIPA-soluble cortex lysates from LDLR transgenic mice and non-

transgenic (NTG) mice were probed with anti-LDLR antibody (Novus). **(B–D)** Regional expression patterns of LDLR in B line mice were characterized by immunostaining with anti-HA antibody to detect HA-tagged LDLR protein. LDLR was expressed in the cortex **(B)**, dentate gyrus of hippocampus **(C)**, and Purkinje cell dendrites of cerebellum **(D)**. **(E–G)** Cellular expression profile of the LDLR transgene was examined by using anti-HA or anti-LDLR antibody. **(E)** Cortical sections were stained by double-immunofluorescence labeling for HA (red) and the neuronal marker NeuN (green). **(F)** Cell lysates from primary neurons or astrocytes isolated from LDLR B line transgenic (TG) and NTG mice were analyzed by probing with either anti-LDLR (Novus) or anti-LDLR (Dr. Bu) antibody, respectively. **(G)** Expression of HA-tagged LDLR transgene in primary neurons and astrocytes was confirmed by western blotting with anti-HA antibody. Scale bar: 30μm. See also Figure S1.

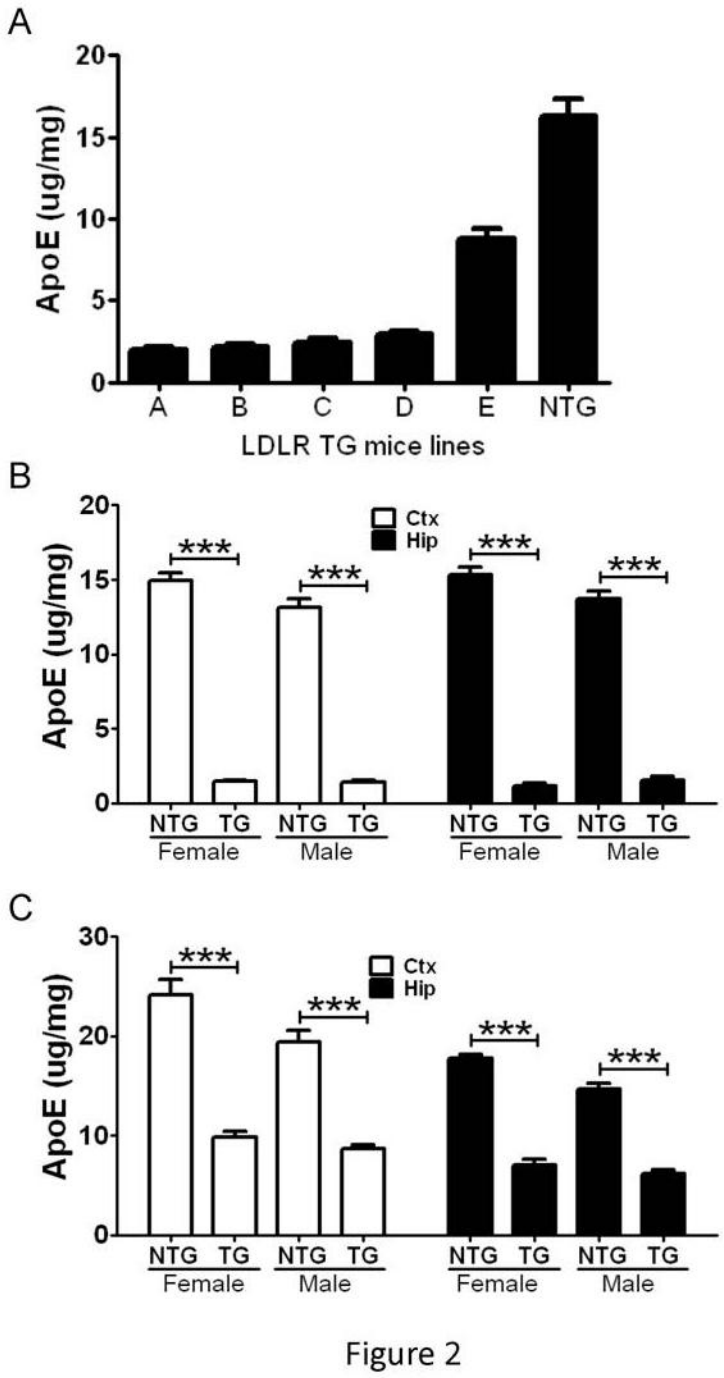

Figure 2

Figure 2. Reduction of Brain ApoE Protein Levels by LDLR Overexpression. (A) Cortex from 5 LDLR transgenic lines and NTG mice were homogenized with PBS at 3 months of age. Levels of apoE protein in PBS-extracted fraction were analyzed by apoE ELISA. (n=4 per group). **(B)** Hemizygous LDLR B line mice were bred with APP/PS1

transgenic mice. Levels of PBS-soluble apoE in the cortex (Ctx) and hippocampus (Hip) were measured from APP/PS1 mice without the LDLR transgene (NTG) and from APP/PS1/LDLR (TG) mice. To prevent any confounding effect from amyloid plaque formation and sex difference, mice were analyzed by sex at 2.5 months of age. (n=5–10 per group). **(C)** The progeny of hemizygous LDLR E line bred with APP/PS1 mice were similarly analyzed for apoE protein levels in the Ctx and Hip. There was a 55–60% reduction of apoE levels in LDLR TG mice, compared with NTG mice. (n=6–8 per group). Values are mean ± SEM. See also Figure S2 and S3.

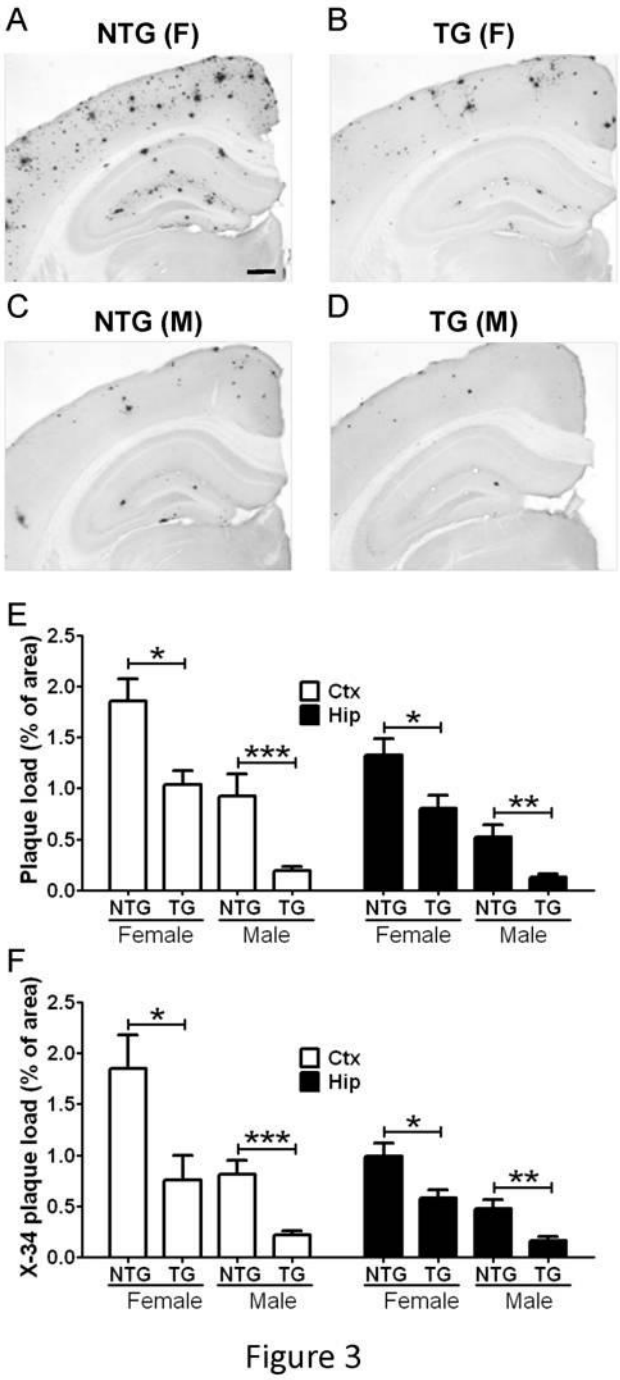

Figure 3

Figure 3. Inhibition of Plaque Formation by Strong LDLR Overexpression. Brain sections from APP/PS1 mice without LDLR transgene (NTG) **(A and C)** and APP/PS1/LDLR B line transgenic mice (TG) **(B and D)** were immunostained for Aβ

using the 3D6 antibody. Scale bar: 300μm. **(E)** The extent of plaque deposition detected by 3D6 antibody was quantified from cortex (Ctx) and hippocampus (Hip) of APP/PS1 and APP/PS1/LDLR transgenic mice. Female and male mice were analyzed separately at 7 months of age. (n=6–12 per group). **(F)** Brain sections from APP/PS1 and APP/PS1/LDLR TG mice were stained with X-34 dye that recognizes compact fibrillar plaques. X-34 positive fibrillar plaque loads in the Ctx and Hip were analyzed by applying an unbiased stereological method. (n=6–12 per group).

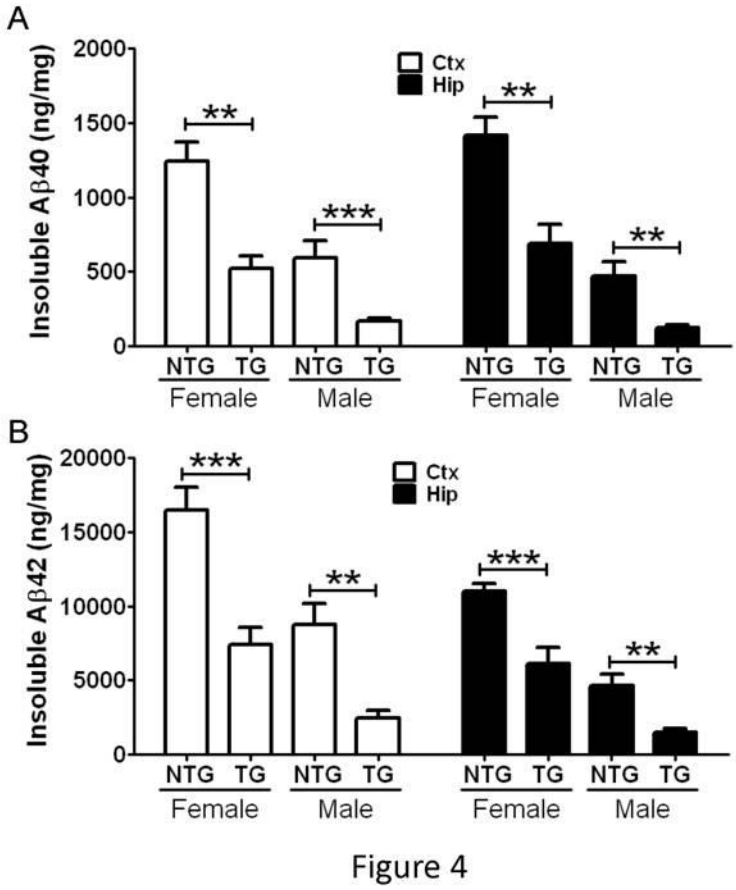

Figure 4. Decrease of Aβ Accumulation in APP/PS1/LDLR Transgenic Mice.

Cortical (Ctx) and hippocampal (Hip) tissues from 7 month-old APP/PS1 (NTG) and APP/PS1/LDLR B line transgenic mice (TG) were sequentially homogenized by using PBS and guanidine buffer. PBS-insoluble Aβ40 **(A)** and Aβ42 **(B)** levels were measured from Ctx and Hip by using a sandwich Aβ ELISA. (n=6–12 per group). Values are mean ± SEM. See also Table S1.

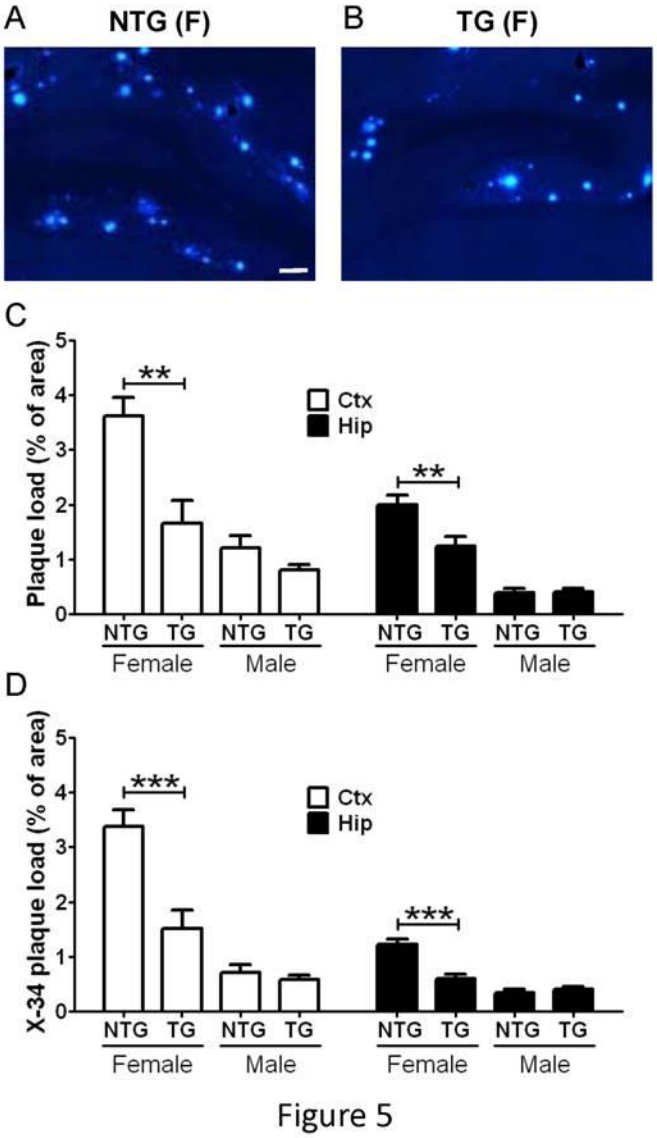

Figure 5

Figure 5. Two-fold Overexpression of LDLR Prevents Amyloid Formation.

Hippocampal sections from 7 month-old female APP/PS1 (NTG) **(A)** and APP/PS1/LDLR E line transgenic mice (TG) **(B)** were stained with fibrillar plaque-specific X-34 dye. Scale bar: 100μm. **(C)** The extent of plaque deposition detected by 3D6 antibody was quantified from cortex (Ctx) and hippocampus (Hip) of APP/PS1 and APP/PS1/LDLR E line transgenic mice. There was no statistically significant difference

between genotypes in male mice. **(D)** X-34 positive fibrillar plaque load was analyzed from Ctx and Hip of APP/PS1 and APP/PS1/LDLR transgenic mice. (n=8–13 per group). See also Table S1.

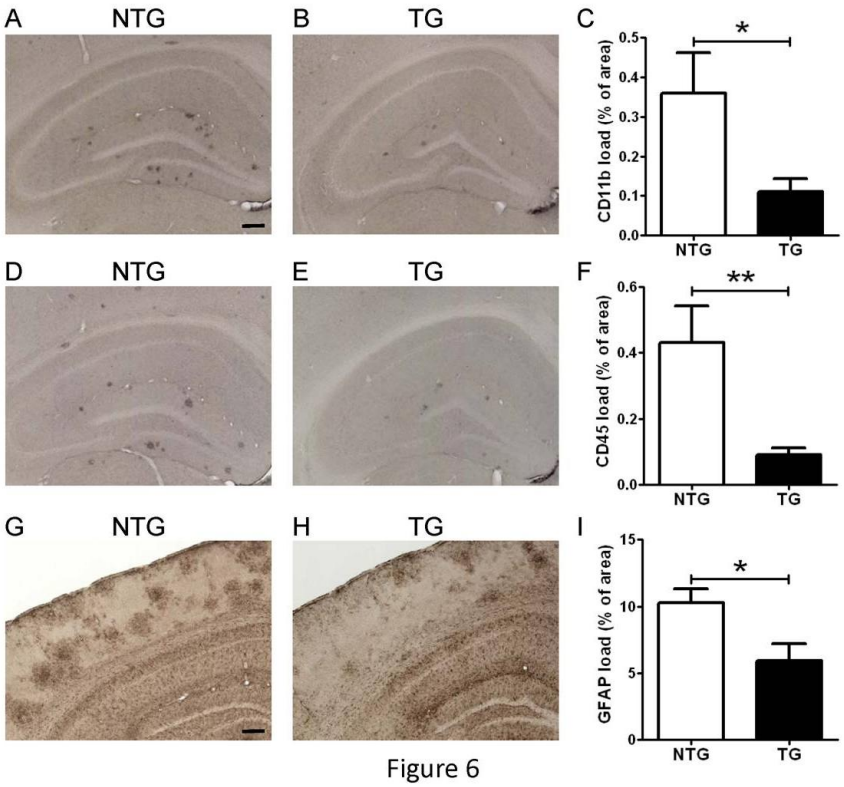

Figure 6

Figure 6. Attenuation of Neuroinflammatory Responses in APP/PS1/LDLR Mice.

Hippocampal sections from male APP/PS1 (NTG) and APP/PS1/LDLR B line transgenic mice (TG) were immunostained with an antibody against the microglial marker CD11b **(A–B)** and CD45 **(D–E)**. Scale bar: 150μm. The percent area covered by CD11b staining **(C)** and CD45 staining **(F)** was quantified from APP/PS1 and APP/PS1/LDLR B line. (n=8–10 per group). Cortical sections from female APP/PS1 **(G)** and APP/PS1/LDLR B line transgenic mice **(H)** were immunostained with anti-GFAP antibody, a marker of astrogliosis. Scale bar: 180μm. **(I)** The percent area covered by GFAP staining was quantified. (n=6–8 per group). Scale bar for higher magnification inserts: 40μm. All mice were 7 months old. See also Figure S4.

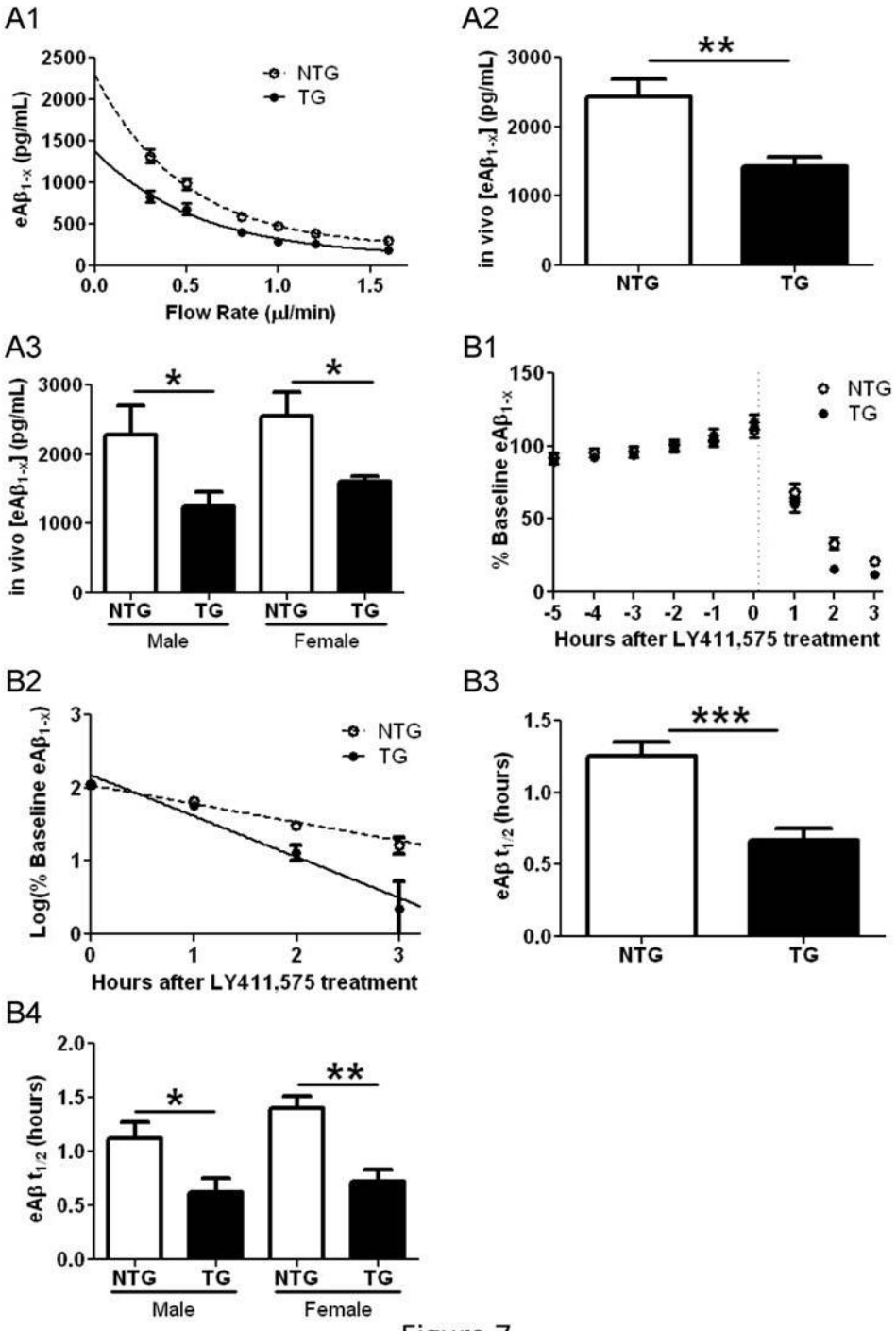

Figure 7

Figure 7. Steady State ISF eAβ Levels and Elimination Half-life Are Altered in APP/PS1 Mice Overexpressing LDLR. (A1) An exponential decay regression was used to fit the concentrations of $eA\beta_{1-x}$ obtained at each flow rate for individual mice in both

groups. The equations of the individual regressions were used to calculate the value at X=0 for each mouse in both groups. **(A2)** The mean in vivo steady state concentrations for ISF $eA\beta_{1\text{-}x}$ (in pg/mL) calculated from the method in A1 were 2426 ± 260.5 and 1432 ± 124.8 for APP/PS1 (NTG) and APP/PS1/LDLR (TG) mice, respectively (n=12 per group; *P*=0.0036, student's *t* test with Welch's correction). **(A3)** The mean in vivo steady state concentrations for ISF $eA\beta_{1\text{-}x}$ (in pg/mL) were significantly lower in APP/PS1/LDLR (TG) mice than in APP/PS1 (NTG) mice when comparing within the same sex (n=6 per group; *P*=0.049 and 0.040 for male and female comparisons, respectively) **(B1)** After a six-hour baseline of ISF $eA\beta_{1\text{-}x}$ was achieved, levels of the peptide rapidly decreased for both groups studied within several hours of a 10 mg/kg i.p. injection of the gamma secretase inhibitor LY411,575. **(B2)** The plot of the common logarithm of percent baseline ISF $eA\beta_{1\text{-}x}$ concentrations versus time was linear in both groups studied, suggesting net first-order kinetics. Data shown represent timepoints at which Aβ levels had not yet plateaued. The slope from the individual linear regressions from log(% eAβ) vs. time for each mouse was used to calculate the mean half-life ($t_{1/2}$) of elimination for eAβ from the ISF in (B3). **(B3)** The mean $eA\beta t_{1/2}$ (in hours) was 1.25 ± 0.0989 (n=13) and 0.671 ± 0.0833 (n=12) in NTG and TG mice, respectively. **(B4)** In NTG and TG male mice, the $eA\beta t_{1/2}$ (in hours) was 1.13 ± 0.147 (n=7) and 0.625 ± 0.126 (n=6), respectively. In NTG and TG female mice, the $eA\beta t_{1/2}$ (in hours) was 1.39 ± 0.112 (n=6) and 0.717 ± 0.117 (n=6), respectively. Differences were significant for comparisons between males as well as those made for females of each genotype (*P*=0.028 and 0.0018, respectively). See also Figure S5 and Table S2.

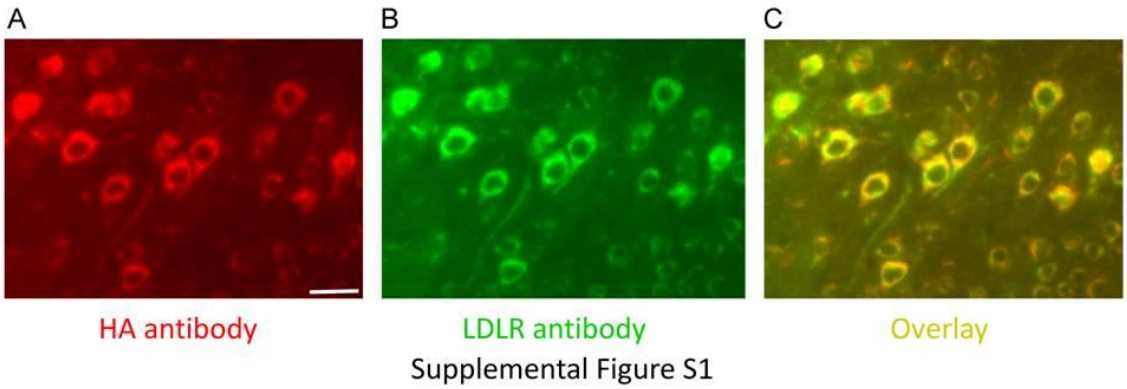

Supplementary Figure 1, related to Figure 1. Overlapping Staining Signal from HA Antibody and LDLR Antibody. Cortical sections from LDLR B line mice were stained by double-immunofluorescence labeling for HA **(A)** and LDLR (Abcam) **(B)**. **(C)** Since the HA epitope tag was inserted in the amino-terminal region of LDLR, HA staining pattern overlapped well with the LDLR staining pattern. Scale bar: 30µm.

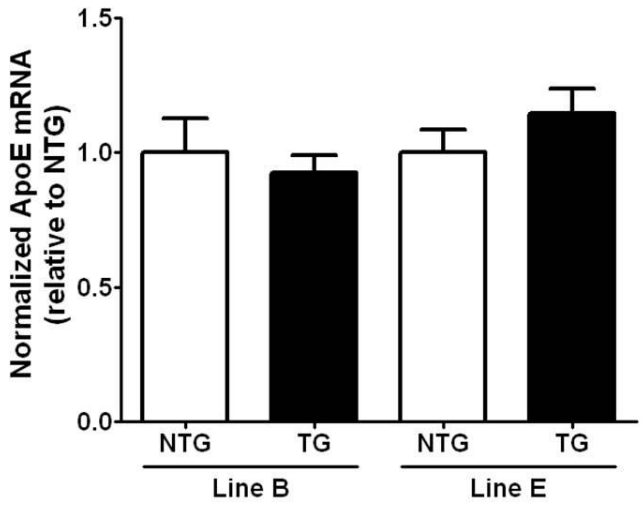

Supplemental Figure S2

Supplementary Figure 2, related to Figure 2. No alteration of apoE mRNA levels in cortex of LDLR transgenic mice. ApoE mRNA was extracted from cortical tissues of 3 month-old LDLR transgenic line B and E as well as their NTG littermates. The levels of apoE mRNA were measured by quantitative RT-PCR. There were no significant differences in apoE mRNA levels between LDLR transgenic mice and their NTG littermates. n=3-6 per group. Values are expressed as mean ± SEM.

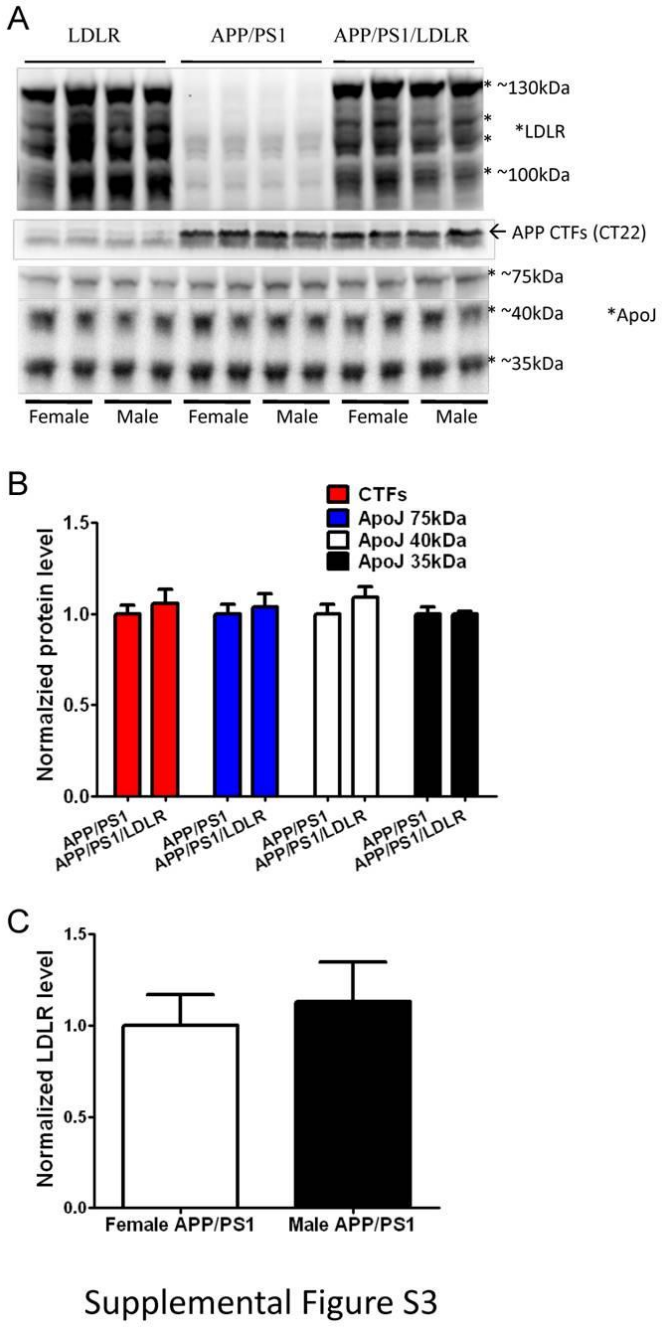

Supplemental Figure S3

Supplementary Figure 3, related to Figure 2. No alteration of APP processing and apoJ levels by LDLR overexpression. (A) Cortical tissues from 2.5 month old mice were lysed in RIPA buffer. Equal amounts of total protein from each mouse were loaded and then western blots were probed for LDLR (Abcam), APP carboxyl-terminal

fragments (CTFs), and ApoJ. The ~75 kDa band represents the disulfide-linked alpha and beta subunit of apoJ while the ~35 and 40 kDa bands represent the alpha and beta subunit, respectively. LDLR bands were used to confirm the genotype of mice. **(B)** Quantitative analyses of western blots were performed using the gel analysis function in NIH ImageJ software. There was no statistical difference for all comparisons. **(C)** Quantitative analyses of LDLR protein levels by western blots between 2.5 month old female and male APP/PS1 mice. LDLR protein levels were not significantly different between female and male mice. n=4 per group. Values are expressed as mean ± SEM.

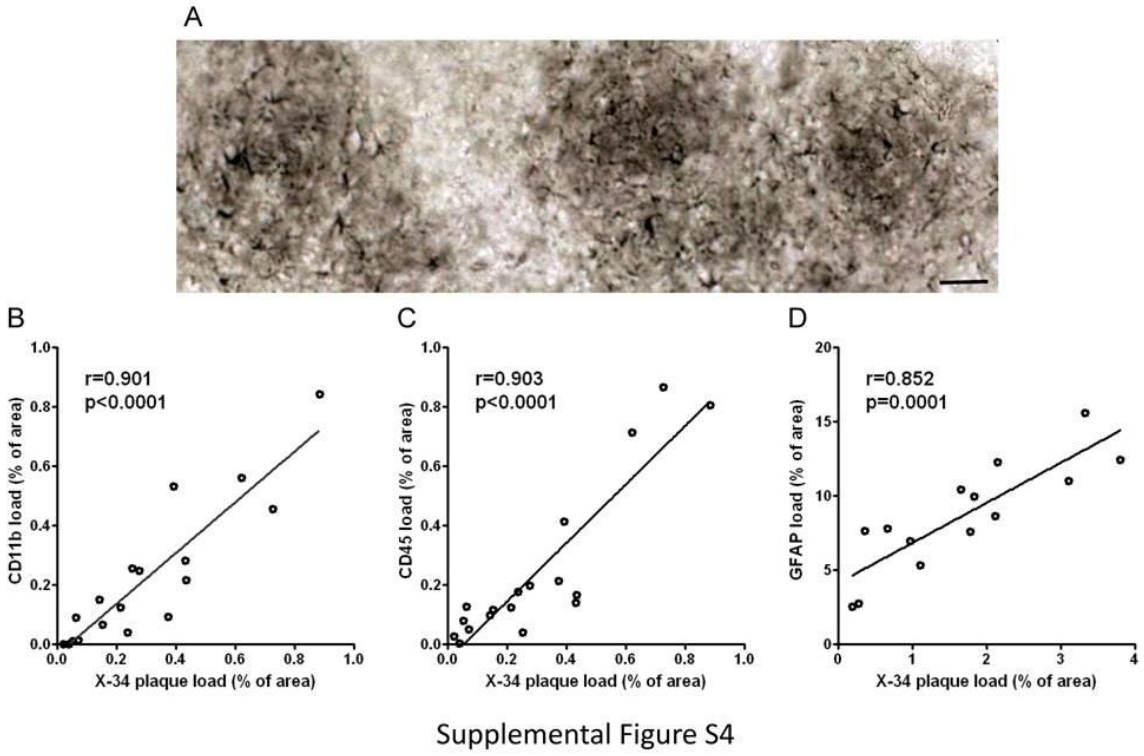

Supplemental Figure S4

Supplementary Figure 4, related to Figure 6. Tight correlation between gliosis and fibrillar plaque load. (A) Cortical sections from APP/PS1 mice were immunostained with anti-GFAP antibody. Reactive astrocytes were increased around amyloid plaques. Scale bar: 50µm. **(B)** Correlation analysis between CD11b-positive microglial load and X-34 positive fibrillar plaque load. Pearson product moment correlation coefficient r = 0.901. **(C)** Correlation analysis between CD45-positive microglial load and X-34 positive fibrillar plaque load. **(D)** Correlation analysis between GFAP-positive astrocyte load and X-34 positive fibrillar plaque load.

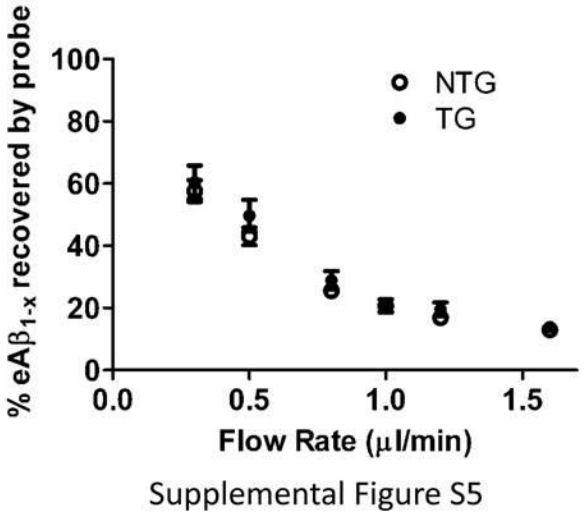

Supplementary Figure 5, related to Figure 7. Percent eAβ_{1-x} recovered by microdialysis probe is equivalent in dialysates collected from APP/PS1/LDLR and APP/PS1 mice. In vivo percent recoveries at each flow rate were determined using the zero flow extrapolated method, revealing no significant difference in eAβ recovery by the microdialysis probe between the groups studied (P>0.05; repeated measures ANOVA with Huynh and Feldt adjustment).

7 Month	Total Aβ40		Total Aβ42	
Line B	**Cortex**	**Hippocampus**	**Cortex**	**Hippocampus**
NTG (F)	1246 ± 132	1427 ± 121	16517 ± 1546	11007 ± 501
TG (F)	529 ± 80 (**)	694 ± 134 (**)	7394 ± 1158 (***)	6140 ± 1094 (***)
NTG (M)	594 ± 119	476 ± 97	8744 ± 1407	4646 ± 754
TG (M)	167 ± 24 (**)	131 ± 21 (**)	2480 ± 510 (**)	1493 ± 232 (**)
Line E	**Cortex**	**Hippocampus**	**Cortex**	**Hippocampus**
NTG (F)	1072 ± 140	1111 ± 113	17670 ± 1712	10600 ± 1091
TG (F)	486 ± 72 (**)	778 ± 105 (*)	11566 ± 1302 (*)	6827 ± 935 (*)
NTG (M)	272 ± 44	241 ± 49	7657 ± 851	2272 ± 415
TG (M)	475 ± 112	293 ± 25	7962 ± 914	2760 ± 205

Supplemental Table S1

Supplementary Table 1, related to Figure 4 and Figure 5. Total Aβ40 and Aβ42 levels in the cortex and hippocampus at 7 months of age. Levels of total (soluble plus insoluble) Aβ in the cortex and hippocampus were measured by using Aβ ELISA. Comparisons were made between APP/PS1 mice (labeled as NTG) and APP/PS1/LDLR transgenic mice (labeled as TG) using 2-tailed Student's t-test. Female (F) and male (M) mice were analyzed separately at 7 months of age. Units are in ng/mg of tissue. (*P<0.05, ***P*<0.01, ****P*<0.001).

2.5 Month	Total Aβ40		Total Aβ42	
Line B	**Cortex**	**Hippocampus**	**Cortex**	**Hippocampus**
NTG (F)	23.15 ± 1.3	29.63 ± 1.0	72.80 ± 5.3	82.26 ± 1.6
TG (F)	26.86 ± 1.2	30.33 ± 1.0	78.58 ± 5.4	86.44 ± 1.8
NTG (M)	22.20 ± 1.4	23.21 ± 1.0	72.14 ± 6.7	77.32 ± 3.2
TG (M)	26.12 ± 1.4	26.00 ± 1.1	74.93 ± 3.7	77.86 ± 2.7
Line E	**Cortex**	**Hippocampus**	**Cortex**	**Hippocampus**
NTG (F)	31.34 ± 1.6	32.36 ± 2.2	51.42 ± 2.1	62.21 ± 2.6
TG (F)	28.58 ± 1.7	33.44 ± 1.9	43.89 ± 2.2 (*)	62.06 ± 2.3
NTG (M)	25.21 ± 1.6	29.12 ± 1.8	39.28 ± 2.2	58.53 ± 1.5
TG (M)	25.92 ± 0.9	30.65 ± 1.1	39.50 ± 2.4	60.50 ± 1.4

Supplemental Table S2

Supplementary Table 2, related to Figure 7. Total Aβ40 and Aβ42 levels in the cortex and hippocampus at 2.5 months of age. Levels of total (soluble plus insoluble) Aβ in the cortex and hippocampus were measured by using Aβ ELISA. Female (F) and male (M) mice were analyzed separately at 2.5 months of age. With the exception of Aβ42 in the cortex of LDLR E line female progeny (*P<0.05), there was no statistically significant difference between NTG and TG mice for any of the measures. Units are in ng/mg of tissue.

Chapter 3.

Overexpression of the low-density lipoprotein receptor enhances brain to blood Aβ clearance in a mouse model of β-amyloidosis

PREFACE

The following work will be submitted as a full research article to a peer-reviewed journal in December 2011. Joseph Castellano performed and designed experiments and analyzed data throughout this work, with experimental assistance from Rashid Deane at the University of Rochester (brain efflux index experiments), Andrew J. Gottesdiener (plaque load quantification), and Floy R. Stewart (histology). Ronald B. DeMattos at Eli Lilly & Co. contributed valuable reagents.

ABSTRACT

Possession of the Apolipoprotein E (*APOE*)-ε4 allele is the strongest genetic risk factor for late-onset, sporadic Alzheimer's disease, likely increasing risk by altering amyloid-β (Aβ) accumulation. We recently demonstrated that the low-density lipoprotein receptor (LDLR) is a major apoE receptor in the brain that strongly regulates amyloid plaque deposition by modulating Aβ clearance. In the current study, we sought to understand the mechanism by which LDLR regulates Aβ accumulation by altering Aβ clearance from the brain interstitial fluid (ISF). We hypothesized that increasing LDLR levels enhances blood-brain barrier-mediated Aβ clearance, thus leading to reduced Aβ accumulation. Using the brain Aβ efflux method, we found that blood-brain barrier-mediated clearance of exogenously administered Aβ is, in fact, enhanced with LDLR overexpression. We next developed a method to directly assess the elimination of centrally-derived, endogenous Aβ into the plasma of mice using an anti-Aβ antibody that prevents degradation of plasma Aβ, allowing its rate of appearance from the brain to be measured. Using this plasma Aβ sequestration technique, we found that LDLR overexpression enhances brain to blood Aβ appearance rate. Together, our results suggest a novel mechanism by which LDLR regulates blood-brain barrier-mediated Aβ clearance, which may serve as a useful therapeutic avenue to target Aβ clearance from the brain.

INTRODUCTION

Alzheimer's disease (AD) is a progressive, neurodegenerative disease with an estimated prevalence of 26 million cases worldwide. Accumulation of soluble Aβ into toxic oligomers and amyloid plaques is widely hypothesized to initiate a pathogenic cascade leading to synaptic dysfunction, neuronal death, and ultimately, loss of cognitive function (Haass and Selkoe, 2007; Hardy and Selkoe, 2002; Selkoe, 2011). Extracellular amyloid plaques have been associated with neuritic dystrophy (D'Amore et al., 2003; Garcia-Alloza et al., 2006; Knowles et al., 1999; Lombardo et al., 2003; Meyer-Luehmann et al., 2008), as well as astrocytic/neuronal hyperactivity and synaptic dysfunction (Busche et al., 2008; Kuchibhotla et al., 2008; Kuchibhotla et al., 2009). In addition to the neurotoxic accumulation of amyloid-β (Aβ) in the brain parenchyma, dementia in AD has been associated with cerebrovascular dysfunction and the accumulation of Aβ in blood vessel walls (Iadecola, 2004; Zlokovic, 2008).

Genetic and biochemical studies have demonstrated that most rare, early-onset forms of familial AD are caused by autosomal dominant mutations that result in aberrant amyloid precursor protein (APP) processing, leading to an overproduction of Aβ or increase in the ratio of Aβ42 to Aβ40. However, much less is known about factors that initiate or regulate risk and onset of Aβ accumulation in sporadic, late-onset cases of AD that account for the majority of AD cases. Emerging evidence suggests that Aβ may accumulate in sporadic, late-onset AD as a result of its faulty clearance from the brain (Mawuenyega et al., 2010b). The strongest identified genetic risk factor for sporadic, late-onset AD is the *APOE* ε4 allele, which increases AD risk and decreases onset by 10-15 years in a dose-dependent fashion (Corder et al., 1994; Corder et al., 1993; Saunders

et al., 1993; Verghese et al., 2011). *APOE* status is hypothesized to modulate AD risk and age of onset by regulating the onset of amyloid deposition (Castellano et al., 2011; Morris et al., 2010; Reiman et al., 2009; Schmechel et al., 1993; Sunderland et al., 2004; Tiraboschi et al., 2004). A recent study in which complexes of human apoE and Aβ were injected into wildtype mouse brain demonstrated that apoE4 impedes the clearance of Aβ compared to complexes of Aβ and apoE2 or apoE3 (Deane et al., 2008). Using a mouse model that develops human apoE isoform-dependent β-amyloidosis (Bales et al., 2009), we recently provided direct in vivo evidence that human apoE isoforms differentially regulate soluble Aβ clearance from the brain interstitial fluid (ISF) (Castellano et al., 2011). The mechanism by which human apoE isoforms differentially clear Aβ remains unclear.

Aβ is eliminated from the brain ISF through various routes, including cellular uptake and degradation, ISF bulk flow, and blood-brain barrier (BBB)-mediated transport. ApoE has been shown to impede the clearance of Aβ across the BBB, and various members of the low-density lipoprotein receptor (LDLR) family have been implicated in mediating apoE-independent or apoE-dependent Aβ clearance across the BBB (Bell et al., 2007; Deane et al., 2008; Deane et al., 2004). Although LRP1 has been well characterized for its role in BBB-mediated Aβ clearance (Bell et al., 2007; Deane et al., 2008; Deane et al., 2004), whether LDLR mediates Aβ clearance across the BBB is unclear. Recent studies have identified LDLR as a major CNS apoE receptor that regulates amyloid deposition in various mouse models of β-amyloidosis (Cao et al., 2006; Fryer et al., 2005a; Katsouri and Georgopoulos, 2011; Kim et al., 2009b). Although we demonstrated that LDLR overexpression decreases amyloid deposition by altering the

steady state concentration of Aβ in the ISF (Kim et al., 2009b), the mechanism by which LDLR regulates ISF Aβ clearance remains to be defined. To this end, we used the brain efflux index (BEI) method to demonstrate a novel role for LDLR in BBB-mediated Aβ clearance. To directly assess the rate of appearance of Aβ in the blood from the brain, we created mice that express Aβ solely within the CNS with and without LDLR overexpression. We next sequestered endogenously produced, brain-derived Aβ with an anti-Aβ antibody in the blood of these mice, finding that LDLR overexpression increases the rate that Aβ enters the blood from the brain.

RESULTS

To further understand the role of LDLR in Aβ metabolism, we created mice in which LDLR is overexpressed in the CNS, which we have previously characterized (Kim et al., 2009b). In young wildtype (NTG) or LDLR-TG (TG) mice, we utilized the brain efflux index (BEI) method (Bell et al., 2007; Deane et al., 2008; Deane et al., 2004; Shibata et al., 2000) to test the hypothesis that LDLR regulates steady state levels of Aβ by enhancing its clearance from the brain. [^{125}I]-radiolabeled, monomeric Aβ40 was co-injected at an equimolar concentration of 12 nM with [^{14}C]-inulin into the brain interstitial fluid (ISF) to compare the clearance kinetics from the brain over various timepoints (15-150 minutes). Unlabeled and radiolabeled Aβ have been shown to exhibit nearly identical clearance kinetics (Bell et al., 2007). [^{14}C]-inulin serves as a reference marker of ISF bulk flow as it does not actively clear across the BBB. Total clearance of Aβ from the brain ISF was significantly faster from the brains of TG mice compared to NTG mice (Figure 1A). Analysis of major components of brain to blood efflux (BBB and ISF bulk flow) revealed that LDLR overexpression increased the BBB-mediated component of Aβ clearance compared to NTG mice, as indicated by the greater slope in TG vs. NG mice (Figure 1B). Notably, the contribution of ISF bulk flow to total Aβ clearance was minimal (Figure 1B), consistent with previous studies (Deane et al., 2008; Deane et al., 2004; Shibata et al., 2000). Given the purported role of apoE in BBB integrity (Fullerton et al., 2001; Hafezi-Moghadam et al., 2007; Methia et al., 2001), it is possible that LDLR overexpression may alter BBB permeability. We monitored the elimination of [^{14}C]-inulin over the entire timecourse for both groups, which revealed that

[^{14}C]-inulin was cleared in a slow, passive manner to a similar extent in both groups (Supplementary Figure 1A), strongly suggesting an intact BBB in TG mice.

Based on the passive elimination kinetics of inulin from the brain ISF and the total clearance of [^{125}I]-Aβ40, we employed our kinetic model (see Methods) to calculate the relative contribution of ISF bulk flow and BBB transport to Aβ clearance in NTG and TG mice (Figure 1C). A significantly greater proportion of total Aβ clearance was attributed to BBB transport in TG mice compared to NTG mice (66.9% compared to 36.3%; Figure 1C). Conversely, less Aβ was retained within the brains of TG mice compared to NTG mice (27.8% compared to 58.6%, respectively). Consistent with our earlier results, the proportion of Aβ clearance attributed to ISF bulk flow did not differ between NTG and TG mice (5.1% compared to 5.3%, respectively). The fractional rate constants (k, min^{-1}) calculated from Equations 2-4 (see Methods) and utilized to determine the rates of Aβ clearance mediated by the BBB, ISF bulk flow, and brain retention, are provided in Table 1. To determine whether cellular degradation within the remaining fraction of Aβ within the brain differed between NTG and TG mice, we performed trichloroacetic acid (TCA) precipitation of brains at early and late timepoints within the timecourse. Of the remaining fraction of brain [^{125}I]-Aβ in each group, the extent of cellular degradation was assessed by performing TCA precipitation of brains at 30 and 120 minutes following injection. We found that the proportion of TCA-precipitable (intact) Aβ did not differ significantly between NTG and TG mice, though a trend was noted towards greater degradation in the brains of TG mice at both timepoints (Supplementary Figure 1B). Together, our results suggest that LDLR enhances BBB-mediated clearance of Aβ.

The rapid degradation of Aβ in the periphery ($t_{1/2}$ = 2-3 min) precludes a direct and sensitive measurement of the rate of Aβ appearance from the brain (Barten et al., 2005; Ghiso et al., 2004). To begin to directly assess the rate of brain to blood Aβ appearance, we first crossbred LDLR-TG mice with the PDAPP (APPV717F) mouse model of β-amyloidosis. PDAPP mice have been previously reported to produce APP/Aβ solely within the CNS (DeMattos et al., 2001; Games et al., 1995; Johnson-Wood et al., 1997), allowing the brain to blood fate of Aβ to be followed in vivo. To characterize the effect of LDLR overexpression on Aβ accumulation in PDAPP mice, we aged PDAPP mice expressing normal levels of LDLR (NTG) and PDAPP mice overexpressing LDLR (TG) to 10 months of age. We immunostained brain sections from mice of each group using an anti-Aβ antibody (3D6). In both the hippocampus, TG mice exhibited a marked decrease in Aβ deposition compared to NTG mice (Figure 2A). Quantification of the extent of each region occupied by Aβ deposition revealed that LDLR overexpression decreased Aβ burden by 2.7-fold and 4.8-fold in hippocampus and cortex, respectively (Figure 2B). We next used the congophilic dye, X-34, to compare amyloid plaque load in 10 month-old NTG and TG mice (Figure 2C), which revealed a significant decrease in amyloid plaque load in hippocampus and cortex as a result of LDLR overexpression in PDAPP mice (Figure 2D). Based on the role of LDLR in receptor-mediated endocytosis of apoE from the extracellular space, we next assessed whether LDLR overexpression influences apoE concentration in young PDAPP mice, prior to the onset of Aβ deposition. We found that LDLR overexpression decreased apoE concentration in hippocampal homogenates by 2.9-fold compared mice expressing normal levels of LDLR (Figure 3A), which was similar to the 2.5-fold decrease in apoE observed in cortical homogenates

(Figure 3B). These results are consistent with previous findings that LDLR is a major receptor for apoE in the CNS (Fryer et al., 2005a; Kim et al., 2009b), further validating PDAPP mice overexpressing LDLR as a useful model to understand the role of LDLR in altering brain to blood clearance of Aβ.

To directly compare peripheral appearance rates of Aβ entering from the brain in NTG and TG mice, we sought to develop a method by which centrally-derived, endogenously secreted Aβ could be sequestered over time in the periphery, thus protecting it from rapid degradation. Based on earlier work characterizing the ability of anti-Aβ antibodies to rapidly sequester Aβ in the periphery and prolong its half-life (DeMattos et al., 2001; DeMattos et al., 2002a; Seubert et al., 2008), we identified a high-affinity anti-Aβ antibody specific for the central domain of Aβ (HJ5.1). Following intravenous injection of biotinylated HJ5.1 in PDAPP mice, we performed serial retro-orbital bleeds over the course of several hours to quantify the concentration of antibody in plasma following injection. Consistent with the long half-life of antibodies in the peripheral circulation, including anti-Aβ antibodies (DeMattos et al., 2001), the concentration of HJ5.1 in plasma of PDAPP mice was stable over the entire timecourse and was in significant molar excess of circulating Aβ (Figure 4A). To address the possibility that intravenously administered antibody enters the CNS, potentially altering Aβ metabolism in the brain, we harvested mice at the end of the timecourse following HJ5.1 injection and quantified the amount of antibody in the brain. In both hippocampal and cortical homogenates, we found a small fraction of the injected antibody (2.65×10^{-3} % to 1.75×10^{-2} %) had entered the brain (Supplementary Table 1). To further assess whether this small fraction could alter brain Aβ metabolism and to test the possibility that

antibody in the periphery may alter the equilibrium of Aβ efflux from brain to blood over this acute timecourse (DeMattos et al., 2001), we performed hippocampal in vivo microdialysis in PDAPP mice intravenously injected with HJ5.1. Compared to baseline levels of Aβ in the brain ISF, we did not observe any changes in the metabolism of ISF Aβ over the 5-hour period following intravenous antibody administration (Figure 4B-C). While it is possible that anti-Aβ antibodies may alter soluble Aβ concentration in the brain in a chronic setting, HJ5.1 does not alter soluble Aβ concentration in the brain over the acute timecourse in the current paradigm.

To compare the rate of Aβ appearance from brain to blood in PDAPP mice expressing wildtype levels of LDLR or overexpressing LDLR, we collected blood samples serially at various timepoints from mice of both groups following intravenous administration of HJ5.1. The concentration of CNS-derived human Aβ in plasma samples was determined using quantitative mass spectrometry. As shown in a representative experiment (Figure 5A), the kinetics of Aβ appearance were reliably linear for the duration of the timecourse, reflecting the rapid sequestration of Aβ entering the periphery from the brain. The appearance rate of human Aβ was significantly faster in TG mice compared to NTG mice (92 ± 4.8 pg $mL^{-1}min^{-1}$ vs. 69 ± 6.9 pg $mL^{-1}min^{-1}$; Figure 5B), strongly suggesting a role for LDLR in mediating brain to blood Aβ clearance. Notably, these results directly demonstrate in vivo that LDLR regulates the rate at which Aβ enters the blood from the brain.

DISCUSSION

The accumulation of soluble Aβ into high-order species and amyloid plaques throughout life is hypothesized to be a critical initiating event in AD pathogenesis (Hardy and Selkoe, 2002; Selkoe, 2011). Recent data have emerged suggesting that Aβ accumulates in the vast majority of AD cases, which are sporadic with late-onset, as a result of impaired Aβ clearance and not increased synthesis (Mawuenyega et al., 2010b). Moreover, we recently provided in vivo evidence that human apoE isoforms differentially regulate soluble Aβ clearance from the brain ISF (Castellano et al., 2011), with the slowest Aβ clearance observed in mice expressing *APOE* ε4, the strongest identified genetic risk factor for AD (Verghese et al., 2011). Based on previous evidence that receptors for apoE modulate Aβ metabolism (Bu, 2009), we sought to elaborate the previously unappreciated role of LDLR in Aβ metabolism. Recent work has identified that LDLR is a major apoE receptor in the CNS (Fryer et al., 2005a). Modulating the expression of LDLR has profound consequences on the accumulation of Aβ (Cao et al., 2006; Katsouri and Georgopoulos, 2011; Kim et al., 2009b), likely through its effects on the metabolism of soluble Aβ in the ISF (Kim et al., 2009b). In the current study, we investigated the mechanism by which LDLR overexpression enhances the clearance of soluble Aβ from the brain ISF. Using the brain efflux index (BEI) method (Deane et al., 2008; Shibata et al., 2000), we show that LDLR mediates clearance of exogenously administered Aβ across the blood-brain barrier but not does not significantly alter its clearance by ISF bulk flow. We then created mice that overexpress LDLR in the context of CNS expression of human Aβ using the PDAPP mouse model of β-amyloidosis. We found that LDLR overexpression in young PDAPP mice markedly decreases apoE levels

and decreases Aβ deposition in aged PDAPP mice. We next developed a method to sequester human Aβ entering the peripheral circulation from the brain using a high affinity anti-Aβ antibody, allowing us to directly assess the effect of LDLR on the rate of Aβ appearance from brain to blood. Using this method, we found that LDLR overexpression significantly increases the appearance rate of endogenously produced Aβ from the brain to blood. Together, our results suggest a novel mechanism whereby LDLR regulates brain Aβ accumulation via BBB-mediated Aβ clearance from the ISF.

Previous work has identified that several members of the LDLR family of receptors, including LRP1, LRP1B, SorLA, and apoER2, influence the trafficking and processing of the amyloid precursor protein (APP) (Andersen et al., 2005; Bu, 2009; Cam et al., 2004; Cam et al., 2005; Fuentealba et al., 2007). For example, LRP1 has been shown to interact with APP, regulating its internalization, trafficking, and its subsequent processing to Aβ (Cam et al., 2005; Kinoshita et al., 2001; Trommsdorff et al., 1998; Ulery et al., 2000). Although we did not observe any changes in APP expression or processing in the brains of mice overexpressing LDLR (Kim et al., 2009b), our work strongly suggests that LDLR influences Aβ metabolism by affecting its clearance from the brain into blood, a mechanism previously suggested for LRP1 and VLDLR (Bell et al., 2007; Deane et al., 2008; Deane et al., 2004; Yamada et al., 2008). ApoE strongly promotes amyloid plaque deposition (Bales et al., 1997; DeMattos et al., 2004) and has been shown to impede the clearance of Aβ from the brain ISF (Bell et al., 2007; Deane et al., 2008; DeMattos et al., 2004). Thus, it is likely that the reduction of apoE levels with LDLR overexpression facilitates greater ISF Aβ clearance across the BBB. Given recent data that the effect of LDLR on Aβ deposition is, in part, independent of apoE expression

(Katsouri and Georgopoulos, 2011), it is possible that LDLR directly facilitates clearance of Aβ across the BBB, as has been suggested for LRP1 (Deane et al., 2004). Moreover, while our data revealed only subtle trends towards greater Aβ degradation as a result of LDLR overexpression, we cannot rule out a role for LDLR in mediating Aβ degradation within particular cell types, the magnitude of which may have been too subtle to detect in whole brain homogenates. Our present results demonstrate a novel role for LDLR in BBB-mediated Aβ clearance, warranting further investigation into the contribution of this clearance pathway to apoE isoform-dependent Aβ clearance. This regulation may be especially relevant given that the affinity of apoE for LDLR is related to apoE isoform (Knouff et al., 2004; Weisgraber, 1994; Yamamoto et al., 2008).

The rapid degradation of Aβ once it enters the blood from the brain precludes direct and reliable measurement of its influx rate (Barten et al., 2005; Ghiso et al., 2004), presenting an obstacle to understanding mechanisms of BBB-mediated Aβ clearance. We reasoned that an anti-Aβ antibody would effectively sequester CNS-derived Aβ within the blood, allowing its appearance rate to be directly measured. We previously hypothesized that anti-Aβ antibody treatment in the periphery leads to a rapid rise in plasma Aβ by altering the efflux of Aβ from the brain (DeMattos et al., 2001; DeMattos et al., 2002a). In contrast, our present results demonstrate that peripheral administration of the HJ5.1 (anti-$A\beta_{13\text{-}28}$) antibody does not alter the metabolism of Aβ within the brain in the acute phase (5 hours) during which we analyzed Aβ influx into the circulation. A recent study suggested that the anti-Aβ antibody, m266, alters Aβ metabolism in the CNS by entering the CNS and sequestering Aβ (Yamada et al., 2009). However, in our study, the small fraction of antibody that entered the brain did not alter Aβ levels in the ISF,

perhaps a reflection of its lower affinity for Aβ as compared to the m266 antibody. Furthermore, our plasma sequestration results were in agreement with results obtained using the BEI method (Figure 1), further validating the BEI method as a useful technique to assess the contribution of different clearance components in overall Aβ clearance from the brain. Provided a suitable antibody is available that does not alter brain Aβ metabolism, the plasma sequestration technique we report herein may be useful to screen drugs targeting Aβ clearance from the brain to the blood, while representing a useful tool for probing the biology of brain apoE receptors and their role in Aβ metabolism.

Our findings that LDLR mediates BBB-mediated Aβ clearance provide rationale for targeting apoE receptors in the brain, and specifically in brain endothelial cells, as an additional means to reducing Aβ accumulation. Given that LDLR has very few identified ligands compared to other apoE receptors (Bu, 2009), strategies aimed at modulating LDLR expression will likely be relatively specific to Aβ/apoE metabolism, representing novel therapeutic avenues for AD prevention and treatment.

METHODS

Aβ preparation and radioiodination. Aβ40 peptide was synthesized by the Keck Foundation Biotechnology Resource Laboratory (Yale University, New Haven, CT). Solid-phase Fmoc (9-fluorenylmethoxycarbonyl) polypeptide synthesis was used to synthesize the Aβ peptide, followed by purification (reverse-phase HPLC) and structural characterization. Peptides were stored as lyophilized powder at -80°C prior to use. Using the lactoperoxidase method (Thorell and Johansson, 1971), Aβ40 was iodinated with [^{125}I] and resolved by HPLC prior to assessing purity by MALDI-TOF mass spectrometry, as previously described (Deane et al., 2008; LaRue et al., 2004). We utilized reduced monoiodinated Aβ with specific activity of ~60 μCi/μg (confirmed by MALDI-TOF mass spectrometry).

Mice

The "B" line of mice expressing the LDLR transgene (Kim et al., 2009b) were crossbred with wildtype mice and maintained on a mixed background comprised of B6/C3/CBA. Mice overexpressing the LDLR transgene (TG) and their NTG littermates were aged to 4-5 months for BEI experiments. Homozygous PDAPP (APPV717F) mice on a mixed background comprised of DBA/2J, C57BL/6J, and Swiss Webster were crossbred with heterozygous mice expressing the LDLR transgene (TG). Heterozygous PDAPP mice expressing normal levels of LDLR or expressing the LDLR transgene were aged to 3-4 months (biochemistry, in vivo microdialysis, plasma sequestration experiments) or 10 months (immunohistochemistry). Comparisons between groups were made using sex-matched littermates on the same genetic background. Animal procedures were performed

according to protocols accepted by the Animal Studies Committee at Washington University School of Medicine.

Quantitative measurement of apoE, HJ5.1, and ISF Aβ

ApoE measurements were made by sensitive sandwich ELISA (mouse monoclonal antibody, HJ6.2, for capture and biotinylated mouse monoclonal antibody, HJ6.3, for detection), using pooled mouse plasma (C57/B6J) for apoE standard (Fryer et al., 2005a). Concentration of biotinylated mouse monoclonal antibody, HJ5.1, recovered from plasma or brain tissue was assayed by ELISA. Samples were added to plates bound with a saturating amount of Aβ40 (50 ng/mL) that had been captured by coated 3D6 antibody; biotinylated HJ5.1 was used to standardize concentration. Measurements of ISF [$A\beta_{1\text{-}X}$] from fractions collected during in vivo microdialysis were made by sandwich ELISA using synthetic Aβ40 as the standard (American Peptide). Briefly, plates were coated with m266 antibody (anti-$A\beta_{13\text{-}28}$), and bound Aβ was detected using biotinylated 3D6 antibody (anti-$A\beta_{1\text{-}5}$).

Brain Tissue processing and quantification of Aβ/amyloid burden

Following transcardial perfusion with heparinized phosphate-buffered saline (PBS), brains were removed and fixed in 4% paraformaldehyde overnight, followed by immersion in 30% sucrose. Brains were sectioned on a freezing-sliding microtome at a thickness of 50 μm. Coronal sections were collected from the rostral anterior commissure through the caudal extent of the hippocampus before staining with biotinylated 3D6 antibody (anti-$A\beta_{1\text{-}5}$) or X-34 dye. The NanoZoomer slide scanner system (Hamamatsu Photonics) was used to scan slides in batch mode, which allowed for

the capture of images in brightfield (Aβ immunostaining) or fluorescent mode (X-34 staining). NDP viewer software was utilized to export acquired images from slides prior to quantitative analysis (Image J software, National Institutes of Health [NIH]). Three sections for each mouse, each separated by 300 μm (corresponding to bregma -1.7 mm, -2.0 mm, -2.3 mm in mouse brain atlas), were used for determination of the percentage of area occupied by immunoreactive Aβ or amyloid burden (X-34-positive signal) in a blinded fashion. Slides were uniformly thresholded to minimize false-positive signal, as previously described (Castellano et al., 2011; Kim et al., 2009b).

Biochemistry

After transcardial perfusion with heparinized PBS, brains were extracted, microdissected, and immediately frozen at -80°C. For apoE ELISAs, hippocampal or cortical tissue was manually dounce-homogenized with 75 strokes in radioimmunoprecipitation assay (RIPA) buffer [50 mM tris-HCl (pH 7.4), 150 mM NaCl, 0.25% deoxycholic acid, 1% NP-40, 1 mM EDTA] containing a cocktail of protease inhibitors (Roche) or PBS containing cocktail of protease inhibitors (Roche) for HJ5.1B ELISAs. Total protein concentration in brain homogenates was determined with a BCA protein assay kit (Pierce).

Brain efflux index (BEI) method

Experiments were performed as described previously (Deane et al., 2008; Deane et al., 2004; Shibata et al., 2000). Stainless steel guide cannulae were stereotaxically implanted into caudate-putamen of mice that had been anesthetized with ketamine (100 mg/kg) and xylazine (10 mg/kg). Coordinates for implantation were as follows: bregma – 1.9 mm,

0.9 mm lateral from midline, 2.9 mm below dura. Following recovery from surgery to allow time for BBB repair for large molecules and before substantial chronic, reactive processes had occurred (Bell et al., 2007; Cirrito et al., 2003; Deane et al., 2005; Deane et al., 2004), mice were co-injected with a solution (0.5 μL) containing [^{14}C]-inulin and [^{125}I]-Aβ40 in artificial cerebrospinal fluid into brain ISF at 0.1 μL/min. Mice were sacrificed at various timepoints after injection (from 15 min to 150 min), and brains were immediately isolated and prepared for radioactivity analysis and TCA precipitation to analyze the molecular forms of tracer compounds, exactly as previously described (Deane et al., 2008; Shibata et al., 2000).

BEI calculations and analysis

Calculations were performed as previously described (Bell et al., 2007; Deane et al., 2008; Deane et al., 2004; Shibata et al., 2000). In brief, the percentage of [^{125}I]-Aβ40 or [^{14}C]-inulin remaining in the brain at each timepoint following microinfusion was calculated as follows:

% recovery in brain = 100 x (N_b/N_i) (Equation 1),

where N_b is the radioactivity of intact ligand remaining in the brain upon conclusion of the experiment, and N_i is the initial amount of radioactive ligand injected into the brain (in counts per minute [c.p.m.] for TCA-precipitable [^{125}I]-Aβ40 and disintegrations per minute [d.p.m.] for [^{14}C]-inulin). The rate of ISF bulk flow was determined as follows using the rate of clearance of inulin, an inert and polar reference molecule that neither transports across the BBB nor is retained in the brain:

$N_{b,inulin}/N_{i,inulin}$ = (Equation 2),

where k_{inulin} indicates the rate of inulin clearance and t denotes time. Based on our model (Bell et al., 2007; Deane et al., 2008; Shibata et al., 2000), Aβ can be eliminated by BBB transport or elimination via ISF bulk flow into the CSF and cervical lymphatics. Our model incorporates retention within the brain, i.e., binding of Aβ to receptors or chaperone molecules, which may result in degradation or retention within brain. Assuming a multiple timepoint efflux series with departure from linearity at later timepoints, the percentage of [^{125}I]-Aβ40 remaining in the brain is expressed as follows:

$N_{b,A\beta}/N_{i,A\beta} = (a_1 + a_2)$ (Equation 3),

where $a_1 = k_2/(k_1 + k_2)$ and $a_2 = k_1/(k_1 + k_2)$, and k_1 and k_2 denote fractional rate constants for total brain efflux and retention within brain, respectively. The fractional rate constant for Aβ clearance mediated by the BBB, k_3, was calculated as the difference between fractional rate constants for total efflux and ISF bulk flow:

$k_3 = k_1 - k_{inulin}$ (Equation 4)

MLAB mathematical modeling (Civilized Software, Inc.) was used to fit the compartmental model to elimination data with inverse square weightage. Fractional rate constants were obtained by nonlinear regression curve fitting (GraphPad Prism 5.0).

In vivo microdialysis

In vivo microdialysis in freely behaving mice was performed essentially as described to assess the effect of intravenous HJ5.1 administration on steady state levels of ISF Aβ in young heterozygous PDAPP mice (Castellano et al., 2011; Cirrito et al., 2003; Kim et al., 2009a). Briefly, stereotaxic surgery was performed to implant guide cannulae in the

caudal extent of hippocampus (bregma -3.1 mm, -2.5 mm lateral from midline, 1.2 mm below dura, 12° off vertical). Using a syringe pump (Stoelting), 0.15% bovine serum albumin (RPI) in artificial cerebrospinal fluid was perfused continuously at a flow rate of 1.0 μL min^{-1} through an implanted 38 kDa MWCO microdialysis probe (BR-2; Bioanalytical Systems, Inc.) to dialyze ISF analytes collected every 60 minutes with a refrigerated fraction collector.

Plasma Sequestration and serial retro-orbital bleeds

Plasma sequestration experiments were performed by administering 250 μg HJ5.1 (generated in-house) by intrajugular injection under brief isoflurane exposure. To sample blood at various timepoints (20, 45, 75, 120, and 240 min) following intrajugular injection, serial retro-orbital bleeds (~110 μL/sample) were performed using heparinized capillary tubes (Chase Scientific Glass, Rockwood, TN) under brief isoflurane exposure. For each mouse, plasma was collected 14-16 hours prior to injection ("pre-bleed") to serve as a baseline sample. Plasma was isolated by spinning blood collected in EDTA-coated microcentrifuge tubes at 7575 x g at 4°C for 9 min; plasma samples were frozen at -80°C until measurement by mass spectrometry. For experiments in Figure 5, plasma samples were pooled by timepoint in pairs (n = 12-14 mice/group) for mass spectrometry detection (n = 6-7/group). Rates were calculated from slopes of individual linear regressions over the entire timecourse (n = 6-7 per group). Human Aβ was immunoprecipitated using 6E10 and quantified against a standard curve during SISAQ quantitative mass spectrometry (Stable Isotope Spike Absolute Quantitation [SISAQ™], C2N Diagnostics, Saint Louis, MO). Briefly, samples were spiked with [^{15}N]-labeled Aβ 40 peptide Aβ in the sample was immunoprecipitated using an N-terminal human-

specific Aβ antibody (6E10). Immunoprecipitated Aβ was trypsin-digested and tryptic peptides were analyzed by mass spectrometry. The ratio of unlabeled to labeled $A\beta_{17-28}$ peptide was normalized against a SISAQ standard curve, allowing quantification of Aβ in the original plasma samples.

Statistics

Unless indicated otherwise within figure legends, differences between groups were assessed using two-tailed student's *t* test. For nonparametric distributions, Mann-Whitney U test was performed. Levels of significance were indicated as follows: $*P<0.05$, $**P<0.01$, $***P<0.001$. Measurements are reported as mean ± SEM. Analyses were performed using GraphPad Prism 5.0 software.

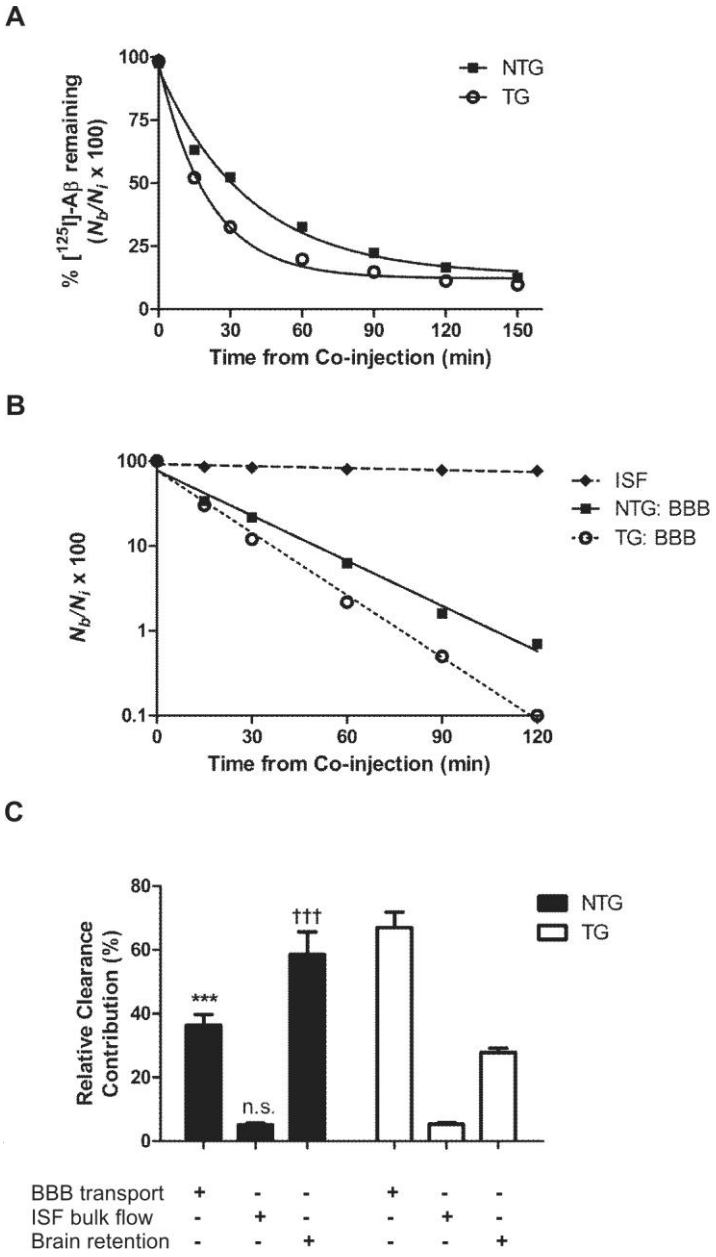

Figure 1. LDLR enhances clearance of radiolabeled Aβ from the brain. (A) Percentage remaining for 12 nM [^{125}I]-Aβ40 microinjected in ISF of caudate-putamen in NTG (closed square) and TG (open circle) mice sacrificed at various timepoints. Percentage recovery was calculated from Equation 1 (Methods). **(B)** Time-dependent clearance of [^{125}I]-Aβ40 by passive ISF bulk flow (closed diamond) and across the BBB (NTG; closed square and TG, open circle) calculated from data in Figure 1A and

Equation 4 (Methods). **(C)** Using fractional rate constants calculated in Table 1, relative contributions of clearance of [^{125}I]-Aβ40 by the BBB, ISF bulk flow, as well as retention within brain were calculated for NTG (black bars) and TG (white bars) mice. Each component is indicated with "+" below figure. Complete timecourse includes 32-41 mice (n=4-6 mice/timepoint for each group). Values in **(A)** and **(C)** are represented as mean ± SEM. When two-way ANOVA was significant (with genotype and component as factors), differences among clearance components were assessed using Tukey's post hoc test for multiple comparisons. ***P<0.001, % BBB for NTG vs. TG. †††P<0.001, brain retention for NTG vs. TG. *N.S.*, no significant difference between ISF bulk flow components between NTG and TG.

	TG k (min^{-1})	NTG k (min^{-1})
Total Efflux (k_1)	0.03326 ± 0.00428	0.01885 ± 0.00202
BBB Transport (k_3)	0.03081 ± 0.00472	0.01652 ± 0.00245
ISF Bulk Flow (k_{inulin})	0.00244 ± 0.00045	0.00232 ± 0.00043
Brain Retention (k_2)	0.01278 ± 0.00085	0.02664 ± 0.00605

Table 1. Fractional rate constants (k, min^{-1})for [^{125}I]-Aβ40 and [^{14}C]-Inulin in TG and NTG mice. Values are mean ± SEM from N=32-41 mice/group.

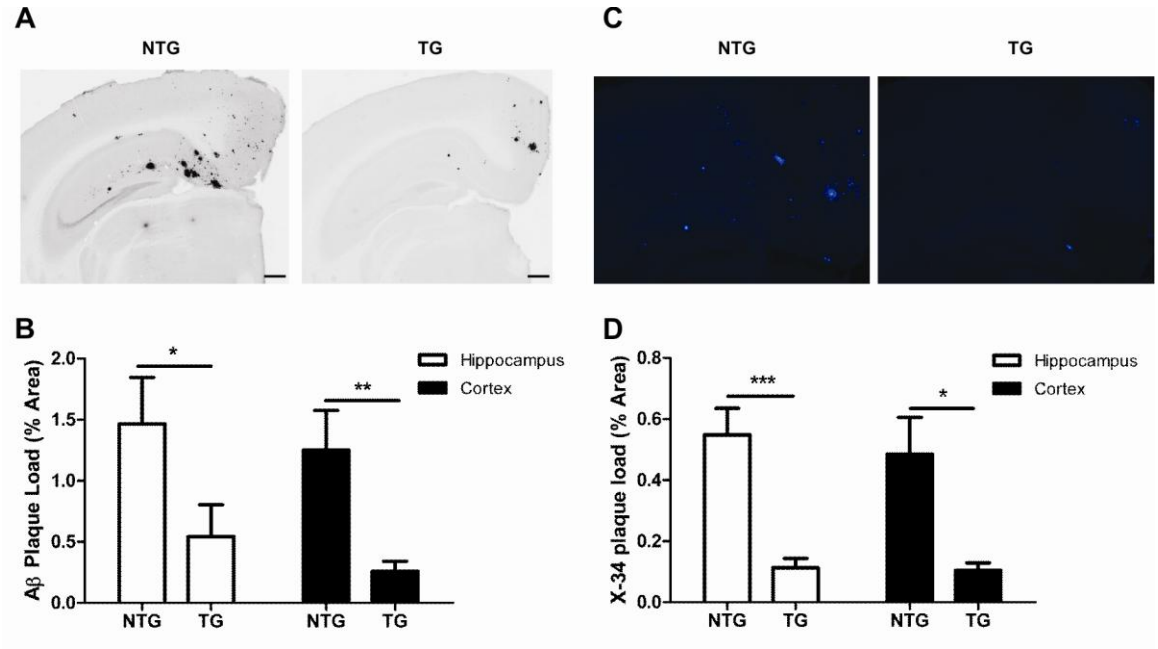

Figure 2. LDLR overexpression in PDAPP mice markedly decreases brain Aβ/amyloid deposition. (A) Representative coronal brain sections from 10-month-old, sex-matched PDAPP$^{+/-}$ mice expressing normal levels of LDLR (NTG) and PDAPP$^{+/-}$ mice overexpressing LDLR (TG). Aβ immunostaining was performed using anti-Aβ antibody (biotinylated-3D6). Scale bars, 300 μm. **(B)** Quantification of the area of the hippocampus or cortex occupied by Aβ immunostaining (n = 9 mice/group). **(C)** Representative amyloid burden in coronal brain sections from 10-month-old, sex-matched PDAPP$^{+/-}$ mice expressing normal levels of LDLR (NTG) and PDAPP$^{+/-}$ mice overexpressing LDLR (TG). Amyloid was visualized using the congophilic fluorescent dye, X-34. Scale bars, 300 μm. **(D)** Quantification of the area of hippocampus or cortex occupied by X-34 staining (n = 9-10 mice/group). In (B) and (D), groups were compared using Mann-Whitney U test. **P*<0.05, ***P*<0.01, ****P*<0.001. Values represent means ± SEM.

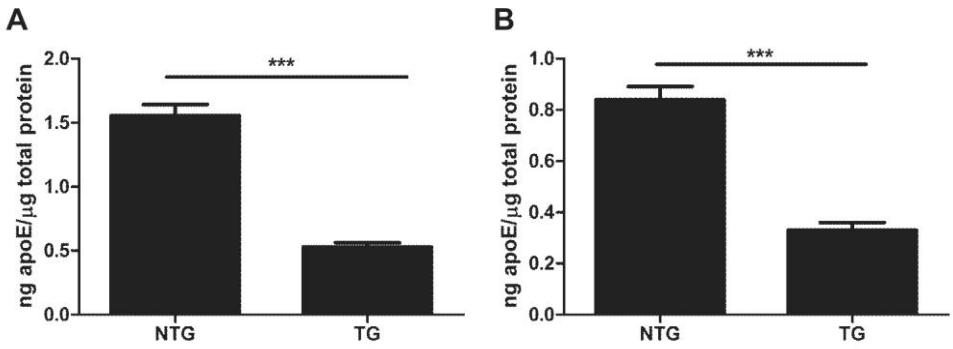

Figure 3. LDLR overexpression in PDAPP mice markedly decreases brain apoE levels. (A) ApoE protein levels measured by sensitive sandwich ELISA in hippocampal homogenates from young mice (3-4 months) to prevent any confounding effect from amyloid plaque deposition (n = 9 mice/group). **(B)** ApoE protein levels measured by sensitive sandwich ELISA in cortical homogenates from young mice (3-4 months) to prevent confounding effects from amyloid plaque deposition (n = 9 mice/group). Differences between groups were assessed using two-tailed student's *t* test (with Welch's correction for **(A)**). ***$P<0.001$. Values represent means ± SEM.

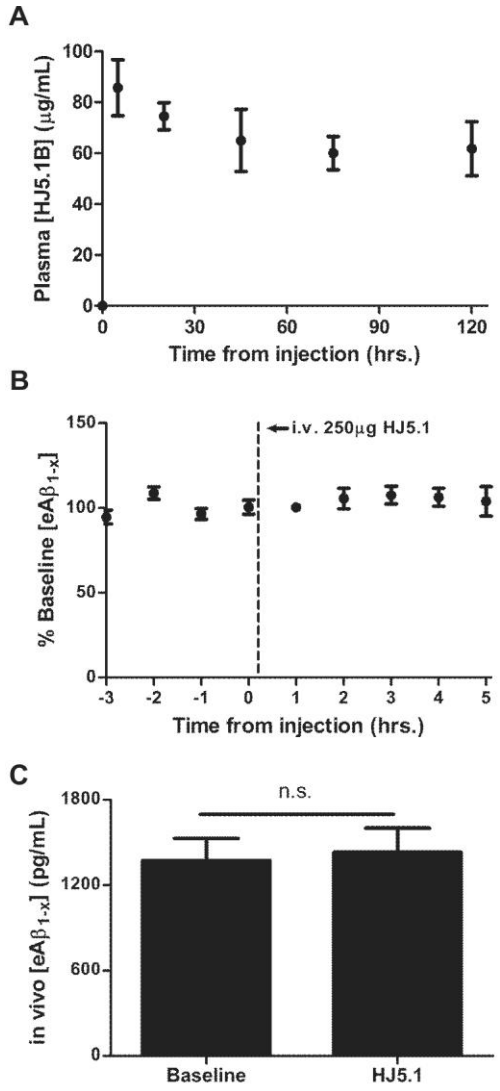

Figure 4. I**ntravenous HJ5.1 administration results in stable antibody steady state levels in plasma without altering brain ISF Aβ metabolism. (A)** Concentration of biotinylated HJ5.1 in plasma samples collected from serial retro-orbital bleeds following intrajugular injection of biotinylated HJ5.1. (n = 4 PDAPP$^{+/-}$ mice; 3-4 months old). **(B)** Effect of intrajugular injection of 250 μg HJ5.1 on soluble, exchangeable ISF $A\beta_{1-x}$ levels following a baseline period of sampling during in vivo microdialysis. (n = 5 PDAPP$^{+/-}$ mice; 3-4 months old). **(C)** Mean effect of HJ5.1 treatment on ISF $A\beta_{1-x}$ compared to mean baseline period preceding treatment. Difference between groups was assessed by

paired student's *t* test, revealing no statistical difference between groups ($p>0.05$). Values represent mean ± SEM.

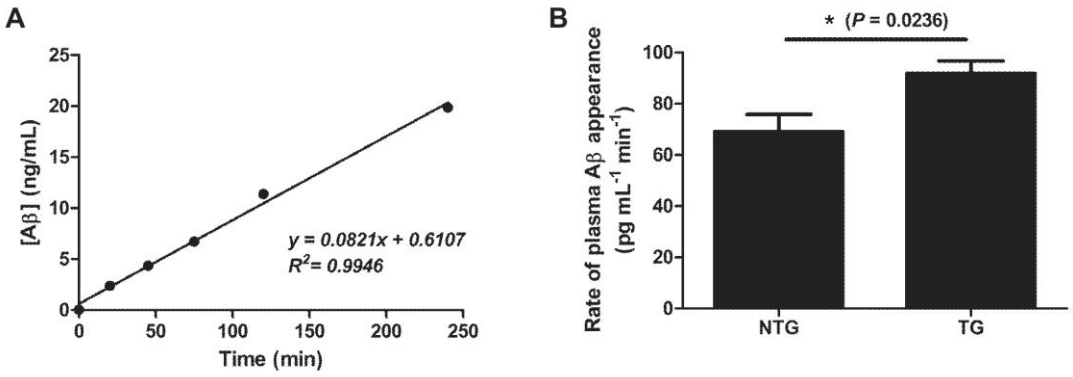

Figure 5. Plasma sequestration of brain Aβ reveals faster brain to blood appearance rate in PDAPP mice overexpressing LDLR. (A) Sample plasma sequestration experiment illustrating kinetics of brain-derived Aβ appearance in plasma collected by serial retro-orbital bleeds following HJ5.1 treatment. Appearance rates were calculated from the slopes of individual linear regressions, e.g., for (A), 82.1 pg mL^{-1} min^{-1}. **(B)** Mean rate of Aβ appearance in $PDAPP^{+/-}$ mice expressing normal levels of LDLR (NTG) or $PDAPP^{+/-}$ mice overexpressing LDLR (TG). (n = 6-7/group; 3.5-4.5 months old). Difference between groups was analyzed using a two-tailed student's *t* test. **P*<0.05. Values in **(B)** represent mean ± SEM.

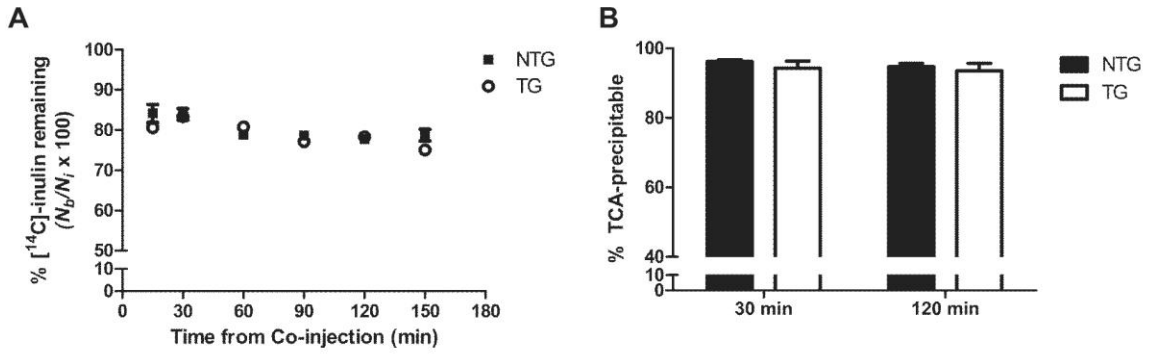

Supplementary Figure 1. LDLR overexpression does not appear to alter ISF bulk flow or the degradation of remaining [^{125}I]-Aβ40. (A) Percentage remaining of co-injected [^{14}C]-inulin over timecourse in experiments from **Figure 1A** in NTG and TG mice. Timecourse includes 32-41 mice (n = 4-6 mice/timepoint for each group; 4-5 months of age). **(B)** Percentage of remaining [^{125}I]-Aβ40 that is precipitable by TCA (intact), representing intact peptide (n = 3-4 mice/timepoint for each group; 4-5 months of age). 2-way ANOVA, with time and genotype as factors, revealed no significant differences among groups. Values represent mean ± SEM.

	Hippocampus	Cortex
[HJ5.1B] ng/mg tissue	0.248 ± 0.0144	0.280 ± 0.0116
% of HJ5.1 injected	$2.65 \times 10^{-3} \pm 4.36 \times 10^{-4}$	$1.75 \times 10^{-2} \pm 6.70 \times 10^{-4}$

Supplementary Table 1. Intravenously administered biotinylated HJ5.1 enters the CNS at low levels. Concentration of biotinylated HJ5.1 in hippocampal or cortical homogenates from PDAPP$^{+/-}$ mice sacrificed 120 min following injection, as determined by sensitive sandwich ELISA. (n = 4; 3-4 months old). Values represent means ± SEM.

Chapter 4.

Human apoE isoforms differentially regulate brain amyloid-β peptide clearance

PREFACE

This work appeared in *Science Translational Medicine* on June 29, 2011. The experiments in this chapter were designed and performed by Joseph Castellano with technical assistance from Floy Stewart (histology) and Hong Jiang (CSF collection). Joseph Castellano and Jungsu Kim performed in vivo stable isotopic labeling kinetics experiments with mass spectrometry assistance from Kwasi Mawuenyega (laboratory of Randall Bateman) and Bruce Patterson. Anne Fagan and John Morris provided human data from the Washington University ADRC for analysis by Joseph Castellano. Alison Goate, Carlos Cruchaga, and Kelly Bales (Pfizer) provided human CSF apoE data. Ronald DeMattos (Eli Lilly & Co.) and Steven Paul (Cornell University) provided valuable reagents.

ABSTRACT

The apolipoprotein E (*APOE*) ε4 allele is the strongest genetic risk factor for late-onset, sporadic Alzheimer's disease (AD). The *APOE* ε4 allele dramatically increases AD risk and decreases age of onset, likely through its strong effect on the accumulation of amyloid-β (Aβ) peptide. In contrast, the *APOE* ε2 allele appears to decrease AD risk. Most rare, early-onset forms of familial AD are caused by autosomal dominant mutations that often lead to overproduction of Aβ42 peptide. However, the mechanism by which *APOE* alleles differentially modulate Aβ accumulation in sporadic, late-onset AD is less clear. In a cohort of cognitively normal individuals, we report that reliable molecular and neuroimaging biomarkers of cerebral Aβ deposition vary in an apoE isoform-dependent manner. We hypothesized that human apoE isoforms differentially affect Aβ clearance or synthesis in vivo, resulting in an apoE isoform-dependent pattern of Aβ accumulation later in life. Performing in vivo microdialysis in a mouse model of β-amyloidosis expressing human apoE isoforms (PDAPP/TRE), we find that the concentration and clearance of soluble Aβ in the brain interstitial fluid depends on the isoform of apoE expressed. This pattern parallels the extent of Aβ deposition observed in aged PDAPP/TRE mice. Importantly, apoE isoform-dependent differences in soluble Aβ metabolism are observed not only in aged PDAPP/TRE mice but also in young PDAPP/TRE mice, well before the onset of Aβ deposition in amyloid plaques. Additionally, amyloidogenic processing of amyloid precursor protein and Aβ synthesis, as assessed by in vivo stable isotopic labeling kinetics, do not vary according to apoE isoform in young PDAPP/TRE mice. Our results suggest that *APOE* alleles contribute to

AD risk by differentially regulating clearance of Aβ from the brain, suggesting that Aβ clearance pathways may be useful therapeutic targets for AD prevention.

INTRODUCTION

Alzheimer's disease (AD) is the leading cause of dementia in the elderly, with an estimated prevalence of 26 million cases worldwide. Because the number of cases and associated costs are projected to increase dramatically, effective strategies aimed at prevention and preclinical intervention will likely depend on our understanding of how major risk factors contribute to the disease process. The prevailing hypothesis of AD pathogenesis posits that accumulation of brain amyloid-β (Aβ) peptide initiates a pathogenic cascade that culminates in neurodegeneration and dementia (Hardy and Selkoe, 2002). The Aβ peptide is generated through sequential proteolytic processing of the amyloid precursor protein (APP) by β- and γ-secretases. Strong biochemical and genetic evidence has demonstrated that most rare, early-onset forms of familial AD are caused by autosomal dominant mutations that result in abnormal processing of APP, leading to overproduction of Aβ or an increase in the ratio of Aβ42 to Aβ40. Much less is known about the factors that initiate or modulate the onset of brain Aβ accumulation in the more common (>99%) sporadic, late-onset form of AD. The best established genetic risk factor for sporadic, late-onset AD is the apolipoprotein E (*APOE*) ε4 allele, the presence of which dramatically increases risk for developing AD and decreases age of onset by 10 to 15 years; in contrast, the *APOE* ε2 allele confers protection against developing AD (Corder et al., 1994; Corder et al., 1993; Saunders et al., 1993; Verghese et al., 2011). *APOE* status has been found to modulate the onset of extracellular amyloid plaque deposition, one of the key pathognomonic features of the disease (Morris et al., 2010; Reiman et al., 2009). Strong evidence demonstrating accelerated onset of amyloid deposition in *APOE* ε4-carriers has led to the hypothesis that *APOE* genotype

differentially modulates AD risk and onset through effects on Aβ metabolism (Morris et al., 2010; Reiman et al., 2009; Schmechel et al., 1993; Tiraboschi et al., 2004). Consistent with this hypothesis, we and others have reported human apoE isoform-dependent differences in amyloid plaque deposition in APP-transgenic mice (E4 > E3 > E2) (Bales et al., 2009; Dodart et al., 2005; Fagan et al., 2002; Fryer et al., 2005b; Holtzman et al., 2000a). Although it has been hypothesized that apoE isoforms differentially modulate Aβ accumulation through effects on Aβ clearance, direct in vivo evidence demonstrating apoE isoform-dependent differences in brain Aβ clearance or synthesis has been lacking. Here, we provide in vivo evidence that apoE isoforms differentially modulate brain Aβ burden in a manner that corresponds to early apoE isoform-dependent differences in Aβ clearance. Specifically, we used in vivo microdialysis to measure the concentration of soluble Aβ and its clearance from the brain interstitial fluid (ISF) of young and aged PDAPP/TRE mice. This mouse model of β-amyloidosis overexpresses human APP carrying an autosomal dominant familial AD-linked mutation (V717F) and also expresses each of the human apoE isoforms under the control of the mouse apoE regulatory elements. We found that the soluble Aβ concentration in ISF and its clearance depends on the human apoE isoform expressed in a manner that parallels the pattern of Aβ deposition in old PDAPP/TRE mice. Finally, using an in vivo stable isotopic labeling kinetics technique, we found no differences in fractional synthesis rates (FSRs) of Aβ among PDAPP/TRE mice, consistent with biochemical evidence suggesting no apoE isoform-dependent changes in amyloidogenic processing of APP. Together, our results provide direct in vivo evidence for a

mechanism whereby apoE isoform-dependent differences in Aβ clearance modulate the onset of Aβ accumulation in transgenic mice and in humans.

RESULTS

Biomarkers of cerebral Aβ deposition differ according to *APOE* genotype in humans

Several groups have now validated molecular and neuroimaging biomarkers of the neuropathological hallmarks of AD (Fagan et al., 2006; Fagan et al., 2007; Jack et al., 2008; Rowe et al., 2007; Shaw et al., 2009). In particular, low concentrations of Aβ42 in the cerebrospinal fluid (CSF) reflect the presence of cerebral Aβ deposition, likely as a result of Aβ42 being sequestered into amyloid plaques, changing the equilibrium between the brain and CSF pools of Aβ (Clark et al., 2003; Fagan et al., 2009; Sunderland et al., 2003). Additionally, the [^{11}C]-benzothiazole radiotracer, Pittsburgh Compound B (PIB), as well as other tracers, can bind to fibrillar Aβ plaques, allowing for visualization of brain amyloid in individuals during positron emission tomography (PET) (Ikonomovic et al., 2008; Klunk et al., 2004; Leinonen et al., 2008). A preponderance of evidence supports the interpretation that PIB uptake and CSF Aβ42 are reliable surrogate markers of amyloid plaque pathology in living subjects (Fagan et al., 2006; Fagan et al., 2007; Jack et al., 2008; Rowe et al., 2007; Shaw et al., 2009). A recent study revealed that CSF and neuroimaging biomarkers of amyloid pathology are more prevalent in cognitively normal *APOE* ε4-carriers relative to individuals who have no *APOE* ε4 alleles (that is, have the *APOE* ε3 and/or *APOE* ε2 alleles) (Morris et al., 2010). Additionally, the *APOE* ε4 allele increases brain amyloid burden assessed by PIB-PET imaging in a gene dose-dependent manner (Reiman et al., 2009). To study the impact of *APOE* ε2, ε3, and ε4 alleles on the development of cerebral Aβ deposition in the absence of AD dementia, we analyzed a cohort of cognitively normal individuals younger than age 70, an age after

which the presence of AD dementia may confound the analyses. From this cohort, we analyzed the concentration of Aβ42 in the CSF from *APOE* ε4/ε4, *APOE* ε3/ε4, and *APOE* ε3/ε3 individuals; because *APOE* ε2 homozygous individuals are exceptionally rare, CSF Aβ42 was analyzed in ε2/ε3 individuals. Although various demographic features of our cohort, such as age, sex, and education level, did not differ by *APOE* genotype, the mean concentration of CSF Aβ42 was significantly lower in *APOE* ε4/ε4 individuals compared to individuals of all other *APOE* genotypes in the cohort (Table 1). Given that a CSF Aβ42 concentration lower than 500 pg/mL has been utilized as a reliable threshold for the presence of cerebral Aβ deposition in humans (Fagan et al., 2009; Fagan et al., 2007; Morris et al., 2010; Tapiola et al., 2009), we determined the proportion of individuals in each genotype with CSF Aβ42 lower than 500 pg/mL. We found that there was a significantly greater proportion of *APOE* ε4/ε4 individuals with CSF Aβ42 lower than 500 pg/mL compared to *APOE* ε3/ε4, ε3/ε3, and ε2/ε3 individuals (Fig. 1A). We next identified individuals in the cohort who had received PIB-PET scans within 2 years of lumbar puncture for CSF analysis. On the basis of previous studies (Mintun et al., 2006; Morris et al., 2010), individuals with mean cortical binding potential (MCBP) for PIB >0.18 were considered PIB-positive (PIB+). We found that the proportion of PIB+ individuals also follows a strong *APOE* allele-dependent pattern (Fig. 1B). These results demonstrate a clear *APOE* allele-dependent difference in the relative frequency at which individuals exhibit molecular and neuroimaging correlates of amyloid pathology.

Aβ and amyloid deposition in old PDAPP mice is human apoE isoform-dependent

To further investigate the role of apoE isoforms in differentially modulating Aβ metabolism, we used PDAPP mice in which human apoE isoforms are expressed under control of the mouse regulatory elements (PDAPP/TRE) (Bales et al., 2009). After allowing each cohort of mice to age to 20-21 months, we immunostained brain sections using an anti-Aβ antibody (3D6) and quantified the extent of Aβ deposition covering the hippocampus. Consistent with a previous report (Bales et al., 2009), we observed marked differences in Aβ deposition depending on the isoform of apoE expressed (Fig. 2A-C). Quantification revealed that hippocampal Aβ burden in 20- to 21-month-old PDAPP/E4 mice was approximately 2-fold and 4.6-fold higher than in PDAPP/E3 and PDAPP/E2 mice, respectively (Fig. 2D). ApoE is strongly associated with the amount of fibrillar amyloid that deposits into plaques (Bales et al., 1997). Thus, we next characterized amyloid plaque load in the context of human apoE by staining adjacent brain sections from these mice with X-34, a congophilic dye that binds to amyloid. Consistent with the Aβ immunostaining pattern observed, we found that hippocampal amyloid plaque load varied according to apoE isoform (Fig. 2E-H). Together, these results provide clear evidence that apolipoprotein E4 (apoE4) increases Aβ deposition relative to apoE3 and apoE2 in a manner that closely recapitulates the human biomarker findings reported in Figure 1.

Soluble Aβ concentration and clearance in brain ISF of old mice is human apoE isoform-dependent

To investigate the mechanism by which Aβ accumulation in the brain varies according to apoE isoform in PDAPP/TRE mice, we used in vivo microdialysis to dynamically assess ISF Aβ metabolism in the contralateral hippocampus of PDAPP/TRE mice before harvesting for pathological analysis. The concentration of soluble Aβ in the ISF throughout life has been shown to be closely associated with the amount of Aβ that ultimately deposits in the extracellular space of the brain (Cirrito et al., 2003; Kim et al., 2009b; Yan et al., 2009). Because soluble ISF Aβ has been shown to closely reflect extracellular pools of Aβ (Cirrito et al., 2003; Kim et al., 2009b; Yan et al., 2009), we hypothesized that the concentration of soluble Aβ in the ISF would closely follow the pattern of Aβ deposition analyzed from the same mice in Figure 2. Hippocampal ISF was sampled in PDAPP/TRE mice for a stable baseline period during which mice were able to freely behave for the duration of the experiment. We found that the steady state concentration of ISF $A\beta_{1-x}$ (Aβ species containing the N terminus through the central domain of Aβ) varied according to apoE isoform (Fig. 3A). Specifically, the brains of PDAPP/E4 mice had significantly more Aβ in the ISF pool, approximately 2- and 3.8-fold more than PDAPP/E3 and PDAPP/E2 mice, respectively. To understand whether the apoE isoform-dependent differences in soluble Aβ concentration may be the result of altered Aβ clearance from the ISF, we performed clearance microdialysis experiments by analyzing the elimination kinetics of Aβ after halting Aβ production with a potent γ-secretase inhibitor (Cirrito et al., 2003) (Fig. 3B). We found that the half-life ($t_{1/2}$) of ISF Aβ in the hippocampus of PDAPP/E4 mice was 1.1 hours, compared to 0.71 and 0.56

hours, measured from PDAPP/E3 and PDAPP/E2 mice, respectively (Fig. 3C). These results demonstrate that the clearance of endogenous Aβ from brain ISF is impaired in old PDAPP/E4 mice relative to PDAPP/E3 and PDAPP/E2 mice.

ApoE isoform-dependent differences in Aβ concentration and clearance exist before Aβ deposition

Because changes in apoE and Aβ metabolism in the brain ISF early in life can markedly alter Aβ deposition later in life (DeMattos et al., 2004; Kim et al., 2009b), we next asked whether the Aβ deposition pattern observed in old PDAPP/TRE mice may be a result of early apoE isoform-dependent differences in ISF Aβ metabolism. To test this hypothesis, we performed in vivo microdialysis in young PDAPP/TRE mice using a sensitive zero flow extrapolation method. Theoretically, the maximum in vivo steady state concentration of an analyte being dialyzed exists at the point at which there is no flow of the perfusion buffer (Kim et al., 2009b; Menacherry et al., 1992). To obtain this value in the hippocampal ISF of PDAPP/TRE mice, we used several flow rates during microdialysis to extrapolate to the point of zero flow for each mouse (Fig. 4A). As shown in Figure 4B, the mean in vivo steady state concentration of soluble ISF Aβ was highest in PDAPP/E4 mice compared to PDAPP/E3 and PDAPP/E2 mice. The concentration of soluble ISF Aβ at each flow rate also varied strongly according to apoE isoform (Fig. S1A). To address the possibility that microdialysis probe function may differ in the context of different human apoE isoforms, we determined the percent recovery at each flow rate, which revealed no significant differences among PDAPP/TRE mice (Fig. S1B). Since the metabolite urea has been utilized as an independent measure of probe function and recovery in both human and animal brain microdialysis studies

(Brody et al., 2008; Hillered et al., 2005; Ronne-Engstrom et al., 2001; Schwetye et al., 2010), we measured the concentration of urea in the brain ISF of PDAPP/TRE mice. The concentration of urea did not differ among groups, suggesting that probe function was equivalent across experiments in PDAPP/TRE mice (Fig. S1C). Neither the levels of phosphate-buffered saline (PBS)-soluble Aβ40 nor the levels of murine APP in hippocampal lysates from young apoE knock-in mice expressing murine APP differed according to apoE isoform, suggesting that regulation of Aβ concentration by human apoE may depend on the human Aβ sequence, which differs from murine Aβ by three amino acids (Fig S2A-B). We next asked whether the concentration of the more aggregation-prone Aβ42 species varies according to human apoE isoform in young mice in the ISF pool, the site of Aβ deposition in old PDAPP/TRE mice. We found that the concentration of soluble Aβ42 was highest in young PDAPP/E4 mice compared to PDAPP/E3 or PDAPP/E2 mice (Fig. 4C). We also measured levels of PBS-soluble and PBS-insoluble Aβ40 and Aβ42 after sequential extraction of hippocampi from young PDAPP/TRE mice (Table S1). Although the overall pattern was similar to what we observed in the ISF, the effects were of lesser magnitude or nonsignificant trends were evident, perhaps suggesting the extracted pools we measured do not completely reflect the ISF pool of Aβ (Kang et al., 2009; Kim et al., 2009b).

To test the hypothesis that human apoE isoforms differentially regulate the concentration of soluble Aβ in the ISF of young PDAPP/TRE mice through effects on Aβ clearance, we performed clearance microdialysis experiments in young PDAPP/TRE mice. As shown in Figure 4D, Aβ $t_{1/2}$ measured in the hippocampal ISF of PDAPP/E4 mice is significantly longer compared to PDAPP/E3 and PDAPP/E2 mice, respectively.

We next assessed Aβ clearance in PS1ΔE9/APPswe/TRE mice, a mouse model of β-amyloidosis based on autosomal dominant AD-linked mutations in *PSEN1* and *APP* that also expresses one of the human apoE isoforms. We also observed a similar pattern of apoE isoform-dependent Aβ clearance in these mice (Fig. S3), suggesting that the clearance impairment in the context of apoE4 is not an artifact of the PDAPP transgene. Together, these results strongly suggest that the reduced clearance of Aβ from the brain ISF of PDAPP/E4 mice contributes to the increased concentration of Aβ in the ISF, likely resulting in earlier Aβ/amyloid plaque deposition. Several studies have indicated that apoE concentration varies by human apoE isoform (Kim et al., 2009a), raising the possibility that altered apoE concentration may be an endophenotype among *APOE* genotypes that regulates *APOE* allele-dependent Aβ metabolism. We analyzed individuals in our cohort whose CSF had been analyzed by multi-analyte profiling, as previously described (Craig-Schapiro et al., 2011), which revealed that the presence of one ε2 allele of *APOE* was associated with significantly increased concentrations of apoE relative to other *APOE* genotypes (Fig. S4A). The concentration of apoE in the CSF was also significantly lower in *APOE* ε4-carriers (individuals with one or two copies of *APOE* ε4) compared to *APOE* ε3/ε3 individuals, but the concentration of apoE did not differ between those who were *APOE* ε3/ε3 and those who were *APOE* ε4/ε4. Whereas apoE levels from brain homogenates were higher in PDAPP/E2 mice compared to PDAPP/E3 or PDAPP/E4 mice, levels did not differ between PDAPP/E3 and PDAPP/E4 mice (Fig. S4B). Together, these results suggest that whereas higher apoE concentration in the context of apoE2 may underlie more rapid Aβ clearance relative to apoE4, apoE concentration is unlikely to underlie Aβ clearance differences observed in the context of

apoE3 versus apoE4. Moreover, because the extent of apoE lipidation may also play a role in modulating Aβ accumulation (Wahrle et al., 2008), we assessed the size of lipidated apoE particles from the CSF of young and old PDAPP/TRE mice by native polyacrylamide gel electrophoresis (PAGE)/Western blot analysis. Regardless of apoE isoform or age, apoE particles were between 12.2nm and slightly larger than 17nm in size (Fig. S4C).

Amyloidogenic processing of APP does not vary according to human apoE isoform

In the amyloidogenic pathway of APP processing, β-secretase (BACE1) cleaves APP N-terminally at the Aβ domain, leading to the generation of sAPPβ and C99, the latter of which ultimately gives rise to the Aβ peptide. In the context of different human apoE isoforms, amyloidogenic processing of APP may vary according to apoE isoform, contributing to the differences in the concentration of ISF Aβ observed in Figure 4B. To begin to address this possibility, we compared levels of the amyloidogenic metabolite C99 in hippocampal homogenates from young PDAPP/TRE mice. As shown in a representative western blot probed with 82E1 antibody (anti-$A\beta_{1-16}$), which recognizes C99, relative levels of C99 did not differ among PDAPP/TRE mice (Fig. 5A). Quantification revealed that C99 levels did not vary significantly according to human apoE isoform (Fig. 5B). Additionally, full-length APP levels did not appear to vary significantly among groups (Fig. S5A-B). To further assess whether amyloidogenic processing differs according to apoE isoform, we measured β-secretase activity in hippocampal homogenates from young PDAPP/TRE mice. β-secretase activity was measured by monitoring the fluorescence increase that results from cleavage of a peptide based on the β-cleavage site of APP. On the basis of the quantification shown in Figure

5C, there were no significant differences in reaction velocity among PDAPP/TRE mice, suggesting that apoE isoform-dependent differences in β-secretase activity are unlikely to account for differences in soluble ISF Aβ concentration in young PDAPP/TRE mice. Overall, our results in PDAPP/TRE mice are consistent with a previous in vitro study showing no effect of apoE isoforms on APP processing (Biere et al., 1995).

Rates of Aβ synthesis do not differ according to human apoE isoform

To sensitively assess the rates of Aβ synthesis in the context of human apoE isoforms in PDAPP/TRE mice, we adapted an in vivo stable isotopic labeling kinetics technique previously described in humans (Bateman et al., 2006). Briefly, young PDAPP/TRE mice were intraperitoneally injected with the stable isotope-labeled amino acid [$^{13}C_6$]-leucine, which crosses the blood-brain barrier and incorporates into newly synthesized APP/Aβ during normal protein synthesis in the central nervous system. We next sacrificed mice at 20 and 40 minutes after the injection and immunoprecipitated total Aβ from brain lysates using HJ5.2, an anti-$A\beta_{13\text{-}28}$ antibody. After trypsin digestion of immunoprecipitated Aβ, samples were submitted to liquid-chromatography mass spectrometry (LC-MS), allowing quantification of the relative abundance of labeled to unlabeled Aβ by analyzing mass shifts of predicted MS/MS ions in the spectra (Fig. 6A). To accurately quantify and calibrate the mass spectrometry signals from mouse brain samples, we used cell-secreted Aβ to generate a standard curve based on a known quantity of Aβ labeled with [$^{13}C_6$]-leucine (Fig. 6B). We next calculated fractional synthesis rates (FSR) of Aβ based on the rate of increase in the amount of labeled to unlabeled Aβ between 20 and 40 minutes after injection, normalized to the average enrichment of plasma leucine. We found no significant differences in Aβ FSRs among

young PDAPP/TRE mice (Fig. 6C), strongly suggesting that apoE isoforms do not differentially modulate Aβ synthesis in vivo.

DISCUSSION

Despite significant advances in our understanding of the pathological events leading to AD, the causes of Aβ accumulation are only reasonably well understood for a small subset of individuals with AD who have autosomal dominant mutations, resulting in early-onset, familial AD. Most AD cases are sporadic, and in these individuals, the factors leading to Aβ accumulation are not well understood. Because effective AD treatments will likely depend on intervening during the preclinical (presymptomatic) phase of AD (Holtzman, 2008; Perrin et al., 2009), understanding how environmental and genetic risk factors modulate pathological hallmarks of the disease will be critical. The strongest genetic risk factor for late-onset, sporadic AD is the *APOE* ε4 allele, which markedly increases risk and reduces the age of onset (Roses, 1996), likely by accelerating the onset of brain Aβ accumulation (Morris et al., 2010; Reiman et al., 2009; Schmechel et al., 1993; Tiraboschi et al., 2004). Indeed, we showed in a cohort of cognitively normal individuals less than 70 years of age that biomarkers of brain amyloid accumulation were present at a relative frequency that corresponded to *APOE* genotype, that is, ε4 > ε 3 > ε 2. Consistent with this observation, we found that old PDAPP/TRE mice developed Aβ/amyloid deposition in an apoE isoform-dependent pattern, that is, E4> E3> E2, a finding that extends previous reports of apoE isoform-dependent Aβ deposition in various mouse models (Bales et al., 2009; Fagan et al., 2002; Fryer et al., 2005b; Holtzman et al., 2000a). Because the concentration of Aβ in the extracellular space of the brain reflects a balance between its synthesis and clearance rates, we hypothesized that *APOE* genotype differentially modulates Aβ accumulation through effects on Aβ clearance and/or synthesis. To test this hypothesis, we used novel in vivo

methodologies to measure endogenous brain Aβ clearance and synthesis in PDAPP mice expressing human apoE isoforms under control of the endogenous mouse *APOE* promoter. Using in vivo microdialysis, we found that the concentration of ISF Aβ in the hippocampus of young and old PDAPP/E4 mice was greater than in PDAPP/E3 or PDAPP/E2 mice, likely as a result of reduced Aβ clearance in PDAPP/E4 mice. ApoE isoform-dependent Aβ clearance was also observed in PDAPP/TRE mice before the onset of Aβ accumulation. To investigate the impact of apoE isoforms on Aβ synthesis, we developed a sensitive method to measure the FSR of brain Aβ in vivo, adapted from the stable isotopic labeling kinetics technique recently utilized by our group in humans (Bateman et al., 2006). Using this technique, we found that the fractional rates of brain Aβ synthesis from young PDAPP/TRE mice did not differ according to the human apoE isoform expressed, consistent with our biochemical results showing that amyloidogenic processing of APP did not vary by human apoE isoform. Our results strongly suggest that *APOE* genotype differentially modulates the onset of Aβ accumulation via differential regulation of Aβ clearance, although the cellular and molecular mechanisms underlying this regulation remain unclear.

Once the link between *APOE* genotype and AD risk had been described, several groups focused on characterizing the putative apoE/Aβ interaction and the extent to which this interaction influenced the aggregation of Aβ in vitro. While our results suggest that apoE isoforms differentially regulate Aβ accumulation via effects on Aβ clearance, we cannot exclude the possibility that apoE isoforms also modulate Aβ accumulation by directly facilitating Aβ fibrillization. For example, lipid-free apoE4 was found to facilitate Aβ fibrillization in vitro to a greater degree compared to apoE3 [(Ma et

al., 1994; Wisniewski et al., 1994); see (Kim et al., 2009a) for a review]. Perhaps due to differences in experimental conditions, others have reported that apoE isoforms inhibit the process of Aβ aggregation (Beffert and Poirier, 1998; Kim et al., 2009a; Wood et al., 1996), making it difficult to interpret whether they differentially modulate Aβ accumulation in vivo. Several in vitro studies have demonstrated that lipidated apoE2 and apoE3 bind Aβ with greater affinity compared to apoE4 (Aleshkov et al., 1997; Kim et al., 2009a; LaDu et al., 1994; Tokuda et al., 2000; Yang et al., 1997). This observation has prompted some to hypothesize that the stronger interaction between Aβ and apoE2 or apoE3 relative to apoE4 may result in greater Aβ clearance, consistent with the clearance pattern we observed in vivo in the current study. Indeed, several studies have demonstrated that Aβ transport from brain into blood is altered when complexed to human apoE (Bell et al., 2007; Deane et al., 2008). A recent study wherein apoE/Aβ complexes were microinjected into wildtype mouse brain revealed that Aβ bound to apoE4 is cleared more slowly than when Aβ is complexed to apoE3 or apoE2 (Deane et al., 2008). One study found that antagonizing the apoE/Aβ interaction with a small peptide decreased Aβ pathology in the mouse brain, further suggesting that the apoE/Aβ interaction may be relevant to Aβ clearance in vivo (Sadowski et al., 2006). Additional studies are needed to characterize the extent of the apoE/Aβ interaction under more physiological conditions and whether differential apoE/Aβ interactions may underlie our current in vivo results. Aside from Aβ egress from brain to blood, in vitro studies have suggested that cellular uptake and degradation of Aβ may also represent clearance mechanisms that are regulated by human apoE (Beffert et al., 1998; Jiang et al., 2008; Yang et al., 1999). One recent in vitro study found that human apoE isoforms differed in

their ability to facilitate neprilysin-mediated degradation of Aβ42 within microglia, with apoE4 being the least effective in facilitating Aβ degradation compared to apoE2 or apoE3 (Jiang et al., 2008).

Although there are some conflicting studies (Korwek et al., 2009), several groups have reported that the concentration of apoE in the brains of human apoE knock-in mice varies in an apoE isoform-dependent manner, that is, E2 > E3 > E4 (Bales et al., 2009; Fryer et al., 2005a; Riddell et al., 2008). Together with our present results, the isoform-dependent pattern of apoE concentration in humans and in mice raises the possibility that apoE concentration alone may play a role in the pattern of Aβ clearance and subsequent Aβ accumulation, though apoE concentration differences are unlikely to completely account for Aβ metabolism differences in the setting of apoE3 versus apoE4 (Bales et al., 2009). The impact of structural differences among apoE isoforms (Hatters et al., 2009), especially differences in relative affinities for various apoE receptors, may also contribute to differences in Aβ clearance. Future studies delineating the precise contribution of both apoE concentration and isoform may directly bear on therapeutic strategies aimed at targeting apoE. Using a mouse model of human apoE-dependent β-amyloidosis, our present results may be directly relevant to human studies. For example, using in vivo stable isotopic labeling kinetics, our group recently reported that CSF Aβ clearance and not synthesis is impaired in a small cohort of late-onset AD patients, though the effect of *APOE* genotype was not assessed (Mawuenyega et al., 2010a). Coupled with this recent finding, our present results motivate further investigation as to whether Aβ clearance in humans is modulated by *APOE* genotype. These findings further motivate the development of therapies that increase brain Aβ clearance.

MATERIALS AND METHODS

CSF Aβ42, apoE, and PIB-PET assessment in humans

Participants were cognitively normal volunteers (between 43 and 70 years of age at time of participation) for a longitudinal memory and aging study at the Washington University Alzheimer's Disease Research Center. Cognitive status was assessed by clinical evaluation based on whether intra-individual decline existed in performance of typical activity (as a result of loss of cognitive function). "Cognitively normal" corresponds to a "0" on the Clinical Dementia Rating (CDR) scale. TaqMan assays (Applied Biosystems, Foster City, US) for both rs429358 (ABI#C_3084793_20) and rs7412 (ABI#C_904973_10) were used for *APOE* genotyping. The allelic discrimination analysis module of ABI Sequence Detection Software was used for allele calling. Positive controls for the six possible *APOE* genotypes were included on the genotyping plate. Individuals with confirmed causative mutations were excluded. CSF Aβ42 was measured using the Innotest Aβ42 ELISA kit (Innogenetics, Ghent, Belgium) according to previous procedures (Morris et al., 2010). CSF apoE concentration in individuals from our cohort for whom CSF had been analyzed by the company Rules Based Medicine was quantified using multi-analyte profiling (Craig-Schapiro et al., 2011). PIB-PET assessment, performed within 2 years of lumbar puncture to collect CSF, was performed as reported previously (Mintun et al., 2006). All procedures were approved by Washington University's Human Protection Office and written informed consent was obtained from all participants prior to study entry.

Animals

Homozygous PDAPP (APPV717F) mice lacking apoE on a mixed background comprised of DBA/2J, C57BL/6J, and Swiss Webster were crossed with mice expressing *APOE* ε2, ε3, and ε4 under control of mouse regulatory elements on a C57BL/6J background (gift from P. Sullivan at Duke University) (Bales et al., 2009). Resulting mice were intercrossed to generate homozygous PDAPP/TRE mice, which were then maintained via a vertical breeding strategy. Male and female PDAPP/TRE mice were used throughout experiments. For experiments involving TRE mice with murine APP, 2.5 month-old, male littermates on a C57BL/6J background from each *APOE* genotype were purchased from Taconic. All animal procedures were performed according to protocols accepted by the Animal Studies Committee at Washington University School of Medicine.

Tissue preparation and quantification of Aβ/amyloid burden

In vivo microdialysis was performed in the left hemisphere of 20- to 21-month-old mice, after which mice were immediately perfused transcardially, fixing brains in 4% paraformaldehyde overnight. After placing brains in 30% sucrose, the contralateral (noncannulated) hemisphere was sectioned on a freezing-sliding microtome. Serial 50 μm coronal sections were taken from the rostral anterior commissure through the caudal extent of the hippocampus, staining sections with biotinylated 3D6 antibody (anti-$A\beta_{1-5}$) for Aβ immunostaining quantification and X-34 dye for amyloid load quantification. Slides were scanned in batch mode using the NanoZoomer slide scanner system (Hamamatsu Photonics), capturing images in brightfield mode (Aβ immunostaining) or fluorescent mode (X-34). NDP viewer software was used to export images from slides before quantitative analysis using Image J software [National Institutes of Health (NIH)]. Using three sections per mouse separated each by 300 μm (corresponding to bregma -1.7,

-2.0, and -2.3 mm in mouse brain atlas), we determined the percentage of area occupied by immunoreactive Aβ or amyloid (X-34-positive signal) in a blinded fashion, thresholding each slide to minimize false-positive signal, as described (Kim et al., 2009b).

In vivo microdialysis

In vivo microdialysis in 20- to 21-month-old and 3- to 4-month-old PDAPP/TRE mice was performed essentially as described to assess steady state concentrations of various analytes in the hippocampal ISF with a 38 kDa cut-off dialysis probe (Bioanalytical Systems, Inc.) (Cirrito et al., 2003; DeMattos et al., 2004). ISF exchangeable $A\beta_{1-X}$ ($eA\beta_{1-X}$) was collected using a flow rate of 1.0 μl/min, whereas ISF $eA\beta_{x-42}$ and urea were collected using a flow rate of 0.3 μl /min. For clearance experiments, a stable baseline of ISF $eA\beta_{1-X}$ concentration was obtained with a constant flow rate of 1.0 μl/min before intraperitoneally injecting each mouse with 10 mg/kg of a selective γ-secretase inhibitor (LY411,575), which was prepared by dissolving in dimethyl sulfoxide (DMSO)/PBS/propylene glycol. The elimination of $eA\beta_{1-X}$ from the ISF followed first-order kinetics; therefore, for each mouse, $t_{1/2}$ for eAβ was calculated using the slope, k', of the linear regression that included all fractions until the concentration of eAβ stopped decreasing ($t_{1/2} = 0.693/k$, where $k = 2.303k'$). Microdialysis using the zero flow extrapolated method was performed by varying the flow rates from 0.3 μl/min to 1.6 μl/min, as described (Kim et al., 2009b). Zero flow data for each mouse were fit with an exponential decay regression with GraphPad Prism 5.0 software (Menacherry et al., 1992).

Quantitative measurements of ISF eAβ

Quantitative measurements of Aβ collected from in vivo microdialysis fractions were performed using sensitive sandwich ELISAs. For human $A\beta_{1-x}$ quantification, ELISA plates were coated with m266 antibody (anti-$A\beta_{13-28}$), and biotinylated 3D6 antibody (anti-$A\beta_{1-5}$) was used for detection. For $A\beta_{x-42}$ ELISAs, HJ7.4 (anti-$A\beta_{35-42}$) antibody was used to capture, followed by biotinylated HJ5.1 antibody to detect (anti-$A\beta_{13-28}$).

Biochemical analyses of hippocampal homogenates from young PDAPP/TRE mice

After transcardial perfusion with heparinized PBS, brain tissue was microdissected and immediately frozen at -80°C. Hippocampal tissue was manually dounce-homogenized with 75 strokes in radioimmunoprecipitation assay (RIPA) buffer [50 mM tris-HCl (pH 7.4), 150 mM NaCl, 0.25% deoxycholic acid, 1% NP-40, 1 mM EDTA] containing a cocktail of protease inhibitors (Roche). Total protein concentration in hippocampal homogenates was determined with a BCA protein assay kit (Pierce). Equivalent amounts of protein (50 μg) were loaded on 4-12% bis-tris gels (Invitrogen) for SDS-PAGE before transferring protein to 0.2-μm nitrocellulose membranes. Immediately after transfer, blots were boiled for 10 min before blocking and incubation with 82E1 antibody (anti-$A\beta_{1-16;}$ IBL) to detect C99. Loading was normalized by stripping blots and re-probing with α-tubulin antibody (Sigma). Normalized band intensities were quantified using Image J software (NIH).

β-secretase activity in hippocampal lysates was assessed using a commercially available kit (#P2985; Invitrogen) that relies on fluorescence resonance energy transfer (FRET) that results from β-secretase cleavage of a fluorescent peptide based on the APP sequence

(Rhodamine-EVNLDAEFK-Quencher). Briefly, 5 μg of protein per sample was mixed with sample buffer and β-secretase substrate, monitoring fluorescence signal every minute for 120 minutes with a Synergy2 BioTek (BioTek Instruments, Inc.) plate reader (Ex_{545nm}/Em_{585nm}). Because the kinetics of the reaction for all samples were reliably linear in the 20- to 60-min interval, reaction velocity [relative fluorescence units (RFUs) per minute] was calculated and reported over this interval for all samples. Specificity of β-secretase activity was validated using a commercially available β-secretase inhibitor.

In vivo stable isotopic labeling kinetics

FSRs of Aβ were measured in hippocampal lysates from young PDAPP/TRE mice with a method adapted from the in vivo stable isotopic labeling kinetics technique we have previously described in humans (Bateman et al., 2006) (detailed Materials and Methods available in the Supplementary Material). Briefly, after mice were injected intraperitoneally with [$^{13}C_6$]-leucine (200 mg/kg), brain tissue harvesting and plasma collection was performed 20 and 40 min after injection. Whole hippocampus was lysed with 1% Triton X-100 lysis buffer containing protease inhibitors, and Aβ in the extracts was immunoprecipitated with HJ5.2 antibody (anti-$Aβ_{13-28}$). After trypsin digestion of immunoprecipitated Aβ, LC-MS was performed to measure the relative abundance of labeled to unlabeled tryptic Aβ peptide, which was calibrated with a standard curve of Aβ secreted from H4 APP695ΔNL neuroglioma cells. FSR curves were then generated based on the amount of labeled to unlabeled Aβ present 20 and 40 min after [$^{13}C_6$]-leucine injection, normalized to the amount of free leucine in the plasma, which was measured by gas chromatography (GC)-MS.

Statistical analysis

Unless indicated otherwise, differences among group means were assessed using a one-way analysis of variance (ANOVA) followed by Tukey's post hoc test for multiple comparisons when the ANOVA was significant. Levels of significance were indicated as follows: *P<0.05, **P<0.01, ***P<0.001. Analyses were performed using GraphPad Prism 5.0 software; human data were analyzed using SAS 9.2 software.

SUPPLEMENTARY METHODS AND MATERIALS

In vivo stable isotopic labeling kinetics

Mice were intraperitoneally injected with 200 mg/kg of stable isotope $^{13}[C_6]$-labeled leucine (Cambridge Isotope Laboratories, Inc., Andover MA). 20 or 40 minutes following injection, mice were transcardially perfused and tissue was immediately harvested and frozen at -80°C. Whole hippocampus from each mouse was lysed using 1% Triton X-100 lysis buffer, pH 7.6 (150mM NaCl, 50mM Tris-HCl, 1% Triton X-100 with complete protease inhibitor cocktail [Roche, Indianapolis, IN]). Aβ was immunoprecipitated from lysates using HJ5.2 antibody (anti-$A\beta_{13-28}$) that had been conjugated to Protein G-Sepharose 4 fast flow beads (GE Healthcare, Pittsburgh, PA). To prevent antibody elution from the beads, antibodies were crosslinked with freshly prepared 20 mM dimethyl pimelinidate (Sigma, St. Louis, MO). After three washes each of PBS and triethylammonium bicarbonate (Sigma, St. Louis, MO), Aβ was eluted twice with 100% formic acid. Formic acid was then dried, resuspending Aβ with 20% acetonitrile in 25mM triethylammonium bicarbonate prior to trypsin digestion (Promega, Madison, WI); samples were stored at 4°C prior to analysis.

Samples were then subjected to quantitative mass spectrometry to measure Aβ peptide containing $^{13}[C_6]$-leucine and $^{12}[C_6]$-leucine using a TSQ Vantage Triple Stage Quadrupole mass spectrometer, controlled by Xcalibur software (ThermoFisher Scientific, San Jose, CA) and equipped with a PST-MS nanospray source (Phoenix S&T, Chester, PA). Sample injection and liquid chromatography gradients were performed using a NanoLC-2D-Ultra (Eksigent Technologies, Dublin, CA). Prior to analysis, the TSQ Vantage was tuned to select the Aβ tryptic peptide LVFFAEDVGSNK (m/z =

663.340) and optimal conditions were set for a capillary temperature of 350°C, with a spray voltage of 1200 V. Peak widths for Q1 and Q3 were set at 2.0 Da, with a collision pressure in Q2 of 2.0 mTorr and a collision energy of 26 V. For the Aβ tryptic peptide LVFFAEDVGSNK (m/z = 663.340) and its $^{13}[C_6]$-leucine labeled form (m/z = 666.350), the MRM transition ions monitored were 819.384, 966.452 and 1113.521. These MRM transition ions were the three most intense ions and were validated using H4 APP695ΔNL cell-secreted Aβ standards. Standards were prepared by incubating H4 APP695ΔNL neuroglioma cells with known amounts of labeled and unlabeled leucine, followed by collection of media containing newly synthesized Aβ. 5-μL aliquots of samples containing Aβ immunoprecipitated from mouse hippocampal lysates were injected into a Zorbax SB300-C18 3μm particle-size nano-column (Agilent Technologies, Santa Clara, CA), packed in-house (0.15 x 150 mm). Peptide mixtures were separated at a flow rate of 500 nL/min using a gradient mixture of solvents A and B. Solvent A was 0.1% formic acid in water; solvent B was 0.1% formic acid in acetonitrile. The separation gradient program used for the nano-column was as follows: 15% to 65% B in 10 min, 65% to 95% B in 5 min, followed by a gradient back to 15% B in 5 min. The column was re-equilibrated for another 5 min to prepare for injection of the next sample.

Gas chromatography/mass spectrometry (GC/MS) was performed to measure free leucine tracer-to-tracee ratio (TTR) in plasma collected from PDAPP/TRE mice prior to harvesting brain tissue, as previously described (Patterson et al., 1993). Plasma proteins were precipitated with ice-cold acetone, followed by extraction of lipids with hexane solvent. The resulting aqueous fraction was then dried under vacuum (Savant

Instruments, Farmingdale, NY). Free leucine TTR was measured by GC/MS by monitoring ions at m/z ratios of 200 and 203, corresponding to unlabeled and labeled leucine, respectively. Relative fractional synthesis rates of Aβ were calculated from the slope of the Aβ TTR over average leucine enrichment at the 20 min timepoint.

Quantitative measurements of ISF Urea concentration

ISF urea collected in microdialysis fractions was quantified using a commercially available colorimetric assay (Quanti-Chrom Urea Assay Kit, BioAssay Systems, Hayward, CA), as previously described (Brody et al., 2008; Schwetye et al., 2010).

Western blot analysis of young PDAPP/TRE and TRE hippocampal homogenates

Hippocampal tissue from young PDAPP/TRE or TRE mice was manually dounce-homogenized with 75 strokes in radioimmunoprecipitation assay (RIPA) buffer (50mM Tris-HCl; pH 7.4, 150mM NaCl, 0.25% deoxycholic acid, 1% NP-40, 1mM EDTA) containing a cocktail of protease inhibitors (Roche, Indianapolis, IN). For assessment of APP levels in PDAPP/TRE mice, equivalent amounts of protein (7.5 μg) were loaded on 4-12% Bis-Tris gels (Invitrogen, Carlsbad, CA) for SDS-PAGE before transferring protein to 0.2 μm nitrocellulose membranes. Full-length APP (FL-APP) was probed using 6E10 antibody (Covance, Princeton, NJ). For measurement of murine APP in TRE mice, equivalent amounts of protein (25 μg) were loaded on 4-12% Bis-Tris gels (Invitrogen, Carlsbad, CA) for SDS-PAGE before transferring protein to 0.2 μm nitrocellulose membranes. Immediately following transfer, blots were boiled for 10 minutes prior to blocking and incubation with CT20 antibody (anti-APP C-terminal 20 amino acids; Calbiochem) to detect murine APP. Loading for 6E10 or CT20 westerns

was normalized by stripping blots and re-probing with α-tubulin antibody (Sigma, St. Louis, MO). Normalized band intensities were quantified using Image J software (NIH).

Sandwich ELISA for Aβ and apoE from CSF and sequentially extracted hippocampal tissue

Frozen hippocampi from young PDAPP/TRE mice were sequentially homogenized with PBS and 5M Guan-Tris buffer (pH 8.0) containing a cocktail of protease inhibitors (Roche), following by centrifugation at 4°C at 14,000rpm for 30 min. Levels of PBS-soluble (soluble) and Guan-soluble (insoluble) Aβ40 and Aβ42 were measured using sandwich ELISAs; HJ2 (anti-$A\beta_{35-40}$) or HJ7.4 (anti-$A\beta_{37-42}$) were used as capture antibodies, followed by detection with biotinylated HJ5.1 (anti-$A\beta_{13-28}$). ApoE levels in Triton X-100-soluble hippocampal extracts or CSF were quantified using an apoE sandwich ELISA (HJ6.2 for capture and HJ6.1B for detection) with recombinant human apoE as a standard.

Native-polyacrylamide gel electrophoresis/western blot analysis of apoE

Fresh CSF was isolated from the cisterna magna of young and old PDAPP/TRE mice before quantification using apoE sandwich ELISA. Equal amount of apoE (3 ng), determined by ELISA, was loaded in each lane of 4-20% Tris-glycine gel for Native-PAGE (100V at 4°C for 14 hours) before transfer to 0.2 μm nitrocellulose membranes. Blots were probed with anti-apoE antibody (Calbiochem), and migration pattern of lipoproteins in the CSF was assessed using protein mixture of estimated hydrodynamic radii as a standard (GE/Amersham).

	APOE genotype			
	ε2/ε 3	**ε3/ε3**	**ε3/ε4**	**ε4/ε4**
n	32	151	81	19
Female (%)	62.50	64.24	67.90	63.16
Caucasian (%)	87.50	92.05	90.12	84.21
Age at LP, yrs, (SD)	59.28 (7.13)	60.72 (7.17)	60.51 (7.80)	57.58 (8.85)
MMSE	29.28 (0.96)	29.37 (0.94)	29.38 (0.96)	29.32 (1.16)
Education, yrs, (SD)	15.69 (2.76)	15.92 (2.62)	15.83 (2.31)	16.53 (3.42)
Aβ42, pg/mL, (SD)	755.65‡,*** (212.85)	695.58*** (243.87)	619.58** (193.79)	437.39 (183.53)
Tau, pg/mL, (SD)	253.33 (114.68)	248.72 (126.48)	267.54 (131.89)	244.13 (90.58)
pTau, pg/mL, (SD)	50.72 (17.76)	48.18 (19.71)	55.86 (28.83)	51.45 (13.62)

Table 1. Demographic characteristics and biomarker information for cognitively normal individuals according to APOE genotype. Values represent means ± SD. When one-way ANOVA was significant, pair-wise comparisons of APOE genotypes were made with Tukey's post hoc test; only significant differences were indicated (‡$P < 0.05$; **$P < 0.01$; ***$P < 0.001$). ‡ denotes significant difference compared to *APOE* ε3/ε4. ** or *** denotes significant difference compared to *APOE* ε4/ε4. MMSE, Mini Mental State Examination from 0 to 30; LP, lumbar puncture.

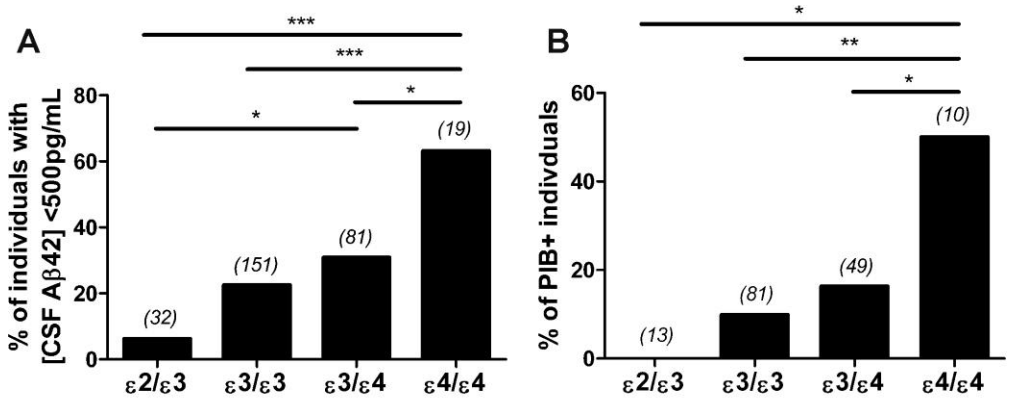

Figure 1. Biomarkers of amyloid differ according to *APOE* genotype in cognitively normal individuals. (A) Percentage of individuals (n=283) with [CSF Aβ42] < 500 pg/mL according to the following *APOE* genotypes: ε2/ε3, ε3/ε3, ε3/ε4, and ε4/ε4. Number in parentheses indicates number of individuals for each group. **(B)** Percentage of PIB+ individuals (n=153) according to *APOE* genotype: ε2/ε3, ε3/ε3, ε3/ε4, and ε4/ε4. Individuals with mean cortical binding potential for Pittsburgh compound B (MCBP) > 0.18 were considered PIB+. Number in parentheses indicates number of individuals for each group. χ^2 analyses for proportions in (A) ($\chi^2(3)=22.1785$, $P=5.99 \times 10^{-5}$) and (B) ($\chi^2(3)=14.4735$, $P=2.33 \times 10^{-3}$) were performed; follow-up χ^2 tests for pairwise comparisons of proportions were performed using Benjamini and Hochberg's linear step-up adjustment to control for type I error. *P<0.05, **P<0.01, ***P<0.001.

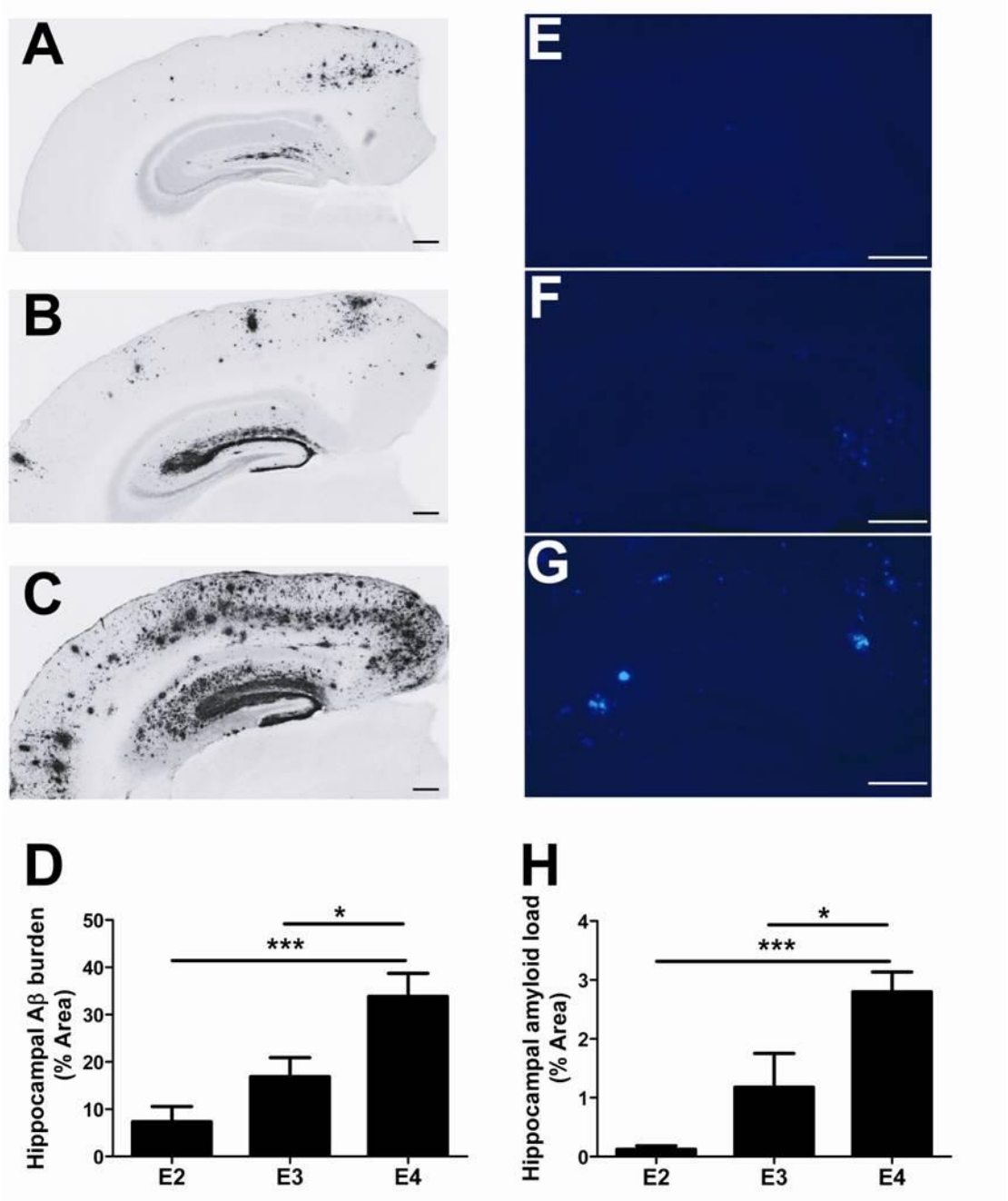

Figure 2. Aβ/amyloid deposition varies according to apoE isoform in old PDAPP/TRE mice. (A-C) Representative coronal brain sections from 20- to 21-month-old, sex-matched PDAPP/E2 **(A)**, PDAPP/E3 **(B)**, and PDAPP/E4 **(C)** mice. Aβ immunostaining was performed using anti-Aβ antibody (biotinylated-3D6). Scale bars, 50 μm. **(D)** Quantification of the area of the hippocampus occupied by Aβ

immunostaining (n=7 mice/group). *P<0.05, **P<0.01. **(E-G)** Representative coronal brain sections from 20- to 21-month-old PDAPP/E2 **(E)**, PDAPP/E3 **(F)**, and PDAPP/E4 **(G)** mice. Amyloid was detected using the congophilic fluorescent dye, X-34. Scale bars, 50 μm. **(H)** Quantification of the area of hippocampus occupied by X-34 staining (n=7 mice/group). When one-way ANOVA was significant, differences among groups were assessed using Tukey's post hoc test for multiple comparisons *P<0.05, ***P<0.001. Values represent means ± SEM.

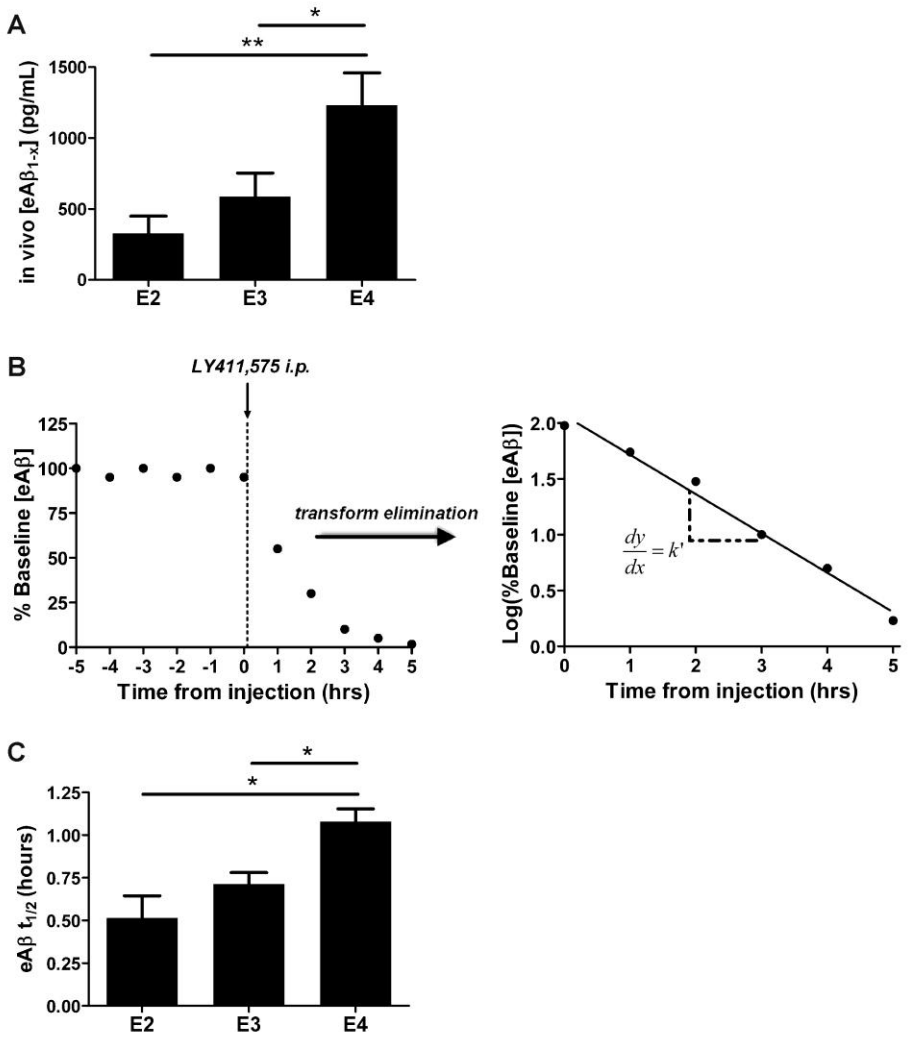

Figure 3. Soluble Aβ concentration and clearance in the brain ISF of old mice is human apoE isoform-dependent. (A) Mean steady state concentrations of $eA\beta_{1\text{-}X}$ (exchangeable Aβ) from sampling hippocampal ISF in old, sex-matched PDAPP/E2, PDAPP/E3, and PDAPP/E4 mice, measured by enzyme-linked immunosorbent assay (ELISA) (n=6 to 7 mice per group; 20 to 21 months old). **(B)** Schematic diagram of a typical clearance experiment in which a stable baseline period is obtained, followed by intraperitoneal (i.p.) injection of LY411,575 (10 mg/kg) to halt Aβ production. Aβ concentrations during the elimination phase are transformed with the common logarithm.

Log-transformed values are fit with a linear regression, allowing calculation of slope, k'. eAβ $t_{1/2}$ = 0.693/k, where k = 2.303k'. **(C)** eAβ $t_{1/2}$ from clearance experiments performed with the mice in (A) after stable baseline measurement of $eA\beta_{1-x}$. When one-way ANOVA was significant, differences among groups were assessed using Tukey's post hoc test for multiple comparisons (**P*<0.05). Values represent means ± SEM.

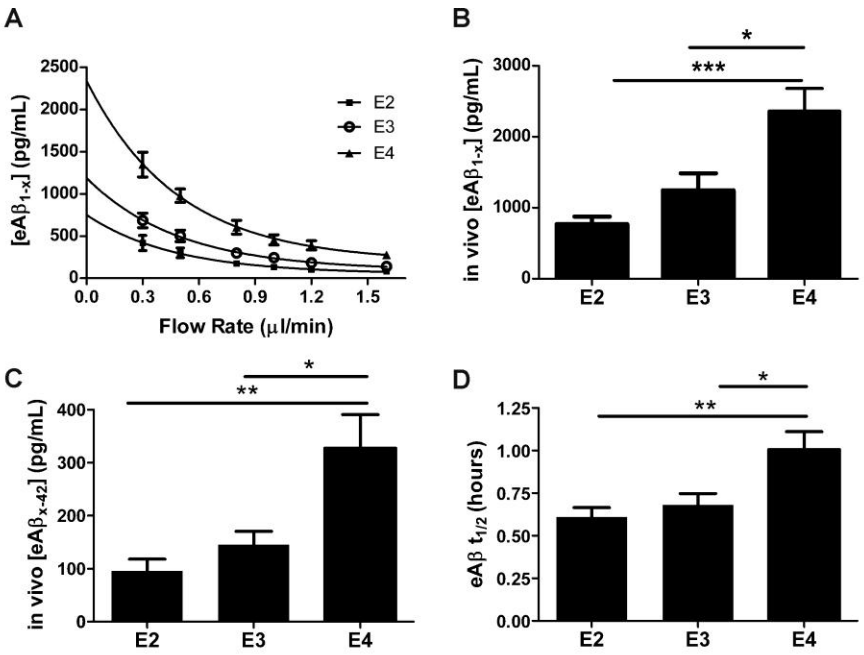

Figure 4. ApoE isoform-dependent differences in soluble Aβ concentration and clearance exist prior to the onset of Aβ deposition. (A) An exponential decay regression was used to fit the concentrations of $eA\beta_{1\text{-}x}$ measured by ELISA at each flow rate for individual mice from groups of young, sex-matched PDAPP/TRE mice (n=6 mice per group; 3 to 4 months old). The equations from the individual regressions were used to calculate $[eA\beta_{1\text{-}x}]$ at x=0 for each mouse, representing the in vivo concentration of $eA\beta_{1\text{-}x}$ recoverable by microdialysis. **(B)** Mean in vivo concentrations of $eA\beta_{1\text{-}x}$ (pg/mL) calculated from the method in (A). **(C)** Mean concentrations of $A\beta_{x\text{-}42}$ (pg/mL) collected from the hippocampal ISF of young, sex-matched PDAPP/TRE mice using a flow rate of 0.3 μl/min (n=8 mice per group; 3-4 months old). **(D)** eAβ $t_{1/2}$ from clearance experiments in young, sex-matched PDAPP/TRE mice after stable baseline measurement of $eA\beta_{1\text{-}x}$ (n=10 to 11 mice per group; 3 to 4 months old). When one-way ANOVA was significant, differences among groups were assessed using Tukey's post

hoc test for multiple comparisons *P<0.05, **P<0.01, ***P<0.001. Values represent means ± SEM.

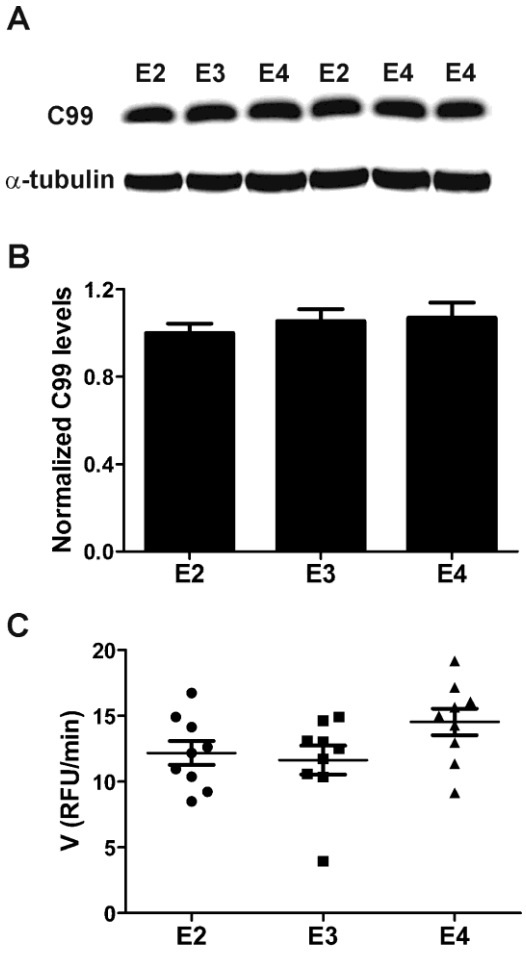

Figure 5. Amyloidogenic processing of APP does not vary according to human apoE isoform. (A) Representative Western blot of the proximal amyloidogenic metabolite, C99, from hippocampal homogenates (extracted with RIPA buffer) from young, sex-matched PDAPP/TRE mice. C99 was detected using 82E1 antibody. All bands were normalized to α-tubulin band intensity (n=9 mice per group; 3 to 4 months old). **(B)** Quantification of C99 levels after normalizing each band's intensity to α-tubulin band intensity. **(C)** Quantification of β-secretase activity in hippocampal homogenates from young PDAPP/TRE mice using a sensitive FRET assay. Homogenates were incubated with fluorescent APP substrate, resulting in β-cleavage that could be followed by fluorescence increase (emission, 585 nm). The interval over which kinetics were linear

was used for quantification of reaction velocity [relative fluorescence units (RFU)/min] for each sample. One-way ANOVA revealed no significant differences among groups. Values represent means ± SEM.

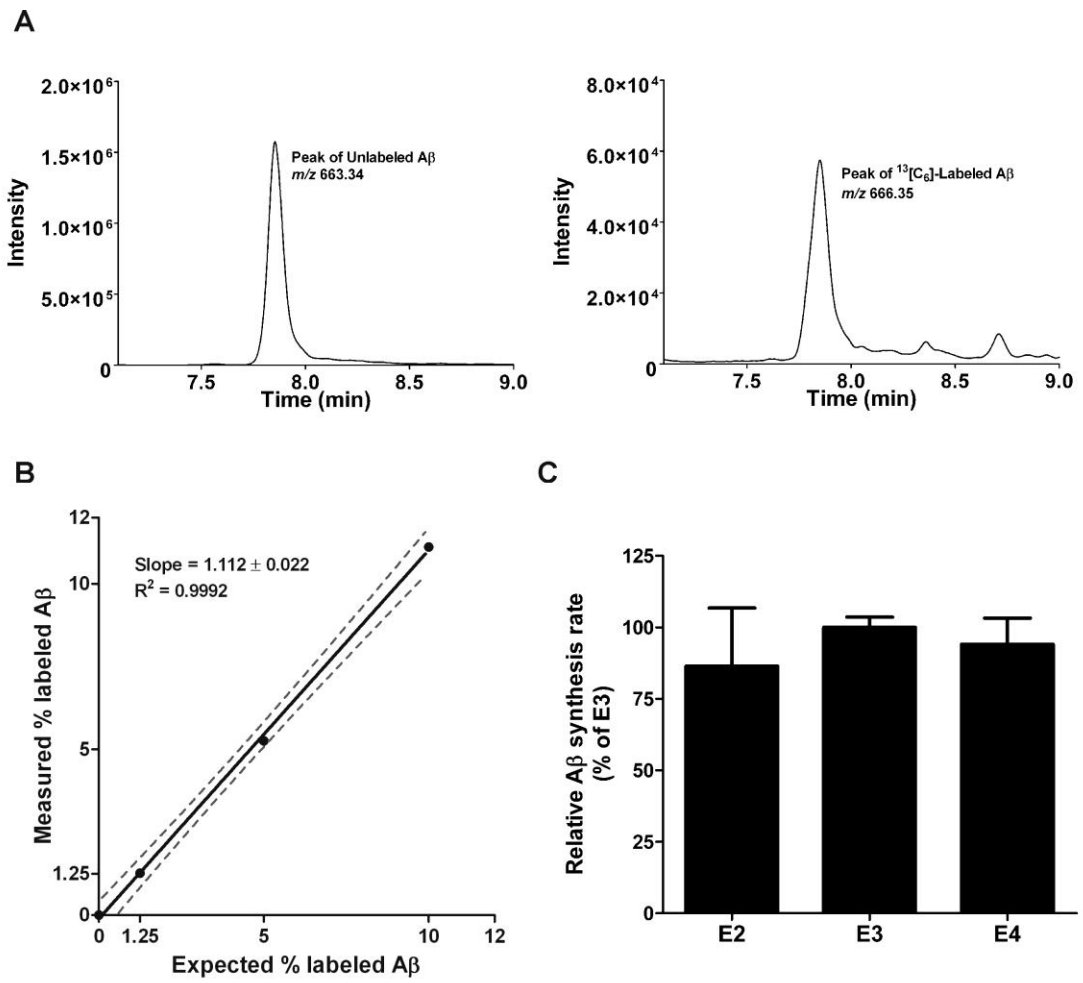

Figure 6. Rates of Aβ synthesis do not differ according to human apoE isoform in PDAPP/TRE mice. (A) Aβ detection in hippocampal lysates from young PDAPP/TRE mice by TSQ Vantage triple quadrupole mass spectrometry. Left, representative total ion count multiple reaction monitoring (MRM) peak of the unlabeled Aβ tryptic peptide, LVFFAEDVGSNK, (m/z = 663.340). Right, MRM peak for [$^{13}C_6$]-leucine labeled Aβ (m/z = 666.350). **(B)** Standard curve generated with known quantity of [$^{13}C_6$]-leucine labeled and unlabeled Aβ. Aβ secreted from H4-APP695ΔNL neuroglioma cells incubated with labeled/unlabeled leucine was immunoprecipitated with HJ5.2 antibody (anti-$A\beta_{13\text{-}28}$), followed by trypsin digestion. $A\beta_{17\text{-}28}$ fragments were analyzed on a TSQ

Vantage mass spectrometer. The expected percentage of labeled Aβ versus measured percentage was fit by linear regression. Variance is reported with 95% confidence interval. **(C)** Relative FSRs of Aβ from hippocampi of PDAPP/TRE mice intraperitoneally injected with [$^{13}C_6$]-leucine (200mg/kg) (n=5 to 6 mice per group; 4 to 5 months old). Relative FSRs of Aβ were calculated from the ratio of [$^{13}C_6$]-leucine labeled to unlabeled Aβ. [$^{13}C_6$]/[$^{12}C_6$]-Aβ ratio was normalized to the ratio of labeled to unlabeled free leucine in plasma (determined by GC-MS). Mass spectrometry data were normalized with the media standard curve in (B). One-way ANCOVA (analysis of covariance) revealed no significant differences among groups. Values represent means ± SEM.

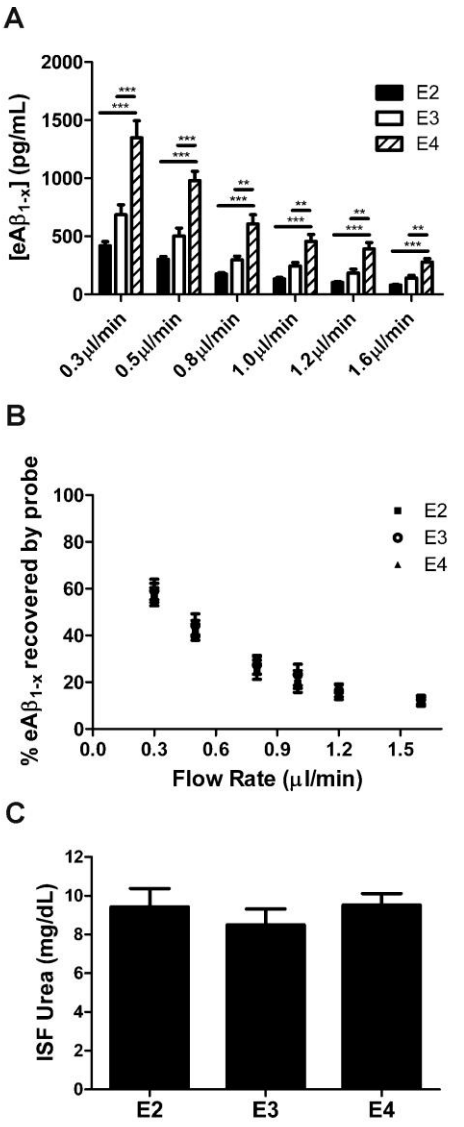

Figure S1. eA$\beta_{1\text{-}x}$ concentration measured with equivalent microdialysis probe function differs according to apoE isoform. (A) Mean concentrations of eA$\beta_{1\text{-}x}$ at each flow rate for zero flow extrapolation experiments performed in Fig. 4A. 2-way repeated-measures ANOVA was performed using genotype and flow rate as factors followed by pairwise comparisons of genotypes by flow rate using Tukey's post-hoc test (***P*<0.01, ****P*<0.001) **(B)** In vivo percent recovery by the microdialysis probe at each flow rate for each experiment in (A) was determined using the zero flow extrapolated method as

previously described (Cirrito et al., 2003; Kim et al., 2009b; Menacherry et al., 1992), revealing no significant difference in $eA\beta_{1-x}$ recovery by the probe among groups as assessed by 2-way repeated measures ANOVA with Huynh and Feldt adjustment. **(C)** Mean concentrations of urea (mg/dL) collected from the hippocampal ISF of young, sex-matched PDAPP/TRE mice using a flow rate of 0.3 μl/min (n=8 mice/group; 3-4 months old). Values represent mean ± SEM.

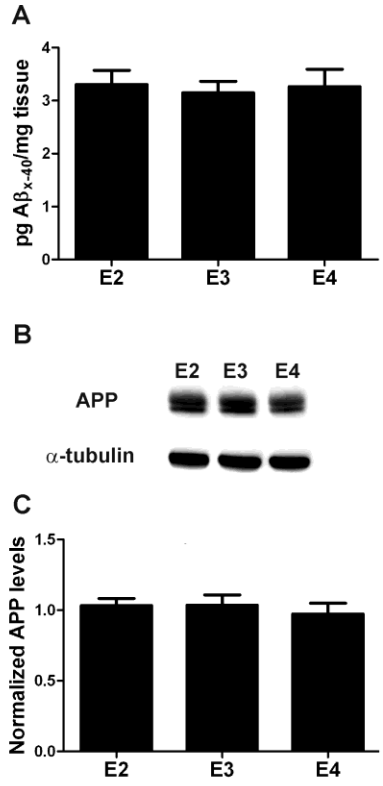

Figure S2. PBS-soluble Aβ40 levels and APP levels do not vary according to apoE isoform in the context of murine APP/Aβ. (A) Mean PBS-soluble $A\beta_{x\text{-}40}$ levels quantified by sandwich ELISA after homogenization of hippocampi from young, male TRE mice (n=5/group). 1-way ANOVA revealed no significant differences among groups. **(B)** Representative western blot probed with CT20 antibody (anti-APP) to detect murine APP from hippocampal homogenates from mice in (A). **(C)** Quantification of APP protein levels after normalization to α-tubulin band intensity (n=5/group). 1-way ANOVA revealed no significant differences among groups. Values represent mean ± SEM.

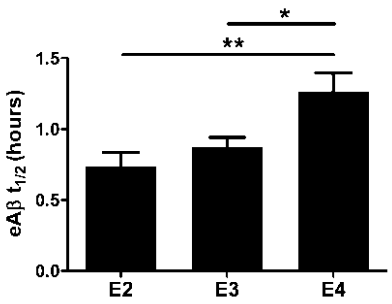

Figure S3. Soluble Aβ clearance from the ISF is apoE isoform-dependent in young PSAPP/TRE mice. Clearance microdialysis experiments were performed in young PS1ΔE9/APPswe/human apoE knockin mice (PSAPP/TRE) on a BL6/SJL/C3 background (n=5-7 mice/group; 3 months old). After stable baseline measurement of $eA\beta_{1\text{-}x}$, mice were injected with 10 mg/kg LY411,575 and $eA\beta t_{1/2}$ (hrs.) was calculated as in experiments in Fig. 3-4. 1-way ANOVA followed by Tukey's post-hoc test for multiple comparisons was performed (*P<0.05,**P<0.01). Values represent mean ± SEM.

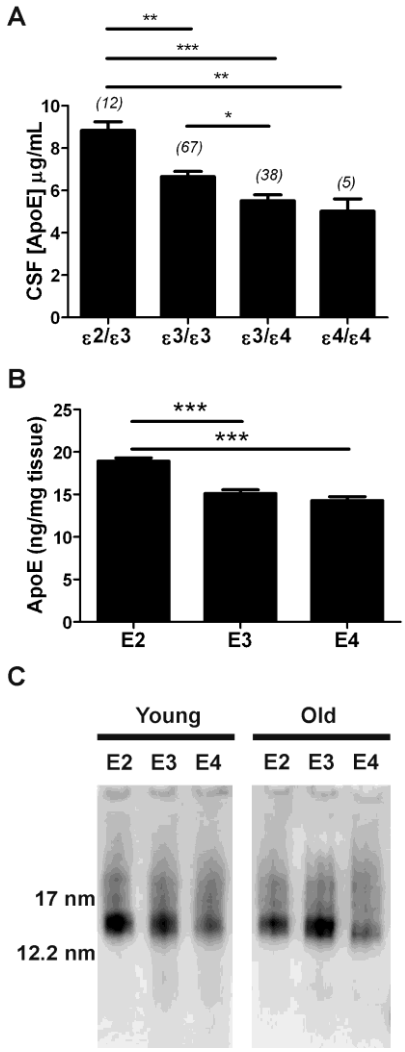

Figure S4. ApoE concentration is higher in the context of apoE2 in both humans and in PDAPP/TRE mice. (A) ApoE protein levels in the CSF of cognitively normal individuals were quantified using multi-analyte profiling. Number in parentheses indicates number of individuals in each group. Since 1-way ANOVA was significant, differences among groups were assessed using Tukey's post-hoc test for multiple comparisons (**P*<0.05, ***P*<0.01, ****P*<0.001). **(B)** ApoE protein levels measured by human apoE-specific sandwich ELISA after 1% Triton X-100 extraction of hippocampi dissected from young PDAPP/TRE mice (3.5 month-old; n=16-18 mice/group). 1-way

ANOVA followed by Tukey's post-hoc test for multiple comparisons was performed (*P<0.05, **P<0.01, ***P<0.001). **(C)** Representative Native-PAGE/western blot probed with anti-apoE antibody (Calbiochem) after loading 3 ng apoE/lane from CSF of young (4 months) and old (17 months) PDAPP/TRE mice (n=4/genotype for each age). 12.2 nm and 17 nm sizes correspond to estimated hydrodynamic radii from protein marker.

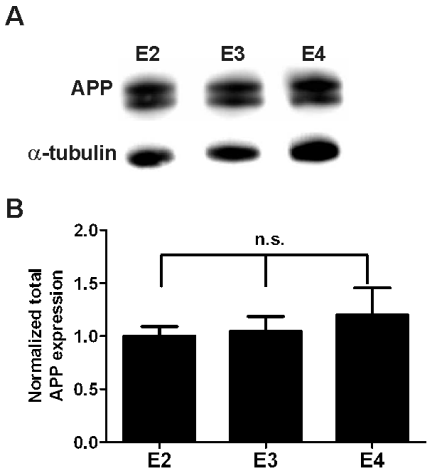

Figure S5. Full-length total APP levels do not differ according to apoE isoform. (A) Representative western blot of RIPA-soluble total (mature and immature) full-length APP from hippocampal homogenates from young, sex-matched PDAPP/TRE mice. APP was detected using 6E10 antibody. All bands were normalized to α-tubulin band intensity (n=9 mice/group; 3-4 months old). **(B)** Quantification of total APP levels after normalizing each band's intensity to α-tubulin band intensity. All samples were represented relative to the PDAPP/E2 group mean. 1-way ANOVA revealed no significant differences among groups. Values represent mean ± SEM.

	APOE genotype		
	PDAPP/E2	**PDAPP/E3**	**PDAPP/E4**
Soluble Aβ40	10.83***** ± 0.36	10.34****** ± 0.70	12.55 ± 0.21
Soluble Aβ42	2.83 ± 0.19	2.66***** ± 0.14	3.29 ± 0.18
Insoluble Aβ40	87.52 ± 3.09	79.55 ± 3.66	84.02 ± 3.29
Insoluble Aβ42	43.39 ± 1.74	41.09***** ± 2.79	53.07 ± 3.89

Table S1. Serial extraction of Aβ40 and Aβ42 from hippocampi of young PDAPP/TRE mice. All values represent mean (pg/mg tissue) ± SEM. PBS-soluble (soluble) and Guan-soluble (insoluble) Aβ40 or Aβ42 was quantified using sandwich ELISAs following serial tissue extraction of hippocampi from young, sex-matched PDAPP/TRE mice with PBS, followed by 5M Guan-Tris buffer (n=8-9/group). When 1-way ANOVA was significant, pairwise comparisons of *APOE* genotypes were made using Tukey's post-hoc test; only significant differences were indicated (**P*<0.05,***P*<0.01). (* or **) denotes significant difference compared to PDAPP/E4 at the indicated levels of significance.

Chapter 5.

Conclusion and Future Directions

Summary

A multitude of autosomal dominant mutations in *APP*, *PSEN1,* and *PSEN2* have been identified that cause early-onset, familial AD (FAD). While identification of the link between these mutations and early-onset, FAD has been fundamental to our current understanding of AD pathogenesis, the cause(s) of sporadic, late-onset AD remains unclear. Characterizing the role of genetic or environmental risk factors in modulating AD pathogenesis will likely be useful in understanding initiating events in sporadic, late-onset AD. Despite a variety of susceptibility genes being linked to AD, including *CLU, CR1, PICALM, CD33, BIN1, MS4A4A, CD2AP, EPHA1,* and *ABCA7* (Holtzman et al., 2011), the *ε4* allele of *APOE* is the strongest identified genetic risk factor for AD. The underlying mechanism for this association remains unclear. Thus, the overall aim of this dissertation was to characterize the role of apoE in regulating the metabolism of the Aβ peptide, the accumulation of which is central to AD pathogenesis.

To begin to assess the effect of apoE on Aβ metabolism in vivo, we manipulated levels of a major apoE receptor in the brain in order to modulate the concentration of apoE (Chapter 2). Specifically, we created several lines of mice overexpressing the low-density lipoprotein receptor (LDLR) and crossbred these mice with the PS1ΔE9/APPswe (PSAPP) mouse model of β-amyloidosis. In addition to reducing brain apoE levels, LDLR overexpression markedly reduced hippocampal and cortical Aβ and amyloid burden, with concomitant decreases in plaque-associated neuroinflammatory response. To investigate the mechanism by which LDLR overexpression decreases Aβ deposition, we aged both groups of mice to 3 months of age to assess Aβ metabolism prior to the onset of Aβ deposition. Compared to mice expressing normal levels of LDLR,

overexpression of LDLR reduced the steady state concentration of Aβ in the brain interstitial fluid (ISF), as assessed by in vivo microdialysis. Consistent with reduced steady state concentration of Aβ in the ISF, we found that the half-life of Aβ in the ISF of PSAPP mice overexpressing LDLR was significantly shorter than that measured in the ISF of PSAPP mice. Together, our results suggest that modulation of apoE levels by LDLR overexpression strongly regulates the steady state concentration of Aβ in the ISF via effects on its clearance.

Aβ can be eliminated from the brain ISF through various proposed routes, including bulk ISF flow, cellular uptake and degradation, and blood-brain barrier (BBB)-mediated transport. To further characterize the mechanism by which LDLR enhances ISF Aβ clearance, we utilized several in vivo methodologies to assess how LDLR mediates Aβ clearance from the brain ISF (Chapter 3). We first employed the brain efflux index (BEI) method to show that LDLR overexpression increased the elimination of radiolabeled Aβ40 that was microinjected into the brain parenchyma. Next, we demonstrated that the elimination of a reference bulk flow marker was not altered by LDLR overexpression, suggesting the presence of an intact BBB in these mice. Moreover, we separated the overall efflux of radiolabeled Aβ40 for both groups into components of BBB and ISF bulk flow clearance, revealing that LDLR overexpression predominantly enhanced BBB-mediated Aβ clearance. We next developed a method to sensitively and directly assess the rate of Aβ appearance in the blood from the brain to confirm our findings obtained with the BEI method in the setting of endogenous Aβ production. To measure the rate of Aβ appearance in the periphery, we sequestered CNS-derived human Aβ as it entered the blood by intravenous administration of an anti-Aβ

antibody (HJ5.1), sampling the blood by serial retro-orbital bleeds. Following validation of the effect of LDLR overexpression on apoE levels and Aβ accumulation in the PDAPP mouse model, we used in vivo microdialysis to demonstrate that peripheral administration of HJ5.1 was not sufficient to alter Aβ metabolism within the brain acutely over a period of several hours. Finally, we used this plasma sequestration method to demonstrate that LDLR overexpression significantly increased the rate of human Aβ appearance from brain into blood. These results suggest a mechanism by which LDLR overexpression reduces Aβ accumulation by enhancing Aβ clearance from brain into blood.

We next investigated the role of *APOE* genotype in modulating Aβ accumulation in cognitively normal humans and in PDAPP mice in which human apoE isoforms were expressed (Chapter 4). In both humans and in mice, we found that cerebral Aβ deposition varied in a manner that corresponded to *APOE* genotype. We next utilized in vivo microdialysis in both young and amyloid plaque-laden mice, which revealed that the concentration and clearance of Aβ from the ISF differed according to the apoE isoform expressed. In other words, apoE4 impaired ISF Aβ clearance relative to apoE2 or apoE3, consistent with the greater Aβ accumulation observed in the context of apoE4. To examine whether human apoE isoforms regulate the synthesis of Aβ, we utilized an in vivo stable isotopic labeling kinetics method in young mice, which demonstrated that fractional synthesis rates of Aβ did not vary significantly according to human apoE isoform. Given the apoE isoform-dependent differences in brain apoE concentration we observed, we infused recombinant apoE particles (rApoE2 and rApoE4) during in vivo microdialysis to demonstrate that intrinsic differences in apoE isoforms contribute to

differences in the steady state concentration of ISF Aβ (Appendix A). Overall, our results suggest a mechanism by which *APOE* alleles influence Aβ accumulation through differential regulation of Aβ clearance from the brain ISF. Furthermore, our results motivate therapeutic strategies that target apoE receptors, apoE expression, or other mediators involved in Aβ clearance for AD prevention and treatment.

LDLR and the role of apoE in regulating Aβ clearance

Following the initial reports that *APOE* genotype was strongly related to AD risk and age of onset (Verghese et al., 2011), several studies suggested the presence of an apoE/Aβ interaction (Kim et al., 2009a). Given that apoE is secreted into the brain extracellular space, evidence of an interaction led to the hypothesis that apoE regulates the accumulation of Aβ in the brain extracellular space. In an attempt to understand how apoE regulates the concentration of Aβ in the brain ISF, we reduced the concentration of brain apoE by overexpressing LDLR, leading to enhanced BBB-mediated Aβ clearance. One potential mechanism to account for this effect is that LDLR is overexpressed at the BBB, leading to enhanced clearance of Aβ/apoE complexes. Alternatively, the markedly reduced concentration of apoE as a result of LDLR overexpression in neurons and astrocytes may allow unbound ISF Aβ to more efficiently clear directly across the BBB using other apoE receptors (Deane et al., 2004). Aside from the effect of reducing apoE concentration and its implication for putative apoE/Aβ interactions in the ISF, it is also possible that LDLR directly mediates Aβ clearance at the BBB, as suggested for LRP1 (Deane et al., 2004), another LDLR family member. Indeed, a recent study provided evidence for an apoE-independent role for LDLR in regulating Aβ accumulation in the

hippocampus, but not the cortex of 5X-FAD mice (Katsouri and Georgopoulos, 2011). Early during the course of this dissertation, we attempted to create mice that overexpressed LDLR while lacking apoE expression to test the possibility that some component of the enhanced Aβ clearance was independent of changes in apoE concentration. For reasons that remain unclear, these mice were not viable. Emerging data from our laboratory, however, suggest an apoE-independent role for LDLR in uptake of Aβ into astrocytes (Jacob Basak et al., *under review*). Specifically, overexpression of LDLR enhances Aβ uptake and degradation within astrocytes in a manner that does not appear to require apoE. Surface plasmon resonance and immunoprecipitation studies suggested the presence of an LDLR/Aβ interaction, raising the possibility that LDLR may directly mediate Aβ clearance in vivo. Given that the mice we created to assess this possibility were not viable, one future direction for this work will be to virally overexpress LDLR in adult APP-Tg mice expressing or lacking apoE. In vivo microdialysis could then be performed in infected mice of both groups to evaluate whether LDLR enhances ISF Aβ clearance in the absence of apoE.

Regulation of Aβ metabolism by LDLR in the context of human apoE

In Chapter 4, we found that human apoE isoforms differentially regulate the clearance of Aβ from the ISF; however, the detailed molecular mechanism for this isoform-dependent clearance remains unclear. Given that LDLR regulates the clearance of Aβ (Chapters 2 and 3), it will be important to assess the extent to which LDLR regulates Aβ clearance from the ISF in the context of human apoE expression. Interestingly, the affinity of human apoE for LDLR varies according to isoform, with apoE2 binding to LDLR with a 1-2% affinity compared to apoE3 or apoE4 (Knouff et al.,

2004; Weisgraber, 1994; Yamamoto et al., 2008). To investigate the impact of LDLR on Aβ metabolism in the context of human apoE isoforms, we first attempted to produce ApoE2 and ApoE4 knockin mice that overexpress LDLR. While LDLR-Tg/ApoE2 mice were viable, we did not obtain any litters of ApoE4 knockin mice that overexpressed LDLR. To circumvent this issue, we created adeno-associated viruses (AAV2/8) expressing human LDLR or GFP (as negative control) under the control of the phosphoglycerate kinase (PGK) promoter (see Appendix B). These viruses will be stereotaxically injected into the hippocampi of adult PDAPP/E2 and PDAPP/E4 mice (10-11 months old) to assess the effect of LDLR overexpression on Aβ deposition following a 6-month infection period. Given that LDLR does not regulate the concentration of apoE2, we hypothesize that LDLR overexpression will reduce Aβ deposition only in the context of apoE4. Alternatively, reduced Aβ deposition in the context of apoE2 would suggest an in vivo role for LDLR in directly facilitating Aβ clearance independent of an apoE/LDLR interaction. Serious consideration of therapeutic strategies that target LDLR will likely require further elaboration of the role of LDLR in Aβ metabolism in the context of human apoE.

Delineating the roles of apoE concentration and isoform

The isoform-dependent pattern of apoE concentration reported by several groups in humans and in mice raises the possibility that the concentration of apoE alone may be regulate the differential pattern of Aβ clearance we demonstrated in Chapter 4. The mechanism by which apoE concentration varies by isoform (E2 > E3 > E4) remains unknown, though a recent in vitro study suggested that the degradation of apoE4 is

greater than that of the other isoforms (Riddell et al., 2008). Perhaps as a result of methodological differences or differences in the pool of apoE extracted, not all studies have reported an isoform-dependent pattern of brain apoE concentration (Korwek et al., 2009; Sullivan et al., 2004). One important future direction will be to attempt to resolve this controversy by measuring apoE in the brain ISF of behaving human apoE knockin mice. Our current in vivo microdialysis method utilizes molecular weight cut-off membranes of 38 kDa (Cirrito et al., 2003) or 100 kDa (Yamada et al., 2011), which are unable to dialyze large particles containing apoE (>250 kDa). Recent advancements have been made in microdialysis probe membrane technology (Takeda et al., 2011), allowing for measurement of high molecular weight molecules, i.e., up to 1 MDa in size. In preliminary experiments, we recently measured murine apoE in the brain ISF, though work is ongoing to characterize the size and concentration of the dialyzed apoE with this method. To clarify the role of human apoE concentration in regulating Aβ metabolism, apoE microdialysis in APP-Tg/human apoE knockin mice would permit the simultaneous measurement of Aβ and apoE in the ISF, allowing sensitive intra-animal correlations between apoE and Aβ concentrations to be made. Assuming that apoE concentration does, in fact, differ according to isoform, we reasoned that infusion of apoE particles into the brain ISF of PDAPP/TRE mice would effectively normalize apoE concentration, allowing us to examine the effect of intrinsic isoform differences on Aβ metabolism. We demonstrated that acute treatment with recombinant ApoE2 and ApoE4 particles in PDAPP/E2 and PDAPP/E4 mice (Appendix A) increased the concentration of ISF Aβ in a manner that depended on isoform, i.e., E4 > E2. Emerging data from our laboratory demonstrate that genetic reduction of apoE expression, regardless of isoform, is sufficient

to reduce Aβ deposition in APP/PS1-Tg mice (Kim et al., *in press*). A complementary approach would be to compare the clearance and steady state concentration of ISF Aβ in the brains of APP-Tg mice expressing one or two copies of apoE2 or apoE4. Together, these studies will advance our understanding of whether apoE4 represents a toxic gain of function or loss of function with respect to AD pathogenesis.

Concluding Remarks

The accumulation of Aβ is widely considered to be a critical event in AD pathogenesis, though the cause(s) for this accumulation is unclear in sporadic, late-onset AD. In this dissertation, we employed novel in vivo methodologies to examine the roles of apoE concentration and isoform in mouse models of β-amyloidosis. We found that decreasing brain apoE concentration by LDLR overexpression increases Aβ clearance from the ISF, specifically by increasing blood-brain barrier-mediated transport of Aβ. We utilized a mouse model of β-amyloidosis expressing human apoE isoforms to demonstrate that Aβ/amyloid deposition differs according to isoform in a manner that parallels the association between *APOE* genotype and AD risk and age of onset. In young mice prior to the onset of Aβ deposition, we showed that human apoE isoforms differentially regulate Aβ clearance from the ISF. We performed stable isotopic labeling kinetics to demonstrate that human apoE isoforms do not regulate the concentration of ISF Aβ through regulation of Aβ synthesis. Taken together, our results provide a potential mechanism to account for the strong association between *APOE* genotype and AD risk and age of onset. Additionally, these findings expand our understanding of the role of apoE concentration and isoform in AD pathogenesis, while motivating the development of therapeutic strategies targeting Aβ clearance pathways.

Appendix A.

Preparation and infusion of recombinant human apoE particles during in vivo microdialysis

RESULTS AND INTERPRETATION

Convincing evidence exists for accelerated onset of amyloid deposition in *APOE* ε4-carriers, leading to the hypothesis that *APOE* genotype differentially regulates AD risk and onset via effects on Aβ accumulation (Verghese et al., 2011). Using PDAPP/human apoE targeted replacement (PDAPP/TRE) mice that exhibit apoE isoform-dependent levels of Aβ burden (E4 > E3 > E2), we have found that human apoE isoforms differentially modulate endogenous Aβ clearance, but not synthesis, in a manner that corresponds to the apoE isoform-dependent pattern of Aβ accumulation in older mice. Although there are a few conflicting studies (Korwek et al., 2009; Sullivan et al., 2004), several groups have identified that apoE concentration in the brains of human apoE knock-in mice varies according to genotype, that is, E2 >> E3 > E4 (Bales et al., 2009; Fryer et al., 2005a; Ramaswamy et al., 2005; Riddell et al., 2008), consistent with our results in humans and in PDAPP/TRE mice (Castellano et al., 2011). Thus, the isoform-dependent pattern of apoE concentration in humans and in mice raises the possibility that apoE concentration alone may play a role in the pattern of Aβ clearance and subsequent Aβ accumulation, though these differences are unlikely to completely account for differences in Aβ metabolism in the setting of apoE3 versus apoE4 (Bales et al., 2009); see Figure A1. The contribution of apoE concentration versus isoform in regulating Aβ metabolism has not been delineated. To this end, we sought to prepare recombinant apoE particles of each isoform in order to normalize the concentration of apoE after infusion into the brain ISF of mice. After preparation of liposomes containing phospholipids (1-palmitoyl-2-oleoyl-sn-glycero-3-phosphocholine [PoPC]) and cholesterol, we used sodium cholate to create mixed micelles, which was then exchanged for each apoE

isoform to form discoidal complexes of recombinant apoE (rApoE) particles. The dialyzed rApoE particles appeared to be of typical size, as assessed by Native PAGE; moreover, concentrating the particles for the purpose of in vivo microdialysis infusion did not alter the size range of the particles (Figure A2). To confirm the functionality of the rApoE particles prior to in vivo experimentation, we performed a cholesterol efflux assay by adding rApoE particles to neuroblastoma cells that had been incubated with tritiated cholesterol for 24 hours. We observed rapid, time-dependent efflux of [^{3}H]-cholesterol into the media following addition of rApoE particles that was not observed using lipid complexes that did not contain apoE (Figure A3). To acutely assess the effect of apoE2 and apoE4, rApoE2 or rApoE4 particles were directly infused around the implanted 38 kDa microdialysis probe during simultaneous sampling of the brain interstitial fluid (ISF) of freely behaving PDAPP/E2 or PDAPP/E4 mice. Compared to a baseline period of steady state ISF Aβ obtained in PDAPP/E2 mice, treatment with rApoE2 particles appeared to increase steady state levels of ISF Aβ by approximately 15%, although this effect did reach statistical significance (Figure A4). In contrast, infusion of the same amount of rApoE4 particles in PDAPP/E4 mice increased ISF Aβ levels by 31% from baseline levels. Although an equimolar amount of apoE2 and apoE4 was infused in PDAPP/E2 and PDAPP/E4 mice, respectively, the possibility remains that total brain apoE concentration was not effectively normalized between the groups of mice we treated. Thus, we next sought to infuse rApoE2 and rApoE4 particles in PDAPP mice lacking apoE to assess the effect of specific apoE isoforms in a more controlled fashion. We first crossbred homozygous PDAPP mice with mice that lacked apoE, ultimately generating PDAPP$^{+/+}$/ApoE knockout (PDAPP/E KO) mice. Following direct infusions

of rApoE2, rApoE4, and vehicle (ACSF) in young PDAPP/E KO mice, we halted Aβ production with a potent γ-secretase inhibitor (LY411,575) to assess the effect of rApoE particles on Aβ clearance. Though we did not see any statistically significant differences among groups, we noted trends consistent with the effect observed in Figure A4, that is, rApoE4 particles decreased Aβ clearance to a slightly greater extent than rApoE2 particles (Figure A5). Notably, we observed significant mortality or poor outcome following guide cannulation or microdialysis probe implantation in these mice, including membrane blockage due to intraparencyhmal bleeding, rapidly decreasing baseline, increased intracranial pressure, seizure, and death. As a result, nearly 50% of mice utilized could not be included in our analysis. Given the purported roles of apoE in recovery following injury as well as maintenance of the blood-brain barrier (Chen et al., 1997; Fullerton et al., 2001; Hafezi-Moghadam et al., 2007; Methia et al., 2001; Pola et al., 2003), it is highly likely that the BBB in our PDAPP/E KO mice was disrupted, potentially leading to leakage of infused rApoE particles. Our results in Figure A4 suggest that rApoE2 and rApoE4 particle infusion in PDAPP/E2 and PDAPP/E4 mice increases Aβ levels in a manner that is specific to isoform, likely by decreasing Aβ clearance. Overall, however, given the potential concerns raised by the mouse model we utilized (PDAPP/ E KO), the effect of rApoE particles on Aβ metabolism remains inconclusive based on these experiments.

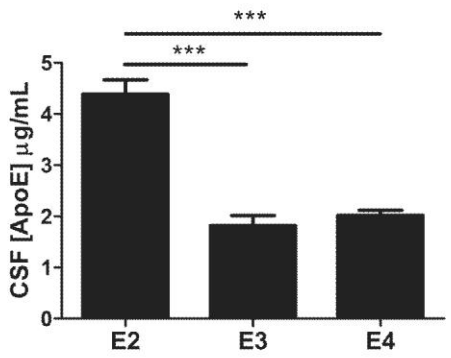

Figure A1. ApoE levels are significantly higher in the CSF of PDAPP/E2 mice. CSF was isolated from the cisternae magnae of young PDAPP/TRE mice and measured by human apoE ELISA (HJ6.2/HJ6.3). (n = 5-6 mice/group; 4 months old). Since one-way ANOVA was significant, pair-wise comparisons were made using Tukey's post hoc test (***P<0.001).

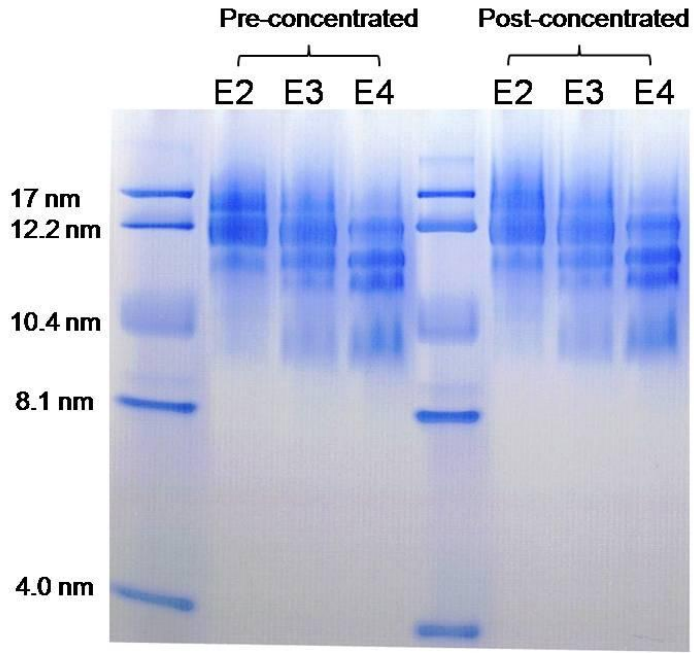

Figure A2. rApoE particles are of typical size and are not affected by concentration. **(Left)** Following dialysis to remove cholate, 8 μg of each sample was loaded on a 4-20% Tris-Glycine gel for Native PAGE to assess size of particles. **(Right)** rApoE particles that were concentrated for in vivo microdialysis experiments were also analyzed by Native PAGE, which suggested no change in size distribution as a result of concentration.

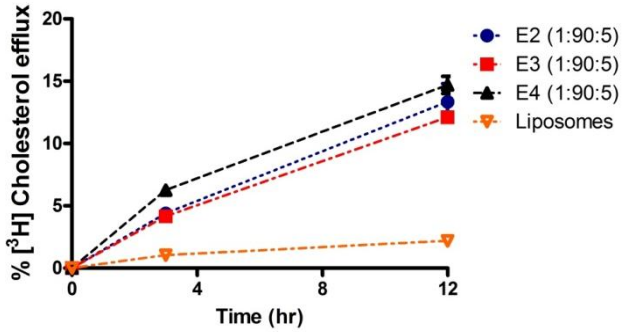

Figure A3. rApoE particles containing human apoE functionally efflux cholesterol. [^{3}H]-cholesterol-labeled H4-APP695ΔNL cells were incubated with 20 µg apoE particles at different timepoints to assess cholesterol efflux relative to liposomes, expressed as the percentage of radiolabeled cholesterol released into the media ([^{3}H]-Cholesterol in media/([^{3}H]-Cholesterol in media + [^{3}H]-Cholesterol in cells)). Cholesterol efflux assays were performed with the assistance of Philip Verghese.

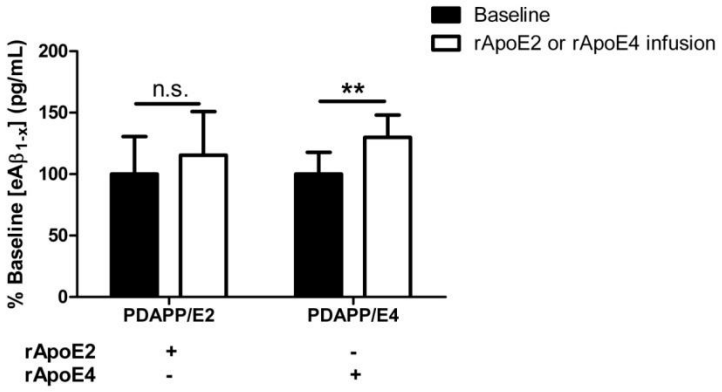

Figure A4. Increase in ISF Aβ after rApoE particle treatment depends on isoform. After a baseline period,1 μg of freshly prepared rApoE2 or rApoE4 particles was infused directly at the site of microdialysis in PDAPP/E2 or PDAPP/E4 mice, respectively. Following infusion at a flow rate of 0.07 μl/min, ISF [eA$\beta_{1\text{-}X}$] was monitored for an additional 6 hours. Values were represented as a percentage of baseline for each group. [A$\beta_{1\text{-}x}$] was measured using sandwich ELISA (266/3D6). Significance of percent increase from baseline to treatment periods was assessed for each group using paired *t* tests (n = 4-7 mice/group; 3-4.5 months old; ***P*<0.01).

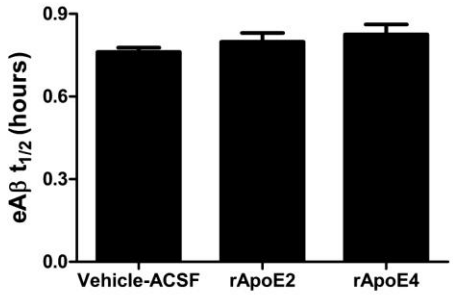

Figure A5. rApoE particle treatment appears to decrease Aβ clearance. Following a baseline period, 1 μg of freshly prepared rApoE2 or rApoE4 particles was infused directly at the site of microdialysis in young PDAPP/E KO mice. Following infusion at a flow rate of 0.07 μl/min, ISF [$eA\beta_{1-X}$] was monitored for an additional 6 hours, immediately followed by γ-secretase inhibition (i.p., 10 mg/kg LY411,575). [$A\beta_{1-x}$] was measured using sandwich ELISA (266/3D6). One-way ANOVA revealed no significant differences among groups. (n = 8 mice/group; 3-5 months old).

Appendix B.

Creation of AAV constructs for human LDLR overexpression

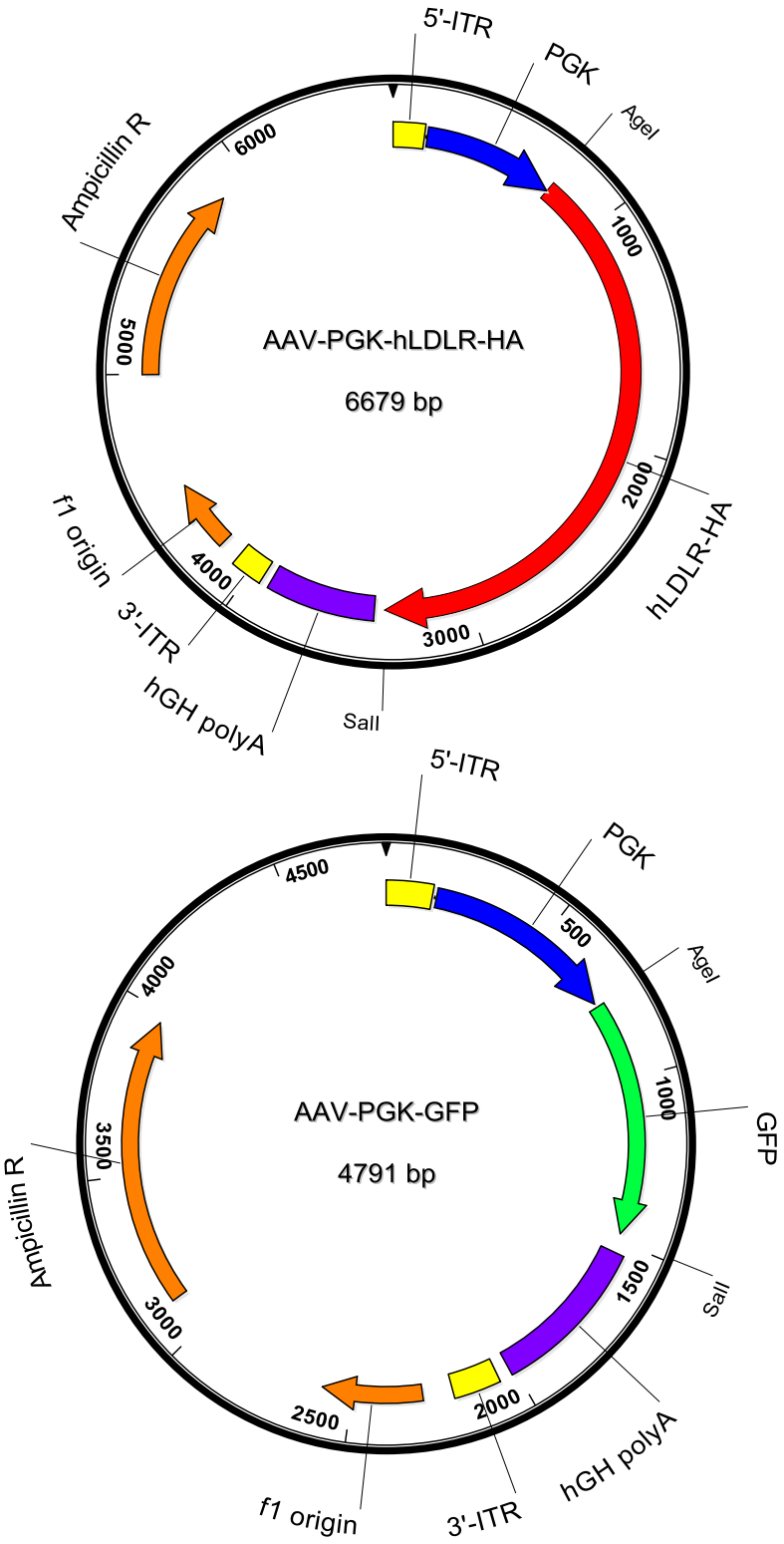

Figure B1. Creation of AAV constructs for human LDLR overexpression. Vector maps depicting sequence features for AAV-PGK-hLDLR-HA (top) and AAV-PGK-GFP

(bottom) constructs generated with the assistance of Qingli Xiao (Jin-Moo Lee laboratory). Constructs were packaged into AAV-2/8 viruses by the Hope Center Viral Vectors Core at Washington University. Viruses will be stereotaxically injected bilaterally into hippocampi of 10-11 month-old PDAPP/E2 and PDAPP/E4 mice, followed by a 6-month infection period after which the effect of hLDLR overexpression on Aβ deposition will be analyzed by immunohistochemistry.

References

Aleshkov, S., Abraham, C.R., and Zannis, V.I. (1997). Interaction of nascent ApoE2, ApoE3, and ApoE4 isoforms expressed in mammalian cells with amyloid peptide beta (1-40). Relevance to Alzheimer's disease. Biochemistry *36*, 10571-10580.

Alzheimer, A., Stelzmann, R.A., Schnitzlein, H.N., and Murtagh, F.R. (1995). An English translation of Alzheimer's 1907 paper, "Uber eine eigenartige Erkankung der Hirnrinde". Clin Anat *8*, 429-431.

Andersen, K., Launer, L.J., Dewey, M.E., Letenneur, L., Ott, A., Copeland, J.R., Dartigues, J.F., Kragh-Sorensen, P., Baldereschi, M., Brayne, C., *et al.* (1999). Gender differences in the incidence of AD and vascular dementia: The EURODEM Studies. EURODEM Incidence Research Group. Neurology *53*, 1992-1997.

Andersen, O.M., Reiche, J., Schmidt, V., Gotthardt, M., Spoelgen, R., Behlke, J., von Arnim, C.A., Breiderhoff, T., Jansen, P., Wu, X., *et al.* (2005). Neuronal sorting protein-related receptor sorLA/LR11 regulates processing of the amyloid precursor protein. Proc Natl Acad Sci U S A *102*, 13461-13466.

Bales, K.R., Liu, F., Wu, S., Lin, S., Koger, D., DeLong, C., Hansen, J.C., Sullivan, P.M., and Paul, S.M. (2009). Human APOE isoform-dependent effects on brain beta-amyloid levels in PDAPP transgenic mice. J Neurosci *29*, 6771-6779.

Bales, K.R., Verina, T., Cummins, D.J., Du, Y., Dodel, R.C., Saura, J., Fishman, C.E., DeLong, C.A., Piccardo, P., Petegnief, V., *et al.* (1999). Apolipoprotein E is essential for amyloid deposition in the APP(V717F) transgenic mouse model of Alzheimer's disease. Proc Natl Acad Sci U S A *96*, 15233-15238.

Bales, K.R., Verina, T., Dodel, R.C., Du, Y., Altstiel, L., Bender, M., Hyslop, P., Johnstone, E.M., Little, S.P., Cummins, D.J., *et al.* (1997). Lack of apolipoprotein E dramatically reduces amyloid beta-peptide deposition. Nat Genet *17*, 263-264.

Bandaru, V.V., Troncoso, J., Wheeler, D., Pletnikova, O., Wang, J., Conant, K., and Haughey, N.J. (2009). ApoE4 disrupts sterol and sphingolipid metabolism in Alzheimer's but not normal brain. Neurobiol Aging *30*, 591-599.

Barten, D.M., Guss, V.L., Corsa, J.A., Loo, A., Hansel, S.B., Zheng, M., Munoz, B., Srinivasan, K., Wang, B., Robertson, B.J., *et al.* (2005). Dynamics of {beta}-amyloid reductions in brain, cerebrospinal fluid, and plasma of {beta}-amyloid precursor protein transgenic mice treated with a {gamma}-secretase inhibitor. J Pharmacol Exp Ther *312*, 635-643.

Bateman, R.J., Munsell, L.Y., Morris, J.C., Swarm, R., Yarasheski, K.E., and Holtzman, D.M. (2006). Human amyloid-beta synthesis and clearance rates as measured in cerebrospinal fluid in vivo. Nat Med *12*, 856-861.

Beffert, U., Aumont, N., Dea, D., Lussier-Cacan, S., Davignon, J., and Poirier, J. (1998). Beta-amyloid peptides increase the binding and internalization of apolipoprotein E to hippocampal neurons. J Neurochem *70*, 1458-1466.

Beffert, U., Cohn, J.S., Petit-Turcotte, C., Tremblay, M., Aumont, N., Ramassamy, C., Davignon, J., and Poirier, J. (1999). Apolipoprotein E and beta-amyloid levels in the hippocampus and frontal cortex of Alzheimer's disease subjects are disease-related and apolipoprotein E genotype dependent. Brain Res *843*, 87-94.

Beffert, U., and Poirier, J. (1998). ApoE associated with lipid has a reduced capacity to inhibit beta-amyloid fibril formation. Neuroreport *9*, 3321-3323.

Bell, R.D., Sagare, A.P., Friedman, A.E., Bedi, G.S., Holtzman, D.M., Deane, R., and Zlokovic, B.V. (2007). Transport pathways for clearance of human Alzheimer's amyloid beta-peptide and apolipoproteins E and J in the mouse central nervous system. J Cereb Blood Flow Metab *27*, 909-918.

Bero, A.W., Yan, P., Roh, J.H., Cirrito, J.R., Stewart, F.R., Raichle, M.E., Lee, J.M., and Holtzman, D.M. (2011). Neuronal activity regulates the regional vulnerability to amyloid-beta deposition. Nat Neurosci *14*, 750-756.

Bertram, L., Hsiao, M., McQueen, M.B., Parkinson, M., Mullin, K., Blacker, D., and Tanzi, R.E. (2007a). The LDLR locus in Alzheimer's disease: a family-based study and meta-analysis of case-control data. Neurobiol Aging *28*, 18 e11-14.

Bertram, L., Lange, C., Mullin, K., Parkinson, M., Hsiao, M., Hogan, M.F., Schjeide, B.M., Hooli, B., Divito, J., Ionita, I., *et al.* (2008). Genome-wide association analysis reveals putative Alzheimer's disease susceptibility loci in addition to APOE. Am J Hum Genet *83*, 623-632.

Bertram, L., McQueen, M.B., Mullin, K., Blacker, D., and Tanzi, R.E. (2007b). Systematic meta-analyses of Alzheimer disease genetic association studies: the AlzGene database. Nat Genet *39*, 17-23.

Biere, A.L., Ostaszewski, B., Zhao, H., Gillespie, S., Younkin, S.G., and Selkoe, D.J. (1995). Co-expression of beta-amyloid precursor protein (betaAPP) and apolipoprotein E in cell culture: analysis of betaAPP processing. Neurobiol Dis *2*, 177-187.

Bolmont, T., Haiss, F., Eicke, D., Radde, R., Mathis, C.A., Klunk, W.E., Kohsaka, S., Jucker, M., and Calhoun, M.E. (2008). Dynamics of the microglial/amyloid interaction indicate a role in plaque maintenance. J Neurosci *28*, 4283-4292.

Bookheimer, S., and Burggren, A. (2009). APOE-4 genotype and neurophysiological vulnerability to Alzheimer's and cognitive aging. Annu Rev Clin Psychol *5*, 343-362.

Borchelt, D.R., Davis, J., Fischer, M., Lee, M.K., Slunt, H.H., Ratovitsky, T., Regard, J., Copeland, N.G., Jenkins, N.A., Sisodia, S.S., and Price, D.L. (1996). A vector for

expressing foreign genes in the brains and hearts of transgenic mice. Genet Anal *13*, 159-163.

Bray, N.J., Jehu, L., Moskvina, V., Buxbaum, J.D., Dracheva, S., Haroutunian, V., Williams, J., Buckland, P.R., Owen, M.J., and O'Donovan, M.C. (2004). Allelic expression of APOE in human brain: effects of epsilon status and promoter haplotypes. Hum Mol Genet *13*, 2885-2892.

Brody, D.L., Magnoni, S., Schwetye, K.E., Spinner, M.L., Esparza, T.J., Stocchetti, N., Zipfel, G.J., and Holtzman, D.M. (2008). Amyloid-beta dynamics correlate with neurological status in the injured human brain. Science *321*, 1221-1224.

Brown, M.S., and Goldstein, J.L. (1986). A receptor-mediated pathway for cholesterol homeostasis. Science *232*, 34-47.

Bu, G. (2009). Apolipoprotein E and its receptors in Alzheimer's disease: pathways, pathogenesis and therapy. Nature reviews *10*, 333-344.

Buckner, R.L., Snyder, A.Z., Shannon, B.J., LaRossa, G., Sachs, R., Fotenos, A.F., Sheline, Y.I., Klunk, W.E., Mathis, C.A., Morris, J.C., and Mintun, M.A. (2005). Molecular, structural, and functional characterization of Alzheimer's disease: evidence for a relationship between default activity, amyloid, and memory. J Neurosci *25*, 7709-7717.

Busche, M.A., Eichhoff, G., Adelsberger, H., Abramowski, D., Wiederhold, K.H., Haass, C., Staufenbiel, M., Konnerth, A., and Garaschuk, O. (2008). Clusters of hyperactive neurons near amyloid plaques in a mouse model of Alzheimer's disease. Science *321*, 1686-1689.

Callahan, M.J., Lipinski, W.J., Bian, F., Durham, R.A., Pack, A., and Walker, L.C. (2001). Augmented senile plaque load in aged female beta-amyloid precursor protein-transgenic mice. Am J Pathol *158*, 1173-1177.

Cam, J.A., and Bu, G. (2006). Modulation of beta-amyloid precursor protein trafficking and processing by the low density lipoprotein receptor family. Mol Neurodegener *1*, 8.

Cam, J.A., Zerbinatti, C.V., Knisely, J.M., Hecimovic, S., Li, Y., and Bu, G. (2004). The low density lipoprotein receptor-related protein 1B retains beta-amyloid precursor protein at the cell surface and reduces amyloid-beta peptide production. J Biol Chem *279*, 29639-29646.

Cam, J.A., Zerbinatti, C.V., Li, Y., and Bu, G. (2005). Rapid endocytosis of the low density lipoprotein receptor-related protein modulates cell surface distribution and processing of the beta-amyloid precursor protein. J Biol Chem *280*, 15464-15470.

Cao, D., Fukuchi, K., Wan, H., Kim, H., and Li, L. (2006). Lack of LDL receptor aggravates learning deficits and amyloid deposits in Alzheimer transgenic mice. Neurobiol Aging *27*, 1632-1643.

Carroll, J.C., Rosario, E.R., Chang, L., Stanczyk, F.Z., Oddo, S., LaFerla, F.M., and Pike, C.J. (2007). Progesterone and estrogen regulate Alzheimer-like neuropathology in female 3xTg-AD mice. J Neurosci *27*, 13357-13365.

Caselli, R.J., Dueck, A.C., Osborne, D., Sabbagh, M.N., Connor, D.J., Ahern, G.L., Baxter, L.C., Rapcsak, S.Z., Shi, J., Woodruff, B.K., *et al.* (2009). Longitudinal modeling of age-related memory decline and the APOE epsilon4 effect. N Engl J Med *361*, 255-263.

Castano, E.M., Prelli, F., Wisniewski, T., Golabek, A., Kumar, R.A., Soto, C., and Frangione, B. (1995). Fibrillogenesis in Alzheimer's disease of amyloid beta peptides and apolipoprotein E. Biochem J *306 (Pt 2)*, 599-604.

Castellano, J.M., Kim, J., Stewart, F.R., Jiang, H., DeMattos, R.B., Patterson, B.W., Fagan, A.M., Morris, J.C., Mawuenyega, K.G., Cruchaga, C., *et al.* (2011). Human apoE isoforms differentially regulate brain amyloid-beta peptide clearance. Sci Transl Med *3*, 89ra57.

Chen, J., Li, Q., and Wang, J. (2011). Topology of human apolipoprotein E3 uniquely regulates its diverse biological functions. Proc Natl Acad Sci U S A *108*, 14813-14818.

Chen, Y., Durakoglugil, M.S., Xian, X., and Herz, J. (2010). ApoE4 reduces glutamate receptor function and synaptic plasticity by selectively impairing ApoE receptor recycling. Proc Natl Acad Sci U S A *107*, 12011-12016.

Chen, Y., Lomnitski, L., Michaelson, D.M., and Shohami, E. (1997). Motor and cognitive deficits in apolipoprotein E-deficient mice after closed head injury. Neuroscience *80*, 1255-1262.

Cheng, D., Huang, R., Lanham, I.S., Cathcart, H.M., Howard, M., Corder, E.H., and Poduslo, S.E. (2005). Functional interaction between APOE4 and LDL receptor isoforms in Alzheimer's disease. J Med Genet *42*, 129-131.

Cirrito, J.R., May, P.C., O'Dell, M.A., Taylor, J.W., Parsadanian, M., Cramer, J.W., Audia, J.E., Nissen, J.S., Bales, K.R., Paul, S.M., *et al.* (2003). In vivo assessment of brain interstitial fluid with microdialysis reveals plaque-associated changes in amyloid-beta metabolism and half-life. J Neurosci *23*, 8844-8853.

Clark, C.M., Xie, S., Chittams, J., Ewbank, D., Peskind, E., Galasko, D., Morris, J.C., McKeel, D.W., Jr., Farlow, M., Weitlauf, S.L., *et al.* (2003). Cerebrospinal fluid tau and beta-amyloid: how well do these biomarkers reflect autopsy-confirmed dementia diagnoses? Arch Neurol *60*, 1696-1702.

Cole, S.L., and Vassar, R. (2007). The Alzheimer's disease beta-secretase enzyme, BACE1. Mol Neurodegener *2*, 22.

Corder, E.H., Saunders, A.M., Risch, N.J., Strittmatter, W.J., Schmechel, D.E., Gaskell, P.C., Jr., Rimmler, J.B., Locke, P.A., Conneally, P.M., Schmader, K.E., and et al. (1994).

Protective effect of apolipoprotein E type 2 allele for late onset Alzheimer disease. Nat Genet *7*, 180-184.

Corder, E.H., Saunders, A.M., Strittmatter, W.J., Schmechel, D.E., Gaskell, P.C., Jr., Rimmler, J.B., Locke, P.A., Conneally, P.M., Schmader, K.E., Tanzi, R.E., and et al. (1995). Apolipoprotein E, survival in Alzheimer's disease patients, and the competing risks of death and Alzheimer's disease. Neurology *45*, 1323-1328.

Corder, E.H., Saunders, A.M., Strittmatter, W.J., Schmechel, D.E., Gaskell, P.C., Small, G.W., Roses, A.D., Haines, J.L., and Pericak-Vance, M.A. (1993). Gene dose of apolipoprotein E type 4 allele and the risk of Alzheimer's disease in late onset families. Science *261*, 921-923.

Craft, S., Teri, L., Edland, S.D., Kukull, W.A., Schellenberg, G., McCormick, W.C., Bowen, J.D., and Larson, E.B. (1998). Accelerated decline in apolipoprotein E-epsilon4 homozygotes with Alzheimer's disease. Neurology *51*, 149-153.

Craig-Schapiro, R., Kuhn, M., Xiong, C., Pickering, E.H., Liu, J., Misko, T.P., Perrin, R.J., Bales, K.R., Soares, H., Fagan, A.M., and Holtzman, D.M. (2011). Multiplexed Immunoassay Panel Identifies Novel CSF Biomarkers for Alzheimer's Disease Diagnosis and Prognosis. PLoS One *6*, e18850.

D'Amore, J.D., Kajdasz, S.T., McLellan, M.E., Bacskai, B.J., Stern, E.A., and Hyman, B.T. (2003). In vivo multiphoton imaging of a transgenic mouse model of Alzheimer disease reveals marked thioflavine-S-associated alterations in neurite trajectories. J Neuropathol Exp Neurol *62*, 137-145.

De Strooper, B. (2007). Loss-of-function presenilin mutations in Alzheimer disease. Talking Point on the role of presenilin mutations in Alzheimer disease. EMBO Rep *8*, 141-146.

De Strooper, B., Saftig, P., Craessaerts, K., Vanderstichele, H., Guhde, G., Annaert, W., Von Figura, K., and Van Leuven, F. (1998). Deficiency of presenilin-1 inhibits the normal cleavage of amyloid precursor protein. Nature *391*, 387-390.

Deane, R., Sagare, A., Hamm, K., Parisi, M., Lane, S., Finn, M.B., Holtzman, D.M., and Zlokovic, B.V. (2008). apoE isoform-specific disruption of amyloid beta peptide clearance from mouse brain. J Clin Invest *118*, 4002-4013.

Deane, R., Sagare, A., Hamm, K., Parisi, M., LaRue, B., Guo, H., Wu, Z., Holtzman, D.M., and Zlokovic, B.V. (2005). IgG-assisted age-dependent clearance of Alzheimer's amyloid beta peptide by the blood-brain barrier neonatal Fc receptor. J Neurosci *25*, 11495-11503.

Deane, R., Wu, Z., Sagare, A., Davis, J., Du Yan, S., Hamm, K., Xu, F., Parisi, M., LaRue, B., Hu, H.W., *et al.* (2004). LRP/amyloid beta-peptide interaction mediates differential brain efflux of Abeta isoforms. Neuron *43*, 333-344.

DeMattos, R.B., Bales, K.R., Cummins, D.J., Dodart, J.C., Paul, S.M., and Holtzman, D.M. (2001). Peripheral anti-A beta antibody alters CNS and plasma A beta clearance and decreases brain A beta burden in a mouse model of Alzheimer's disease. Proc Natl Acad Sci U S A *98*, 8850-8855.

DeMattos, R.B., Bales, K.R., Cummins, D.J., Paul, S.M., and Holtzman, D.M. (2002a). Brain to plasma amyloid-beta efflux: a measure of brain amyloid burden in a mouse model of Alzheimer's disease. Science *295*, 2264-2267.

DeMattos, R.B., Cirrito, J.R., Parsadanian, M., May, P.C., O'Dell, M.A., Taylor, J.W., Harmony, J.A., Aronow, B.J., Bales, K.R., Paul, S.M., and Holtzman, D.M. (2004). ApoE and clusterin cooperatively suppress Abeta levels and deposition: evidence that ApoE regulates extracellular Abeta metabolism in vivo. Neuron *41*, 193-202.

DeMattos, R.B., O'Dell M, A., Parsadanian, M., Taylor, J.W., Harmony, J.A., Bales, K.R., Paul, S.M., Aronow, B.J., and Holtzman, D.M. (2002b). Clusterin promotes amyloid plaque formation and is critical for neuritic toxicity in a mouse model of Alzheimer's disease. Proc Natl Acad Sci U S A *99*, 10843-10848.

Dodart, J.C., Marr, R.A., Koistinaho, M., Gregersen, B.M., Malkani, S., Verma, I.M., and Paul, S.M. (2005). Gene delivery of human apolipoprotein E alters brain Abeta burden in a mouse model of Alzheimer's disease. Proc Natl Acad Sci U S A *102*, 1211-1216.

Elder, G.A., Cho, J.Y., English, D.F., Franciosi, S., Schmeidler, J., Sosa, M.A., Gasperi, R.D., Fisher, E.A., Mathews, P.M., Haroutunian, V., and Buxbaum, J.D. (2007). Elevated plasma cholesterol does not affect brain Abeta in mice lacking the low-density lipoprotein receptor. Journal of neurochemistry *102*, 1220-1231.

Evans, K.C., Berger, E.P., Cho, C.G., Weisgraber, K.H., and Lansbury, P.T., Jr. (1995). Apolipoprotein E is a kinetic but not a thermodynamic inhibitor of amyloid formation: implications for the pathogenesis and treatment of Alzheimer disease. Proc Natl Acad Sci U S A *92*, 763-767.

Fagan, A.M., Head, D., Shah, A.R., Marcus, D., Mintun, M., Morris, J.C., and Holtzman, D.M. (2009). Decreased cerebrospinal fluid Abeta(42) correlates with brain atrophy in cognitively normal elderly. Ann Neurol *65*, 176-183.

Fagan, A.M., Mintun, M.A., Mach, R.H., Lee, S.Y., Dence, C.S., Shah, A.R., LaRossa, G.N., Spinner, M.L., Klunk, W.E., Mathis, C.A., *et al.* (2006). Inverse relation between in vivo amyloid imaging load and cerebrospinal fluid Abeta42 in humans. Ann Neurol *59*, 512-519.

Fagan, A.M., Roe, C.M., Xiong, C., Mintun, M.A., Morris, J.C., and Holtzman, D.M. (2007). Cerebrospinal fluid tau/beta-amyloid(42) ratio as a prediction of cognitive decline in nondemented older adults. Arch Neurol *64*, 343-349.

Fagan, A.M., Watson, M., Parsadanian, M., Bales, K.R., Paul, S.M., and Holtzman, D.M. (2002). Human and murine ApoE markedly alters A beta metabolism before and after plaque formation in a mouse model of Alzheimer's disease. Neurobiol Dis *9*, 305-318.

Filipovic, I. (1989). Effect of inhibiting N-glycosylation on the stability and binding activity of the low density lipoprotein receptor. J Biol Chem *264*, 8815-8820.

Fratiglioni, L., Ahlbom, A., Viitanen, M., and Winblad, B. (1993). Risk factors for late-onset Alzheimer's disease: a population-based, case-control study. Ann Neurol *33*, 258-266.

Fryer, J.D., Demattos, R.B., McCormick, L.M., O'Dell, M.A., Spinner, M.L., Bales, K.R., Paul, S.M., Sullivan, P.M., Parsadanian, M., Bu, G., and Holtzman, D.M. (2005a). The low density lipoprotein receptor regulates the level of central nervous system human and murine apolipoprotein E but does not modify amyloid plaque pathology in PDAPP mice. J Biol Chem *280*, 25754-25759.

Fryer, J.D., Simmons, K., Parsadanian, M., Bales, K.R., Paul, S.M., Sullivan, P.M., and Holtzman, D.M. (2005b). Human apolipoprotein E4 alters the amyloid-beta 40:42 ratio and promotes the formation of cerebral amyloid angiopathy in an amyloid precursor protein transgenic model. J Neurosci *25*, 2803-2810.

Fuentealba, R.A., Barria, M.I., Lee, J., Cam, J., Araya, C., Escudero, C.A., Inestrosa, N.C., Bronfman, F.C., Bu, G., and Marzolo, M.P. (2007). ApoER2 expression increases Abeta production while decreasing Amyloid Precursor Protein (APP) endocytosis: Possible role in the partitioning of APP into lipid rafts and in the regulation of gamma-secretase activity. Mol Neurodegener *2*, 14.

Fuentealba, R.A., Liu, Q., Zhang, J., Kanekiyo, T., Hu, X., Lee, J.M., LaDu, M.J., and Bu, G. (2010). Low-density lipoprotein receptor-related protein 1 (LRP1) mediates neuronal Abeta42 uptake and lysosomal trafficking. PLoS One *5*, e11884.

Fullerton, S.M., Shirman, G.A., Strittmatter, W.J., and Matthew, W.D. (2001). Impairment of the blood-nerve and blood-brain barriers in apolipoprotein e knockout mice. Exp Neurol *169*, 13-22.

Games, D., Adams, D., Alessandrini, R., Barbour, R., Berthelette, P., Blackwell, C., Carr, T., Clemens, J., Donaldson, T., Gillespie, F., and et al. (1995). Alzheimer-type neuropathology in transgenic mice overexpressing V717F beta-amyloid precursor protein. Nature *373*, 523-527.

Garai, K., Mustafi, S.M., Baban, B., and Frieden, C. (2010). Structural differences between apolipoprotein E3 and E4 as measured by (19)F NMR. Protein Sci *19*, 66-74.

Garcia-Alloza, M., Dodwell, S.A., Meyer-Luehmann, M., Hyman, B.T., and Bacskai, B.J. (2006). Plaque-derived oxidative stress mediates distorted neurite trajectories in the Alzheimer mouse model. J Neuropathol Exp Neurol *65*, 1082-1089.

Ghiso, J., Shayo, M., Calero, M., Ng, D., Tomidokoro, Y., Gandy, S., Rostagno, A., and Frangione, B. (2004). Systemic catabolism of Alzheimer's Abeta40 and Abeta42. J Biol Chem *279*, 45897-45908.

Glenner, G.G., and Wong, C.W. (1984). Alzheimer's disease: initial report of the purification and characterization of a novel cerebrovascular amyloid protein. Biochem Biophys Res Commun *120*, 885-890.

Goate, A., Chartier-Harlin, M.C., Mullan, M., Brown, J., Crawford, F., Fidani, L., Giuffra, L., Haynes, A., Irving, N., James, L., and et al. (1991). Segregation of a missense mutation in the amyloid precursor protein gene with familial Alzheimer's disease. Nature *349*, 704-706.

Golde, T.E. (2006). Disease modifying therapy for AD? Journal of neurochemistry *99*, 689-707.

Gopalraj, R.K., Zhu, H., Kelly, J.F., Mendiondo, M., Pulliam, J.F., Bennett, D.A., and Estus, S. (2005). Genetic association of low density lipoprotein receptor and Alzheimer's disease. Neurobiol Aging *26*, 1-7.

Gregg, R.E., Zech, L.A., Schaefer, E.J., Stark, D., Wilson, D., and Brewer, H.B., Jr. (1986). Abnormal in vivo metabolism of apolipoprotein E4 in humans. J Clin Invest *78*, 815-821.

Growdon, W.B., Cheung, B.S., Hyman, B.T., and Rebeck, G.W. (1999). Lack of allelic imbalance in APOE epsilon3/4 brain mRNA expression in Alzheimer's disease. Neurosci Lett *272*, 83-86.

Haass, C., Hung, A.Y., Selkoe, D.J., and Teplow, D.B. (1994). Mutations associated with a locus for familial Alzheimer's disease result in alternative processing of amyloid beta-protein precursor. J Biol Chem *269*, 17741-17748.

Haass, C., Schlossmacher, M.G., Hung, A.Y., Vigo-Pelfrey, C., Mellon, A., Ostaszewski, B.L., Lieberburg, I., Koo, E.H., Schenk, D., Teplow, D.B., and et al. (1992). Amyloid beta-peptide is produced by cultured cells during normal metabolism. Nature *359*, 322-325.

Haass, C., and Selkoe, D.J. (2007). Soluble protein oligomers in neurodegeneration: lessons from the Alzheimer's amyloid beta-peptide. Nat Rev Mol Cell Biol *8*, 101-112.

Hafezi-Moghadam, A., Thomas, K.L., and Wagner, D.D. (2007). ApoE deficiency leads to a progressive age-dependent blood-brain barrier leakage. Am J Physiol Cell Physiol *292*, C1256-1262.

Halford, R.W., and Russell, D.W. (2009). Reduction of cholesterol synthesis in the mouse brain does not affect amyloid formation in Alzheimer's disease, but does extend lifespan. Proc Natl Acad Sci U S A *106*, 3502-3506.

Hardy, J. (2006). A hundred years of Alzheimer's disease research. Neuron *52*, 3-13.

Hardy, J., and Selkoe, D.J. (2002). The amyloid hypothesis of Alzheimer's disease: progress and problems on the road to therapeutics. Science *297*, 353-356.

Harold, D., Abraham, R., Hollingworth, P., Sims, R., Gerrish, A., Hamshere, M.L., Pahwa, J.S., Moskvina, V., Dowzell, K., Williams, A., *et al.* (2009). Genome-wide association study identifies variants at CLU and PICALM associated with Alzheimer's disease. Nat Genet *41*, 1088-1093.

Harr, S.D., Uint, L., Hollister, R., Hyman, B.T., and Mendez, A.J. (1996). Brain expression of apolipoproteins E, J, and A-I in Alzheimer's disease. J Neurochem *66*, 2429-2435.

Hatters, D.M., Budamagunta, M.S., Voss, J.C., and Weisgraber, K.H. (2005). Modulation of apolipoprotein E structure by domain interaction: differences in lipid-bound and lipid-free forms. J Biol Chem *280*, 34288-34295.

Hatters, D.M., Peters-Libeu, C.A., and Weisgraber, K.H. (2006). Apolipoprotein E structure: insights into function. Trends Biochem Sci *31*, 445-454.

Hatters, D.M., Voss, J.C., Budamagunta, M.S., Newhouse, Y.N., and Weisgraber, K.H. (2009). Insight on the molecular envelope of lipid-bound apolipoprotein E from electron paramagnetic resonance spectroscopy. J Mol Biol *386*, 261-271.

Herz, J. (2009). Apolipoprotein E receptors in the nervous system. Curr Opin Lipidol *20*, 190-196.

Herz, J., and Bock, H.H. (2002). Lipoprotein receptors in the nervous system. Annu Rev Biochem *71*, 405-434.

Herz, J., and Chen, Y. (2006). Reelin, lipoprotein receptors and synaptic plasticity. Nature reviews *7*, 850-859.

Hillered, L., Vespa, P.M., and Hovda, D.A. (2005). Translational neurochemical research in acute human brain injury: the current status and potential future for cerebral microdialysis. J Neurotrauma *22*, 3-41.

Hirsch-Reinshagen, V., Maia, L.F., Burgess, B.L., Blain, J.F., Naus, K.E., McIsaac, S.A., Parkinson, P.F., Chan, J.Y., Tansley, G.H., Hayden, M.R., *et al.* (2005). The absence of ABCA1 decreases soluble ApoE levels but does not diminish amyloid deposition in two murine models of Alzheimer disease. J Biol Chem *280*, 43243-43256.

Hofmann, S.L., Russell, D.W., Brown, M.S., Goldstein, J.L., and Hammer, R.E. (1988). Overexpression of low density lipoprotein (LDL) receptor eliminates LDL from plasma in transgenic mice. Science *239*, 1277-1281.

Hollingworth, P., Harold, D., Sims, R., Gerrish, A., Lambert, J.C., Carrasquillo, M.M., Abraham, R., Hamshere, M.L., Pahwa, J.S., Moskvina, V., *et al.* (2011). Common variants at ABCA7, MS4A6A/MS4A4E, EPHA1, CD33 and CD2AP are associated with Alzheimer's disease. Nat Genet *43*, 429-435.

Holtzman, D.M. (2008). Alzheimer's disease: Moving towards a vaccine. Nature *454*, 418-420.

Holtzman, D.M., Bales, K.R., Tenkova, T., Fagan, A.M., Parsadanian, M., Sartorius, L.J., Mackey, B., Olney, J., McKeel, D., Wozniak, D., and Paul, S.M. (2000a). Apolipoprotein E isoform-dependent amyloid deposition and neuritic degeneration in a mouse model of Alzheimer's disease. Proc Natl Acad Sci U S A *97*, 2892-2897.

Holtzman, D.M., Fagan, A.M., Mackey, B., Tenkova, T., Sartorius, L., Paul, S.M., Bales, K., Ashe, K.H., Irizarry, M.C., and Hyman, B.T. (2000b). Apolipoprotein E facilitates neuritic and cerebrovascular plaque formation in an Alzheimer's disease model. Ann Neurol *47*, 739-747.

Holtzman, D.M., Morris, J.C., and Goate, A.M. (2011). Alzheimer's disease: the challenge of the second century. Sci Transl Med *3*, 77sr71.

Hong, S., Quintero-Monzon, O., Ostaszewski, B.L., Podlisny, D.R., Cavanaugh, W.T., Yang, T., Holtzman, D.M., Cirrito, J.R., and Selkoe, D.J. (2011). Dynamic Analysis of Amyloid beta-Protein in Behaving Mice Reveals Opposing Changes in ISF versus Parenchymal Abeta during Age-Related Plaque Formation. J Neurosci *31*, 15861-15869.

Hoyt, B.D., Massman, P.J., Schatschneider, C., Cooke, N., and Doody, R.S. (2005). Individual growth curve analysis of APOE epsilon 4-associated cognitive decline in Alzheimer disease. Arch Neurol *62*, 454-459.

Hyman, B.T., West, H.L., Rebeck, G.W., Buldyrev, S.V., Mantegna, R.N., Ukleja, M., Havlin, S., and Stanley, H.E. (1995). Quantitative analysis of senile plaques in Alzheimer disease: observation of log-normal size distribution and molecular epidemiology of differences associated with apolipoprotein E genotype and trisomy 21 (Down syndrome). Proc Natl Acad Sci U S A *92*, 3586-3590.

Iadecola, C. (2004). Neurovascular regulation in the normal brain and in Alzheimer's disease. Nature reviews *5*, 347-360.

Ikonomovic, M.D., Klunk, W.E., Abrahamson, E.E., Mathis, C.A., Price, J.C., Tsopelas, N.D., Lopresti, B.J., Ziolko, S., Bi, W., Paljug, W.R., *et al.* (2008). Post-mortem correlates of in vivo PiB-PET amyloid imaging in a typical case of Alzheimer's disease. Brain *131*, 1630-1645.

Jack, C.R., Jr., Lowe, V.J., Senjem, M.L., Weigand, S.D., Kemp, B.J., Shiung, M.M., Knopman, D.S., Boeve, B.F., Klunk, W.E., Mathis, C.A., and Petersen, R.C. (2008). 11C PiB and structural MRI provide complementary information in imaging of Alzheimer's disease and amnestic mild cognitive impairment. Brain *131*, 665-680.

Jankowsky, J.L., Fadale, D.J., Anderson, J., Xu, G.M., Gonzales, V., Jenkins, N.A., Copeland, N.G., Lee, M.K., Younkin, L.H., Wagner, S.L., *et al.* (2004). Mutant presenilins specifically elevate the levels of the 42 residue beta-amyloid peptide in vivo: evidence for augmentation of a 42-specific gamma secretase. Human molecular genetics *13*, 159-170.

Jiang, Q., Lee, C.Y., Mandrekar, S., Wilkinson, B., Cramer, P., Zelcer, N., Mann, K., Lamb, B., Willson, T.M., Collins, J.L., *et al.* (2008). ApoE promotes the proteolytic degradation of Abeta. Neuron *58*, 681-693.

Johnson-Wood, K., Lee, M., Motter, R., Hu, K., Gordon, G., Barbour, R., Khan, K., Gordon, M., Tan, H., Games, D., *et al.* (1997). Amyloid precursor protein processing and A beta42 deposition in a transgenic mouse model of Alzheimer disease. Proc Natl Acad Sci U S A *94*, 1550-1555.

Kang, J.E., Lim, M.M., Bateman, R.J., Lee, J.J., Smyth, L.P., Cirrito, J.R., Fujiki, N., Nishino, S., and Holtzman, D.M. (2009). Amyloid-beta dynamics are regulated by orexin and the sleep-wake cycle. Science *326*, 1005-1007.

Katsouri, L., and Georgopoulos, S. (2011). Lack of LDL receptor enhances amyloid deposition and decreases glial response in an Alzheimer's disease mouse model. PLoS One *6*, e21880.

Kim, J., Basak, J.M., and Holtzman, D.M. (2009a). The role of apolipoprotein E in Alzheimer's disease. Neuron *63*, 287-303.

Kim, J., Castellano, J.M., Jiang, H., Basak, J.M., Parsadanian, M., Pham, V., Mason, S.M., Paul, S.M., and Holtzman, D.M. (2009b). Overexpression of low-density lipoprotein receptor in the brain markedly inhibits amyloid deposition and increases extracellular A beta clearance. Neuron *64*, 632-644.

Kim, J., Jiang, H., Park, S., Eltorai, E.M., Stewart, F.R., Yoon, H., Basak, J.M., Finn, M.B., and Holtzman, D.M. (*in press*). Haploinsufficiency of human APOE reduces amyloid deposition in a mouse model of Aβ amyloidosis. J Neurosci *In press*.

Kim, J., Onstead, L., Randle, S., Price, R., Smithson, L., Zwizinski, C., Dickson, D.W., Golde, T., and McGowan, E. (2007). Abeta40 inhibits amyloid deposition in vivo. J Neurosci *27*, 627-633.

Kinoshita, A., Whelan, C.M., Smith, C.J., Mikhailenko, I., Rebeck, G.W., Strickland, D.K., and Hyman, B.T. (2001). Demonstration by fluorescence resonance energy transfer of two sites of interaction between the low-density lipoprotein receptor-related protein and the amyloid precursor protein: role of the intracellular adapter protein Fe65. J Neurosci *21*, 8354-8361.

Klunk, W.E., Engler, H., Nordberg, A., Wang, Y., Blomqvist, G., Holt, D.P., Bergstrom, M., Savitcheva, I., Huang, G.F., Estrada, S., *et al.* (2004). Imaging brain amyloid in Alzheimer's disease with Pittsburgh Compound-B. Ann Neurol *55*, 306-319.

Knouff, C., Briand, O., Lestavel, S., Clavey, V., Altenburg, M., and Maeda, N. (2004). Defective VLDL metabolism and severe atherosclerosis in mice expressing human apolipoprotein E isoforms but lacking the LDL receptor. Biochimica et biophysica acta *1684*, 8-17.

Knowles, R.B., Wyart, C., Buldyrev, S.V., Cruz, L., Urbanc, B., Hasselmo, M.E., Stanley, H.E., and Hyman, B.T. (1999). Plaque-induced neurite abnormalities: implications for disruption of neural networks in Alzheimer's disease. Proc Natl Acad Sci U S A *96*, 5274-5279.

Koldamova, R., Staufenbiel, M., and Lefterov, I. (2005). Lack of ABCA1 considerably decreases brain ApoE level and increases amyloid deposition in APP23 mice. J Biol Chem *280*, 43224-43235.

Korwek, K.M., Trotter, J.H., Ladu, M.J., Sullivan, P.M., and Weeber, E.J. (2009). ApoE isoform-dependent changes in hippocampal synaptic function. Mol Neurodegener *4*, 21.

Krul, E.S., Tikkanen, M.J., and Schonfeld, G. (1988). Heterogeneity of apolipoprotein E epitope expression on human lipoproteins: importance for apolipoprotein E function. J Lipid Res *29*, 1309-1325.

Kuchibhotla, K.V., Goldman, S.T., Lattarulo, C.R., Wu, H.Y., Hyman, B.T., and Bacskai, B.J. (2008). Abeta plaques lead to aberrant regulation of calcium homeostasis in vivo resulting in structural and functional disruption of neuronal networks. Neuron *59*, 214-225.

Kuchibhotla, K.V., Lattarulo, C.R., Hyman, B.T., and Bacskai, B.J. (2009). Synchronous hyperactivity and intercellular calcium waves in astrocytes in Alzheimer mice. Science *323*, 1211-1215.

LaDu, M.J., Falduto, M.T., Manelli, A.M., Reardon, C.A., Getz, G.S., and Frail, D.E. (1994). Isoform-specific binding of apolipoprotein E to beta-amyloid. J Biol Chem *269*, 23403-23406.

LaDu, M.J., Gilligan, S.M., Lukens, J.R., Cabana, V.G., Reardon, C.A., Van Eldik, L.J., and Holtzman, D.M. (1998). Nascent astrocyte particles differ from lipoproteins in CSF. J Neurochem *70*, 2070-2081.

Lambert, J.C., Heath, S., Even, G., Campion, D., Sleegers, K., Hiltunen, M., Combarros, O., Zelenika, D., Bullido, M.J., Tavernier, B., *et al.* (2009). Genome-wide association study identifies variants at CLU and CR1 associated with Alzheimer's disease. Nat Genet *41*, 1094-1099.

Lamsa, R., Helisalmi, S., Herukka, S.K., Tapiola, T., Pirttila, T., Vepsalainen, S., Hiltunen, M., and Soininen, H. (2008). Genetic study evaluating LDLR polymorphisms and Alzheimer's disease. Neurobiol Aging *29*, 848-855.

LaRue, B., Hogg, E., Sagare, A., Jovanovic, S., Maness, L., Maurer, C., Deane, R., and Zlokovic, B.V. (2004). Method for measurement of the blood-brain barrier permeability in the perfused mouse brain: application to amyloid-beta peptide in wild type and Alzheimer's Tg2576 mice. J Neurosci Methods *138*, 233-242.

Leinonen, V., Alafuzoff, I., Aalto, S., Suotunen, T., Savolainen, S., Nagren, K., Tapiola, T., Pirttila, T., Rinne, J., Jaaskelainen, J.E., *et al.* (2008). Assessment of beta-amyloid in a frontal cortical brain biopsy specimen and by positron emission tomography with carbon 11-labeled Pittsburgh Compound B. Arch Neurol *65*, 1304-1309.

Levy, E., Carman, M.D., Fernandez-Madrid, I.J., Power, M.D., Lieberburg, I., van Duinen, S.G., Bots, G.T., Luyendijk, W., and Frangione, B. (1990). Mutation of the Alzheimer's disease amyloid gene in hereditary cerebral hemorrhage, Dutch type. Science *248*, 1124-1126.

Liu, Q., Zerbinatti, C.V., Zhang, J., Hoe, H.S., Wang, B., Cole, S.L., Herz, J., Muglia, L., and Bu, G. (2007). Amyloid precursor protein regulates brain apolipoprotein E and cholesterol metabolism through lipoprotein receptor LRP1. Neuron *56*, 66-78.

Lombardo, J.A., Stern, E.A., McLellan, M.E., Kajdasz, S.T., Hickey, G.A., Bacskai, B.J., and Hyman, B.T. (2003). Amyloid-beta antibody treatment leads to rapid normalization of plaque-induced neuritic alterations. J Neurosci *23*, 10879-10883.

Lucin, K.M., and Wyss-Coray, T. (2009). Immune activation in brain aging and neurodegeneration: too much or too little? Neuron *64*, 110-122.

Ma, J., Yee, A., Brewer, H.B., Jr., Das, S., and Potter, H. (1994). Amyloid-associated proteins alpha 1-antichymotrypsin and apolipoprotein E promote assembly of Alzheimer beta-protein into filaments. Nature *372*, 92-94.

Mahley, R.W. (1988). Apolipoprotein E: cholesterol transport protein with expanding role in cell biology. Science *240*, 622-630.

Mahley, R.W., Huang, Y., and Rall, S.C., Jr. (1999). Pathogenesis of type III hyperlipoproteinemia (dysbetalipoproteinemia). Questions, quandaries, and paradoxes. J Lipid Res *40*, 1933-1949.

Mahley, R.W., and Ji, Z.S. (1999). Remnant lipoprotein metabolism: key pathways involving cell-surface heparan sulfate proteoglycans and apolipoprotein E. J Lipid Res *40*, 1-16.

Mahley, R.W., and Rall, S.C., Jr. (2000). Apolipoprotein E: far more than a lipid transport protein. Annu Rev Genomics Hum Genet *1*, 507-537.

Masters, C.L., Simms, G., Weinman, N.A., Multhaup, G., McDonald, B.L., and Beyreuther, K. (1985). Amyloid plaque core protein in Alzheimer disease and Down syndrome. Proc Natl Acad Sci U S A *82*, 4245-4249.

Mawuenyega, K.G., Sigurdson, W., Ovod, V., Munsell, L., Kasten, T., Morris, J.C., Yarasheski, K.E., and Bateman, R.J. (2010a). Decreased Clearance of CNS {beta}-Amyloid in Alzheimer's Disease. Science.

Mawuenyega, K.G., Sigurdson, W., Ovod, V., Munsell, L., Kasten, T., Morris, J.C., Yarasheski, K.E., and Bateman, R.J. (2010b). Decreased clearance of CNS beta-amyloid in Alzheimer's disease. Science *330*, 1774.

Mayeux, R., Ottman, R., Tang, M.X., Noboa-Bauza, L., Marder, K., Gurland, B., and Stern, Y. (1993). Genetic susceptibility and head injury as risk factors for Alzheimer's disease among community-dwelling elderly persons and their first-degree relatives. Ann Neurol *33*, 494-501.

Mayeux, R., Sano, M., Chen, J., Tatemichi, T., and Stern, Y. (1991). Risk of dementia in first-degree relatives of patients with Alzheimer's disease and related disorders. Arch Neurol *48*, 269-273.

Menacherry, S., Hubert, W., and Justice, J.B., Jr. (1992). In vivo calibration of microdialysis probes for exogenous compounds. Anal Chem *64*, 577-583.

Methia, N., Andre, P., Hafezi-Moghadam, A., Economopoulos, M., Thomas, K.L., and Wagner, D.D. (2001). ApoE deficiency compromises the blood brain barrier especially after injury. Mol Med *7*, 810-815.

Meyer-Luehmann, M., Spires-Jones, T.L., Prada, C., Garcia-Alloza, M., de Calignon, A., Rozkalne, A., Koenigsknecht-Talboo, J., Holtzman, D.M., Bacskai, B.J., and Hyman, B.T. (2008). Rapid appearance and local toxicity of amyloid-beta plaques in a mouse model of Alzheimer's disease. Nature *451*, 720-724.

Meyer-Luehmann, M., Stalder, M., Herzig, M.C., Kaeser, S.A., Kohler, E., Pfeifer, M., Boncristiano, S., Mathews, P.M., Mercken, M., Abramowski, D., *et al.* (2003). Extracellular amyloid formation and associated pathology in neural grafts. Nat Neurosci *6*, 370-377.

Meyer, M.R., Tschanz, J.T., Norton, M.C., Welsh-Bohmer, K.A., Steffens, D.C., Wyse, B.W., and Breitner, J.C. (1998). APOE genotype predicts when--not whether--one is predisposed to develop Alzheimer disease. Nat Genet *19*, 321-322.

Mintun, M.A., Larossa, G.N., Sheline, Y.I., Dence, C.S., Lee, S.Y., Mach, R.H., Klunk, W.E., Mathis, C.A., DeKosky, S.T., and Morris, J.C. (2006). [11C]PIB in a nondemented population: potential antecedent marker of Alzheimer disease. Neurology *67*, 446-452.

Morris, J.C., Roe, C.M., Xiong, C., Fagan, A.M., Goate, A.M., Holtzman, D.M., and Mintun, M.A. (2010). APOE predicts amyloid-beta but not tau Alzheimer pathology in cognitively normal aging. Ann Neurol *67*, 122-131.

Mullan, M., Crawford, F., Axelman, K., Houlden, H., Lilius, L., Winblad, B., and Lannfelt, L. (1992). A pathogenic mutation for probable Alzheimer's disease in the APP gene at the N-terminus of beta-amyloid. Nat Genet *1*, 345-347.

Naj, A.C., Jun, G., Beecham, G.W., Wang, L.S., Vardarajan, B.N., Buros, J., Gallins, P.J., Buxbaum, J.D., Jarvik, G.P., Crane, P.K., *et al.* (2011). Common variants at MS4A4/MS4A6E, CD2AP, CD33 and EPHA1 are associated with late-onset Alzheimer's disease. Nat Genet *43*, 436-441.

Pastor, P., Roe, C.M., Villegas, A., Bedoya, G., Chakraverty, S., Garcia, G., Tirado, V., Norton, J., Rios, S., Martinez, M., *et al.* (2003). Apolipoprotein Eepsilon4 modifies Alzheimer's disease onset in an E280A PS1 kindred. Ann Neurol *54*, 163-169.

Patterson, B.W., Carraro, F., and Wolfe, R.R. (1993). Measurement of 15N enrichment in multiple amino acids and urea in a single analysis by gas chromatography/mass spectrometry. Biol Mass Spectrom *22*, 518-523.

Perrin, R.J., Fagan, A.M., and Holtzman, D.M. (2009). Multimodal techniques for diagnosis and prognosis of Alzheimer's disease. Nature *461*, 916-922.

Pietrzik, C.U., Busse, T., Merriam, D.E., Weggen, S., and Koo, E.H. (2002). The cytoplasmic domain of the LDL receptor-related protein regulates multiple steps in APP processing. EMBO J *21*, 5691-5700.

Pitas, R.E., Boyles, J.K., Lee, S.H., Hui, D., and Weisgraber, K.H. (1987). Lipoproteins and their receptors in the central nervous system. Characterization of the lipoproteins in cerebrospinal fluid and identification of apolipoprotein B,E(LDL) receptors in the brain. J Biol Chem *262*, 14352-14360.

Plassman, B.L., Havlik, R.J., Steffens, D.C., Helms, M.J., Newman, T.N., Drosdick, D., Phillips, C., Gau, B.A., Welsh-Bohmer, K.A., Burke, J.R., *et al.* (2000). Documented head injury in early adulthood and risk of Alzheimer's disease and other dementias. Neurology *55*, 1158-1166.

Pola, R., Gaetani, E., Flex, A., Aprahamian, T., Proia, A.S., Bosch-Marce, M., Smith, R.C., and Pola, P. (2003). Peripheral nerve ischemia: apolipoprotein E deficiency results in impaired functional recovery and reduction of associated intraneural angiogenic response. Exp Neurol *184*, 264-273.

Quan, G., Xie, C., Dietschy, J.M., and Turley, S.D. (2003). Ontogenesis and regulation of cholesterol metabolism in the central nervous system of the mouse. Brain Res Dev Brain Res *146*, 87-98.

Raichle, M.E., MacLeod, A.M., Snyder, A.Z., Powers, W.J., Gusnard, D.A., and Shulman, G.L. (2001). A default mode of brain function. Proc Natl Acad Sci U S A *98*, 676-682.

Ramaswamy, G., Xu, Q., Huang, Y., and Weisgraber, K.H. (2005). Effect of domain interaction on apolipoprotein E levels in mouse brain. J Neurosci *25*, 10658-10663.

Reiman, E.M., Chen, K., Liu, X., Bandy, D., Yu, M., Lee, W., Ayutyanont, N., Keppler, J., Reeder, S.A., Langbaum, J.B., *et al.* (2009). Fibrillar amyloid-beta burden in cognitively normal people at 3 levels of genetic risk for Alzheimer's disease. Proc Natl Acad Sci U S A *106*, 6820-6825.

Retz, W., Thome, J., Durany, N., Harsanyi, A., Retz-Junginger, P., Kornhuber, J., Riederer, P., and Rosler, M. (2001). Potential genetic markers of sporadic Alzheimer's dementia. Psychiatr Genet *11*, 115-122.

Riddell, D.R., Zhou, H., Atchison, K., Warwick, H.K., Atkinson, P.J., Jefferson, J., Xu, L., Aschmies, S., Kirksey, Y., Hu, Y., *et al.* (2008). Impact of apolipoprotein E (ApoE) polymorphism on brain ApoE levels. J Neurosci *28*, 11445-11453.

Rodriguez, E., Mateo, I., Llorca, J., Sanchez-Quintana, C., Infante, J., Berciano, J., and Combarros, O. (2006). No association between low density lipoprotein receptor genetic variants and Alzheimer's disease risk. Am J Med Genet B Neuropsychiatr Genet *141B*, 541-543.

Ronne-Engstrom, E., Cesarini, K.G., Enblad, P., Hesselager, G., Marklund, N., Nilsson, P., Salci, K., Persson, L., and Hillered, L. (2001). Intracerebral microdialysis in neurointensive care: the use of urea as an endogenous reference compound. J Neurosurg *94*, 397-402.

Roses, A.D. (1996). Apolipoprotein E alleles as risk factors in Alzheimer's disease. Annu Rev Med *47*, 387-400.

Rowe, C.C., Ng, S., Ackermann, U., Gong, S.J., Pike, K., Savage, G., Cowie, T.F., Dickinson, K.L., Maruff, P., Darby, D., *et al.* (2007). Imaging beta-amyloid burden in aging and dementia. Neurology *68*, 1718-1725.

Ruiz, J., Kouiavskaia, D., Migliorini, M., Robinson, S., Saenko, E.L., Gorlatova, N., Li, D., Lawrence, D., Hyman, B.T., Weisgraber, K.H., and Strickland, D.K. (2005). The apoE isoform binding properties of the VLDL receptor reveal marked differences from LRP and the LDL receptor. J Lipid Res *46*, 1721-1731.

Sadowski, M.J., Pankiewicz, J., Scholtzova, H., Mehta, P.D., Prelli, F., Quartermain, D., and Wisniewski, T. (2006). Blocking the apolipoprotein E/amyloid-beta interaction as a potential therapeutic approach for Alzheimer's disease. Proc Natl Acad Sci U S A *103*, 18787-18792.

Saunders, A.M. (2000). Apolipoprotein E and Alzheimer disease: an update on genetic and functional analyses. J Neuropathol Exp Neurol *59*, 751-758.

Saunders, A.M., Strittmatter, W.J., Schmechel, D., George-Hyslop, P.H., Pericak-Vance, M.A., Joo, S.H., Rosi, B.L., Gusella, J.F., Crapper-MacLachlan, D.R., Alberts, M.J., and

et al. (1993). Association of apolipoprotein E allele epsilon 4 with late-onset familial and sporadic Alzheimer's disease. Neurology *43*, 1467-1472.

Schmechel, D.E., Saunders, A.M., Strittmatter, W.J., Crain, B.J., Hulette, C.M., Joo, S.H., Pericak-Vance, M.A., Goldgaber, D., and Roses, A.D. (1993). Increased amyloid beta-peptide deposition in cerebral cortex as a consequence of apolipoprotein E genotype in late-onset Alzheimer disease. Proc Natl Acad Sci U S A *90*, 9649-9653.

Schneeweis, L.A., Koppaka, V., Lund-Katz, S., Phillips, M.C., and Axelsen, P.H. (2005). Structural analysis of lipoprotein E particles. Biochemistry *44*, 12525-12534.

Schwetye, K.E., Cirrito, J.R., Esparza, T.J., Mac Donald, C.L., Holtzman, D.M., and Brody, D.L. (2010). Traumatic brain injury reduces soluble extracellular amyloid-beta in mice: a methodologically novel combined microdialysis-controlled cortical impact study. Neurobiol Dis *40*, 555-564.

Selkoe, D.J. (2011). Resolving controversies on the path to Alzheimer's therapeutics. Nat Med *17*, 1060-1065.

Seshadri, S., Fitzpatrick, A.L., Ikram, M.A., DeStefano, A.L., Gudnason, V., Boada, M., Bis, J.C., Smith, A.V., Carassquillo, M.M., Lambert, J.C., *et al.* (2010). Genome-wide analysis of genetic loci associated with Alzheimer disease. JAMA *303*, 1832-1840.

Seubert, P., Barbour, R., Khan, K., Motter, R., Tang, P., Kholodenko, D., Kling, K., Schenk, D., Johnson-Wood, K., Schroeter, S., *et al.* (2008). Antibody capture of soluble Abeta does not reduce cortical Abeta amyloidosis in the PDAPP mouse. Neurodegener Dis *5*, 65-71.

Seubert, P., Vigo-Pelfrey, C., Esch, F., Lee, M., Dovey, H., Davis, D., Sinha, S., Schlossmacher, M., Whaley, J., Swindlehurst, C., and et al. (1992). Isolation and quantification of soluble Alzheimer's beta-peptide from biological fluids. Nature *359*, 325-327.

Shaw, L.M., Vanderstichele, H., Knapik-Czajka, M., Clark, C.M., Aisen, P.S., Petersen, R.C., Blennow, K., Soares, H., Simon, A., Lewczuk, P., *et al.* (2009). Cerebrospinal fluid biomarker signature in Alzheimer's disease neuroimaging initiative subjects. Ann Neurol *65*, 403-413.

Shaw, P., Lerch, J.P., Pruessner, J.C., Taylor, K.N., Rose, A.B., Greenstein, D., Clasen, L., Evans, A., Rapoport, J.L., and Giedd, J.N. (2007). Cortical morphology in children and adolescents with different apolipoprotein E gene polymorphisms: an observational study. Lancet Neurol *6*, 494-500.

Shibata, M., Yamada, S., Kumar, S.R., Calero, M., Bading, J., Frangione, B., Holtzman, D.M., Miller, C.A., Strickland, D.K., Ghiso, J., and Zlokovic, B.V. (2000). Clearance of Alzheimer's amyloid-ss(1-40) peptide from brain by LDL receptor-related protein-1 at the blood-brain barrier. J Clin Invest *106*, 1489-1499.

Shoji, M., Golde, T.E., Ghiso, J., Cheung, T.T., Estus, S., Shaffer, L.M., Cai, X.D., McKay, D.M., Tintner, R., Frangione, B., and et al. (1992). Production of the Alzheimer amyloid beta protein by normal proteolytic processing. Science *258*, 126-129.

Sisodia, S.S., and St George-Hyslop, P.H. (2002). gamma-Secretase, Notch, Abeta and Alzheimer's disease: where do the presenilins fit in? Nature reviews *3*, 281-290.

Soutar, A.K., and Naoumova, R.P. (2007). Mechanisms of disease: genetic causes of familial hypercholesterolemia. Nat Clin Pract Cardiovasc Med *4*, 214-225.

Steiner, H., and Haass, C. (2000). Intramembrane proteolysis by presenilins. Nat Rev Mol Cell Biol *1*, 217-224.

Strittmatter, W.J., and Roses, A.D. (1996). Apolipoprotein E and Alzheimer's disease. Annu Rev Neurosci *19*, 53-77.

Sullivan, P.M., Han, B., Liu, F., Mace, B.E., Ervin, J.F., Wu, S., Koger, D., Paul, S., and Bales, K.R. (2009). Reduced levels of human apoE4 protein in an animal model of cognitive impairment. Neurobiol Aging.

Sullivan, P.M., Mace, B.E., Maeda, N., and Schmechel, D.E. (2004). Marked regional differences of brain human apolipoprotein E expression in targeted replacement mice. Neuroscience *124*, 725-733.

Sunderland, T., Linker, G., Mirza, N., Putnam, K.T., Friedman, D.L., Kimmel, L.H., Bergeson, J., Manetti, G.J., Zimmermann, M., Tang, B., *et al.* (2003). Decreased beta-amyloid1-42 and increased tau levels in cerebrospinal fluid of patients with Alzheimer disease. JAMA *289*, 2094-2103.

Sunderland, T., Mirza, N., Putnam, K.T., Linker, G., Bhupali, D., Durham, R., Soares, H., Kimmel, L., Friedman, D., Bergeson, J., *et al.* (2004). Cerebrospinal fluid beta-amyloid1-42 and tau in control subjects at risk for Alzheimer's disease: the effect of APOE epsilon4 allele. Biol Psychiatry *56*, 670-676.

Suzuki, N., Cheung, T.T., Cai, X.D., Odaka, A., Otvos, L., Jr., Eckman, C., Golde, T.E., and Younkin, S.G. (1994). An increased percentage of long amyloid beta protein secreted by familial amyloid beta protein precursor (beta APP717) mutants. Science *264*, 1336-1340.

Taha, A.Y., Chen, C.T., Liu, Z., Kim, J.H., Mount, H.T., and Bazinet, R.P. (2009). Brainstem concentrations of cholesterol are not influenced by genetic ablation of the low-density lipoprotein receptor. Neurochem Res *34*, 311-315.

Takeda, S., Sato, N., Ikimura, K., Nishino, H., Rakugi, H., and Morishita, R. (2011). Novel microdialysis method to assess neuropeptides and large molecules in free-moving mouse. Neuroscience *186*, 110-119.

Tamboli, I.Y., Prager, K., Thal, D.R., Thelen, K.M., Dewachter, I., Pietrzik, C.U., St George-Hyslop, P., Sisodia, S.S., De Strooper, B., Heneka, M.T., *et al.* (2008). Loss of gamma-secretase function impairs endocytosis of lipoprotein particles and membrane cholesterol homeostasis. J Neurosci *28*, 12097-12106.

Tapiola, T., Alafuzoff, I., Herukka, S.K., Parkkinen, L., Hartikainen, P., Soininen, H., and Pirttila, T. (2009). Cerebrospinal fluid {beta}-amyloid 42 and tau proteins as biomarkers of Alzheimer-type pathologic changes in the brain. Arch Neurol *66*, 382-389.

Thies, W., and Bleiler, L. (2011). 2011 Alzheimer's disease facts and figures. Alzheimers Dement *7*, 208-244.

Thorell, J.I., and Johansson, B.G. (1971). Enzymatic iodination of polypeptides with 125I to high specific activity. Biochimica et biophysica acta *251*, 363-369.

Tiraboschi, P., Hansen, L.A., Masliah, E., Alford, M., Thal, L.J., and Corey-Bloom, J. (2004). Impact of APOE genotype on neuropathologic and neurochemical markers of Alzheimer disease. Neurology *62*, 1977-1983.

Tokuda, T., Calero, M., Matsubara, E., Vidal, R., Kumar, A., Permanne, B., Zlokovic, B., Smith, J.D., Ladu, M.J., Rostagno, A., *et al.* (2000). Lipidation of apolipoprotein E influences its isoform-specific interaction with Alzheimer's amyloid beta peptides. Biochem J *348 Pt 2*, 359-365.

Trommsdorff, M., Borg, J.P., Margolis, B., and Herz, J. (1998). Interaction of cytosolic adaptor proteins with neuronal apolipoprotein E receptors and the amyloid precursor protein. J Biol Chem *273*, 33556-33560.

Ulery, P.G., Beers, J., Mikhailenko, I., Tanzi, R.E., Rebeck, G.W., Hyman, B.T., and Strickland, D.K. (2000). Modulation of beta-amyloid precursor protein processing by the low density lipoprotein receptor-related protein (LRP). Evidence that LRP contributes to the pathogenesis of Alzheimer's disease. J Biol Chem *275*, 7410-7415.

Van Broeckhoven, C., Haan, J., Bakker, E., Hardy, J.A., Van Hul, W., Wehnert, A., Vegter-Van der Vlis, M., and Roos, R.A. (1990). Amyloid beta protein precursor gene and hereditary cerebral hemorrhage with amyloidosis (Dutch). Science *248*, 1120-1122.

Van Uden, E., Mallory, M., Veinbergs, I., Alford, M., Rockenstein, E., and Masliah, E. (2002). Increased extracellular amyloid deposition and neurodegeneration in human amyloid precursor protein transgenic mice deficient in receptor-associated protein. J Neurosci *22*, 9298-9304.

Vassar, R., Bennett, B.D., Babu-Khan, S., Kahn, S., Mendiaz, E.A., Denis, P., Teplow, D.B., Ross, S., Amarante, P., Loeloff, R., *et al.* (1999). Beta-secretase cleavage of Alzheimer's amyloid precursor protein by the transmembrane aspartic protease BACE. Science *286*, 735-741.

Verghese, P.B., Castellano, J.M., and Holtzman, D.M. (2011). Apolipoprotein E in Alzheimer's disease and other neurological disorders. Lancet Neurol *10*, 241-252.

Vlassenko, A.G., Vaishnavi, S.N., Couture, L., Sacco, D., Shannon, B.J., Mach, R.H., Morris, J.C., Raichle, M.E., and Mintun, M.A. (2010). Spatial correlation between brain aerobic glycolysis and amyloid-beta (Abeta) deposition. Proc Natl Acad Sci U S A *107*, 17763-17767.

Wahrle, S.E., Jiang, H., Parsadanian, M., Hartman, R.E., Bales, K.R., Paul, S.M., and Holtzman, D.M. (2005). Deletion of Abca1 increases Abeta deposition in the PDAPP transgenic mouse model of Alzheimer disease. J Biol Chem *280*, 43236-43242.

Wahrle, S.E., Jiang, H., Parsadanian, M., Kim, J., Li, A., Knoten, A., Jain, S., Hirsch-Reinshagen, V., Wellington, C.L., Bales, K.R., *et al.* (2008). Overexpression of ABCA1 reduces amyloid deposition in the PDAPP mouse model of Alzheimer disease. J Clin Invest *118*, 671-682.

Wang, J., Tanila, H., Puolivali, J., Kadish, I., and van Groen, T. (2003). Gender differences in the amount and deposition of amyloidbeta in APPswe and PS1 double transgenic mice. Neurobiology of disease *14*, 318-327.

Weisgraber, K.H. (1994). Apolipoprotein E: structure-function relationships. Advances in protein chemistry *45*, 249-302.

West, H.L., Rebeck, G.W., and Hyman, B.T. (1994). Frequency of the apolipoprotein E epsilon 2 allele is diminished in sporadic Alzheimer disease. Neurosci Lett *175*, 46-48.

Wisniewski, T., Castano, E.M., Golabek, A., Vogel, T., and Frangione, B. (1994). Acceleration of Alzheimer's fibril formation by apolipoprotein E in vitro. Am J Pathol *145*, 1030-1035.

Wood, S.J., Chan, W., and Wetzel, R. (1996). Seeding of A beta fibril formation is inhibited by all three isotypes of apolipoprotein E. Biochemistry *35*, 12623-12628.

Wouters, K., Shiri-Sverdlov, R., van Gorp, P.J., van Bilsen, M., and Hofker, M.H. (2005). Understanding hyperlipidemia and atherosclerosis: lessons from genetically modified apoe and ldlr mice. Clin Chem Lab Med *43*, 470-479.

Wyss-Coray, T. (2006). Inflammation in Alzheimer disease: driving force, bystander or beneficial response? Nat Med *12*, 1005-1015.

Yamada, K., Cirrito, J.R., Stewart, F.R., Jiang, H., Finn, M.B., Holmes, B.B., Binder, L.I., Mandelkow, E.M., Diamond, M.I., Lee, V.M., and Holtzman, D.M. (2011). In vivo microdialysis reveals age-dependent decrease of brain interstitial fluid tau levels in P301S human tau transgenic mice. J Neurosci *31*, 13110-13117.

Yamada, K., Hashimoto, T., Yabuki, C., Nagae, Y., Tachikawa, M., Strickland, D.K., Liu, Q., Bu, G., Basak, J.M., Holtzman, D.M., *et al.* (2008). The low density lipoprotein

receptor-related protein 1 mediates uptake of amyloid beta peptides in an in vitro model of the blood-brain barrier cells. J Biol Chem *283*, 34554-34562.

Yamada, K., Yabuki, C., Seubert, P., Schenk, D., Hori, Y., Ohtsuki, S., Terasaki, T., Hashimoto, T., and Iwatsubo, T. (2009). Abeta immunotherapy: intracerebral sequestration of Abeta by an anti-Abeta monoclonal antibody 266 with high affinity to soluble Abeta. J Neurosci *29*, 11393-11398.

Yamamoto, T., Choi, H.W., and Ryan, R.O. (2008). Apolipoprotein E isoform-specific binding to the low-density lipoprotein receptor. Analytical biochemistry *372*, 222-226.

Yan, P., Bero, A.W., Cirrito, J.R., Xiao, Q., Hu, X., Wang, Y., Gonzales, E., Holtzman, D.M., and Lee, J.M. (2009). Characterizing the appearance and growth of amyloid plaques in APP/PS1 mice. J Neurosci *29*, 10706-10714.

Yang, D.S., Small, D.H., Seydel, U., Smith, J.D., Hallmayer, J., Gandy, S.E., and Martins, R.N. (1999). Apolipoprotein E promotes the binding and uptake of beta-amyloid into Chinese hamster ovary cells in an isoform-specific manner. Neuroscience *90*, 1217-1226.

Yang, D.S., Smith, J.D., Zhou, Z., Gandy, S.E., and Martins, R.N. (1997). Characterization of the binding of amyloid-beta peptide to cell culture-derived native apolipoprotein E2, E3, and E4 isoforms and to isoforms from human plasma. J Neurochem *68*, 721-725.

Yokode, M., Hammer, R.E., Ishibashi, S., Brown, M.S., and Goldstein, J.L. (1990). Diet-induced hypercholesterolemia in mice: prevention by overexpression of LDL receptors. Science *250*, 1273-1275.

Yue, X., Lu, M., Lancaster, T., Cao, P., Honda, S., Staufenbiel, M., Harada, N., Zhong, Z., Shen, Y., and Li, R. (2005). Brain estrogen deficiency accelerates Abeta plaque formation in an Alzheimer's disease animal model. Proc Natl Acad Sci U S A *102*, 19198-19203.

Zannis, V.I., Breslow, J.L., Utermann, G., Mahley, R.W., Weisgraber, K.H., Havel, R.J., Goldstein, J.L., Brown, M.S., Schonfeld, G., Hazzard, W.R., and Blum, C. (1982). Proposed nomenclature of apoE isoproteins, apoE genotypes, and phenotypes. J Lipid Res *23*, 911-914.

Zerbinatti, C.V., Wahrle, S.E., Kim, H., Cam, J.A., Bales, K., Paul, S.M., Holtzman, D.M., and Bu, G. (2006). Apolipoprotein E and low density lipoprotein receptor-related protein facilitate intraneuronal Abeta42 accumulation in amyloid model mice. J Biol Chem *281*, 36180-36186.

Zerbinatti, C.V., Wozniak, D.F., Cirrito, J., Cam, J.A., Osaka, H., Bales, K.R., Zhuo, M., Paul, S.M., Holtzman, D.M., and Bu, G. (2004). Increased soluble amyloid-beta peptide and memory deficits in amyloid model mice overexpressing the low-density lipoprotein receptor-related protein. Proc Natl Acad Sci U S A *101*, 1075-1080.

Zhang, Y., Chen, J., and Wang, J. (2008). A complete backbone spectral assignment of lipid-free human apolipoprotein E (apoE). Biomol NMR Assign *2*, 207-210.

Zhang, Y., Vasudevan, S., Sojitrawala, R., Zhao, W., Cui, C., Xu, C., Fan, D., Newhouse, Y., Balestra, R., Jerome, W.G., *et al.* (2007). A monomeric, biologically active, full-length human apolipoprotein E. Biochemistry *46*, 10722-10732.

Zlokovic, B.V. (2008). The blood-brain barrier in health and chronic neurodegenerative disorders. Neuron *57*, 178-201.

Zou, F., Gopalraj, R.K., Lok, J., Zhu, H., Ling, I.F., Simpson, J.F., Tucker, H.M., Kelly, J.F., Younkin, S.G., Dickson, D.W., *et al.* (2008). Sex-dependent association of a common low-density lipoprotein receptor polymorphism with RNA splicing efficiency in the brain and Alzheimer's disease. Human molecular genetics *17*, 929-935.